

**ISTANBUL TECHNICAL UNIVERSITY ★ FACULTY OF MECHANICAL
ENGINEERING
MANUFACTURING ENGINEERING DEPARTMENT**



**DENTAL IMPLANT DESIGN FOR MANDIBULAR FIRST MOLAR TOOTH
AND MATERIAL OPTIMIZATION WITH FINITE ELEMENT ANALYSIS**

SENIOR DESIGN PROJECT

Prepared by

**030120425 Veysel Mert USTA
030110405 Gani Melik ÖNDER**

**Supervisor: Prof. Dr. Ersan ÜSTÜNDAR
Assist. Prof. Erkan GÜNPINAR**

JANUARY 2017

Prepared by

**030120425 Veysel Mert USTA
030110405 Gani Melik ÖNDER**

To our families and the Great Turkish Nation,

PREFACE

We would like to thank Prof. Dr. Ersan ÜSTÜNDAĞ, Assist. Prof. Erkan GÜNPINAR from the School of Mechanical Engineering of Istanbul Technical University and Assist. Prof. Şadiye GÜNPINAR from the Dental Faculty of Abant İzzet Baysal University for their valuable comments and advice.

January 2017

Veysel Mert USTA
Gani Melik ÖNDER

TABLE OF CONTENTS

	<u>Page</u>
PREFACE.....	v
TABLE OF CONTENTS.....	vii
ABREVIATIONS.....	ix
LIST OF TABLES.....	xi
LIST OF FIGURES.....	xiii
ABSTRACT.....	xvii
ÖZET.....	xviii
1. INTRODUCTION.....	1
1.1 Purpose of the Project.....	2
1.2 Design Limitations	2
1.3 Literature Research and Parameter Settings.....	3
1.4 Distribution of Tasks and Gantt Chart.....	13
2. DESIGN OPTIONS AND SELECTION CRITERIA.....	14
2.1 Design Iteration and Advantages of the New Design.....	14
3. DESIGN OF IMPLANT SYSTEM FINITE ELEMENT ANALYSIS	19
3.1 Introduction to ANSYS Workbench.....	19
3.2 Project Schematic.....	19
3.3 Geometry.....	20
3.4 Static Structural.....	24
3.5 Engineering Data.....	26
3.6 Geometry – 2D.....	27
3.7 Geometry – 3D	31
3.8 Symmetry.....	33
3.9 Connections.....	34
3.10 Meshing.....	38
3.10.1 2D Mesh Metrics.....	40
3.10.2 3D Mesh Metrics.....	41
3.10.3 Tabular Data of 2D and 3D Mesh Metrics.....	43
3.11 Loading and Boundary Conditions	44
3.12 Material Analysis on 2D model.....	45
4. RESULTS.....	46
4.1 Total Deformation	46
4.2 Equivalent Stresses On The Entire Model.....	48
4.3 Equivalent Stresses On The Cortical Bone.....	51
4.4 Equivalent Stress On The Trabecular Bone.....	53
4.5 Tabular Data For The Stress and Deformation Results.....	56
4.6 FEM Solution Times.....	57
4.7 Material Analysis Results.....	57
5. EVALUATION, DISCUSSION AND SUGGESTIONS.....	61
6. FINANCIAL COST ANALYSIS.....	63
7. FUTURE WORK.....	64
REFERENCES.....	65
APPENDIX – 1 TECHNICAL DRAWINGS.....	69
APPENDIX – 1 STUDENT RESUMES.....	71

ABREVIATIONS

APDL	: ANSYS Parametric Design Language
Buccolingual	: From buccal side to lingual side
CAD	: Computer Aided Design
CFD	: Computational Fluid Dynamics
CT	: Computer Tomography
FEA	: Finite Element Analysis
FEM	: Finite Element Method
GPa	: Giga Pascal
MPa	: Mega Pascal

LIST OF TABLES

	<u>Page</u>
Table 3.1 : Tabular data for 2D and 3D mesh metrics.....	43
Table 3.2 : Mesh statistics for 2D and 3D meshing.....	43
Table 3.3 : The Young's moduli of some titanium-based alloys [18]. The numbers in front of element names in the first column indicate wt.%.....	47
Table 4.1 : Deformation and stress results on the 2D and 3D parts of the model.....	56
Table 4.2 : Elapsed solution times for the tested models.....	57
Table 5.1 : Tabular data of literature stress and deformation results on the bones.....	62

LIST OF FIGURES

	<u>Page</u>
Figure 1.1 : A - Maggiolo's gold implant design	1
Figure 1.2 : B - Dr. Edward J. Greendfield's lattice cage design	1
Figure 1.3 : C - Per-Ingvar Branemark's system design	1
Figure 1.4 : Osseointegration of the bone on the implant surface.....	2
Figure 1.5 : Section view of the bone geometric model.....	4
Figure 1.6 : Fixed support at the bottom side and frictionless supports at the right and left side.....	4
Figure 1.7 : 100 N axial compression loading.....	5
Figure 1.8 : 20 N bending loading (Buccolingual).....	5
Figure 1.9 : Results table from [9].....	5
Figure 1.10 : 3D models of the dental implant.....	6
Figure 1.11 : Results table from [10].....	6
Figure 1.12 : Models of (a) cylindrical, (b) stepped, (c) v-thread.....	7
Figure 1.13 : Models of (d) rectangular threaded, (e) tapered body of threaded implants, (f) implants with two thread sizes.....	7
Figure 1.14 : (a) Loading directions and fixed support, (b) isometric and (c) section views.....	8
Figure 1.15 : Bone level implant and tissue level implant.....	8
Figure 1.16 : Mesh and node demonstration on the 3D model.....	9
Figure 1.17 : Results of NobelBiocare.....	9
Figure 1.18 : Results of Straumann.....	9
Figure 1.19 : Implant thread height and width.....	10
Figure 1.20 : Mesh model of the implant system.....	10
Figure 1.21 : Different height and width values and their results.....	11
Figure 1.22 : Response curve analysis for jaw bone stresses.....	11
Figure 1.23 : Sensitivity analysis, H=Height – W=Width.....	11
Figure 1.24 : Gantt chart	13
Figure 2.1 : Basic implant parts.....	14
Figure 2.2 : Thread types.....	14
Figure 2.3 : 3D model of new implant design.....	15
Figure 2.4 : Section view of new implant design.....	15
Figure 2.5 : 3D model cortical and trabecular bone (yellow: cortical, brown: trabecular).....	16
Figure 2.6 : 3D model of all parts (white: crown force part, blue: abutment, gray: screw).....	16
Figure 2.7 : The thread profile employed in this project. Radius: 0.05mm.....	17
Figure 2.8 : Tapered helix threads.....	17
Figure 2.9 : Real bone structure	18
Figure 2.10 : Tapered helix thread tap	18
Figure 2.11 : 2D model of all parts	18
Figure 3.1 : Workbench project schematic page	19
Figure 3.2 : Geometry blocks on the project schematic page, Upper one is not exploded and the latter is exploded.....	21
Figure 3.3 : Exploding the parts in the design modeler	22
Figure 3.4 : Unexploded part meshing	23

Figure 3.5 : Exploded part meshing	23
Figure 3.6 : Unexploded part stresses	24
Figure 3.7 : Exploded part stresses	24
Figure 3.8 : Force displacement curve for linear analysis	24
Figure 3.9 : Force displacement curve for nonlinear analysis.....	25
Figure 3.10 : Workbench engineering data page.....	26
Figure 3.11 : Non-threaded screw.....	28
Figure 3.12 : Threaded screw.....	28
Figure 3.13 : The stresses on the cortical bone with screw threads	28
Figure 3.14 : The stresses on the cortical bone without screw threads	28
Figure 3.15 : The stresses on the trabecular bone with screw threads.....	29
Figure 3.16 : The stresses on the trabecular bone without screw threads.....	29
Figure 3.17 : 2D surface bodies of the dental implant and bone models.....	30
Figure 3.18 : Zoomed view of the 2D surface bodies of the entire model.....	31
Figure 3.19 : 3D section view of the model.....	32
Figure 3.20 : Parts of the 3D model.....	33
Figure 3.21 : 90° representation of the 2D surface.....	34
Figure 3.22 : 270° representation of the 2D surface.....	34
Figure 3.23 : Normal Lagrange formulation at left and MPC formulation at right.....	36
Figure 3.24 : Initial contact information of 2d frictional case.....	37
Figure 3.25 : 2D Meshing with triangular elements.....	38
Figure 3.26 : 3D Meshing with tetrahedral elements.....	39
Figure 3.27 : 2D element quality graph of triangular mesh. The average value is 0.96 and it should be close to the value of 1 in order to have excellent mesh quality.....	40
Figure 3.28 : 2D aspect ratio of the triangular elements. The average value is 1.2 while the best value is 1. It should be lower than 20 in order to have fair mesh elements.....	40
Figure 3.29 : 2D skewness of the triangular elements. The average value is 0.056 and the optimum value should be 0. In order to have acceptable results, the skewness value should be lower than 0.9.....	41
Figure 3.30 : 3D element quality graph of tetrahedral mesh. The average value is 0.84 and it should be close to the value of 1 in order to have excellent mesh quality.....	41
Figure 3.31 : 3D aspect ratio of the tetrahedral elements. The average value is 1.82 while the best value is 1. It should be lower than 20 in order to have fair mesh elements.....	41
Figure 3.32 : 3D skewness of the tetrahedral elements. The average value is 0.22 and the optimum value should be 0. In order to have acceptable results, the skewness value should be lower than 0.9.....	42
Figure 3.33 : 2D boundary conditions.....	44
Figure 3.34 : 3D boundary conditions.....	44
Figure 4.1 : 3D bonded condition total deformation of the entire model. Max is 0.0037 mm....	46
Figure 4.2 : 2D bonded condition total deformation of the entire model. Max is 0.0037 mm....	47
Figure 4.3 : 3D frictional condition total deformation of the entire model. Max is 0.0044 mm..	47
Figure 4.4 : 2D frictional condition total deformation of the entire model. Max is 0.0042 mm..	48
Figure 4.5 : 3D bonded condition equivalent stresses on the whole model. Max occurs on the top of the abutment which is 41 MPa and the strength of the abutment is 830 MPa.....	49
Figure 4.6 : 2D bonded condition equivalent stresses on the whole model. Max occurs on the implant which is 41 MPa and the strength of the implant is 830 MPa.....	49
Figure 4.7 : 3D frictional condition equivalent stresses on the whole model. Max occurs on the abutment which is 35 MPa and the strength of the abutment is 830 MPa.....	50

Figure 4.8 : 2D frictional condition equivalent stresses on the whole model. Max occurs on the implant which is 40 MPa and the strength of the implant is 830 MPa.....	50
Figure 4.9 : 3D bonded condition equivalent stress on the cortical bone. Max value is 9.8 and the strength of the cortical bone is 130 MPa.....	51
Figure 4.10 : 2D bonded condition equivalent stress on the cortical bone. Max value is 8.4 MPa and the strength of the cortical bone is 130 MPa.....	52
Figure 4.11 : 3D frictional condition equivalent stress on the cortical bone. Max value is 14 MPa and the strength of the cortical bone is 130 MPa.....	52
Figure 4.12 : 2D frictional condition equivalent stress on the cortical bone. Max value is 14 MPa and the strength of the cortical bone is 130 MPa.....	53
Figure 4.13 : 3D bonded condition equivalent stress on the trabecular bone. Max value is 3.3 MPa and the strength of the trabecular bone is 20 MPa.....	54
Figure 4.14 : 2D bonded condition equivalent stress on the trabecular bone. Max value is 3.5 MPa and the strength of the trabecular bone is 20 MPa.....	54
Figure 4.15 : 3D frictional condition equivalent stress on the trabecular bone. Max value is 4 MPa and the strength of the trabecular bone is 20 MPa.....	55
Figure 4.16 : 2D frictional condition equivalent stress on the trabecular bone. Max value is 4.7 MPa and the strength of the trabecular bone is 20 MPa.....	55
Figure 4.17 : Table of material analysis results. The Young's modulus values begin from 14 GPa to the 110 GPa.....	58
Figure 4.18 : Deformation graph for both bonded and frictional cases.....	59
Figure 4.19 : General max equivalent stress graph for both bonded and frictional case.....	59
Figure 4.20 : Cortical bone max equivalent stress graph for both bonded and frictional case	60
Figure 4.21 : Trabecular bone max equivalent stress graph for both bonded and frictional case.....	60

DENTAL IMPLANT DESIGN FOR MANDIBULAR FIRST MOLAR TOOTH AND MATERIAL OPTIMIZATION WITH FINITE ELEMENT ANALYSIS

ABSTRACT

Dental implants are support elements that are placed on the jaw bone to replace a missing tooth root. Dental implants support the prosthesis parts such as the tooth crown. Implant length and diameter can change due to the type of the missing tooth. With the advance of recent technology, implant design and materials have changed enormously in time. This design project focuses on the desired mechanical properties for a new implant using the finite element method (FEM). By creating an FEM model for the mandibular first molar, it attempted to observe the effects of design changes for optimization. In literature, most of the implant FEMs are three dimensional (3D). These 3D analyses result in high computational costs. In this project it was shown that two dimensional (2D) analyses can provide similar results at a much lower computational cost: The average time of 2D analyses was 10 seconds while the average time of 3D analyses was about 2 hours. These vastly more efficient 2D models were then used to study the effect of different materials and designs on the jaw bone stresses. For instance, it was shown that different titanium-based materials can lower the stresses on the bone by about 15%. Lastly, a financial cost analysis of the project was performed.

ALT BİRİNCİ MOLAR İÇİN DİŞ İMPLANT TASARIMI VE SONLU ELEMANLAR YÖNTEMİYLE MALZEME OPTİMİZASYONU

ÖZET

Diş implantı kaybedilmiş bir dişin kökü görevini yapması için çene kemiğine yerleştirilen destek elemanıdır. Diş implantları daha sonra üzerlerine takılacak diş minesи protezlerine destek oluştururlar. Kaybedilmiş dişin türüne göre implantların boyu ve çapı gibi boyut özellikleri değiştiği gibi gelişen teknolojik bilgiler sayesinde malzemesi ve tasarımları da zaman içerisinde gelişme göstermiştir. Bu tasarım projesi yeni bir implantın tasarımı için gereken mekanik özelliklerin sonlu elemanlar yöntemiyle bilgisayar ortamında test edilmesi için izlenen adımları içermektedir. 2 boyutlu analizler sayesinde alt birinci molar için tasarlanan implantın optimizasyonu için yapılan değişikliklerinin etkileri çok kısa süreler içerisinde saptanabilemektedir. Literatür araştırmasında yapılan analizlerin büyük çoğunluğunun üç boyutlu olduğu görülmüştür. Yapılan üç boyutlu analizler, gereken zaman ve bilgisayar donanımı düşünüldüğünde yüksek maliyetler oluşturmaktadır. Bazı kabuller yapılarak bunların iki boyutlu olarak analizleri yapıldığında belirtilen maliyetler oldukça düşmektedir. Yeni implantın tasarımından sonra üç boyutlu ve iki boyutlu analizleri yapılmış ve sonuçları incelenmiştir. Bu sonuçlara göre 3 boyutlu analizlerin ortalama süresi 2 saat iken 2 boyutlu analizlerin ortalama süreleri 10 saniyedir. Sonuçlarda krtitik nokta olarak çene kemiği üzerinde oluşan stresler incelenmiştir. Farklı malzeme ve tasarımların stresleri etkilediği görülmüştür. Farklı titanyum alaşımaları denenerek kemik yapısı üstüneki streslerin yüzde 15 civarında düşürülebildiği gözlemlenmiştir. Son olarak maliyet analizi yapılmıştır.

1. INTRODUCTION

An implant can be described as a tool that restores, reinforces or improves biological structure. For the human body, there are over 20 implant types just for orthopedics. Implants have also had a significant role in dentistry. In history, lots of different materials were used as dental implants. For example, bamboo in China, copper pegs in Egypt, and sea shells in Maya countries were used as dental implants. In the modern era, dental implants are mostly manufactured using bio-compatible metals such as titanium.

People started to try different metals as implant material in the 19th century. In 1809, French dentist Maggiolo designed a gold implant which was installed into a newly opened extraction socket. In 1886, Harris designed a tooth-root-shaped platinum post with lead coating. In 1889, Edmunds planted a platinum disc with a porcelain crown to his patient's jaw bone. In 1913, Dr. Edward J. Greenfield designed a root form implant as a lattice cage made of platinum and gold. In late 1930s, Venable, Strock, Dahl, Gershkoff and Goldberg made many implant designs and used metal alloys which included basically Co, Cr and Mo. In 1960, Per-Ingvar Branemark introduced titanium as implant material. Branemark developed the "osseointegration" concept on the titanium. Here, the titanium implant was used as anchorage point and screws were used to retain the abutment and crown. This formed the basis of today's implant designs [1].

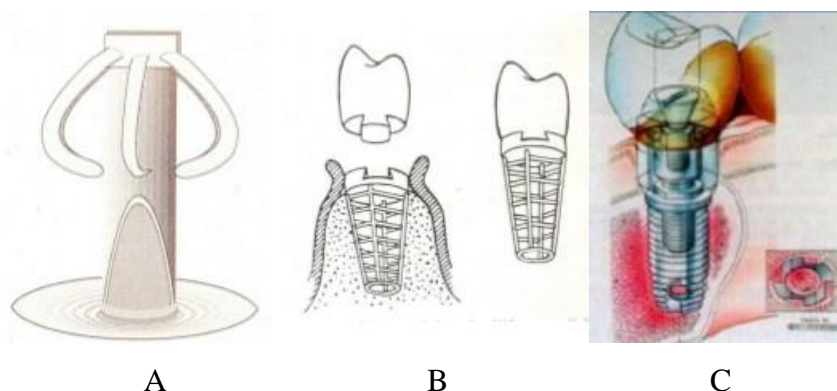


Figure 1.1: A - Maggiolo's gold implant design [1].

Figure 1.2: B - Dr. Edward J. Greendfield's lattice cage design [1].

Figure 1.3: C - Per-Ingvar Branemark's system design [1].

1.1 Purpose of the Project

Dental implants are very reliable prostheses for patients who lost their teeth. Today dental implant success rates are mostly above 90% [2]. Although dental implants have high success rates, some patients occasionally experience catastrophic failures. Fracture of the sub-parts, infections and patient's other sicknesses (e.g., diabetes) and habits (smoking, alcoholism) are some of the causes of dental implant failures. Implant design and materials have been shown to have a big role on implant survivability. In this project, new implant designs were developed and modelled using the finite element method (FEM). It was determined early in the project that 3D FEM models are computationally costly. Therefore, a 2D model was developed that yielded results similar to those by the 3D model, yet it was very fast. Using the 2D model, various design parameters and implant materials were investigated.

1.2 Design Limitations

For realistic simulations, all parameters of the dental implant must be considered carefully. Firstly, materials that are selected for the implant parts must be bio-compatible. Since most implants are used for long periods, they must be in harmony with the live tissues. For dental implants, “osseointegration” is another significant concept within bio-compatibility. Introduced by Prof. Dr. Per-Ingvar Branemark in 1960s [3], it involves bone healing and growing on implants. This growth on the implant surface forms a bonded connection between the implant and the bone.

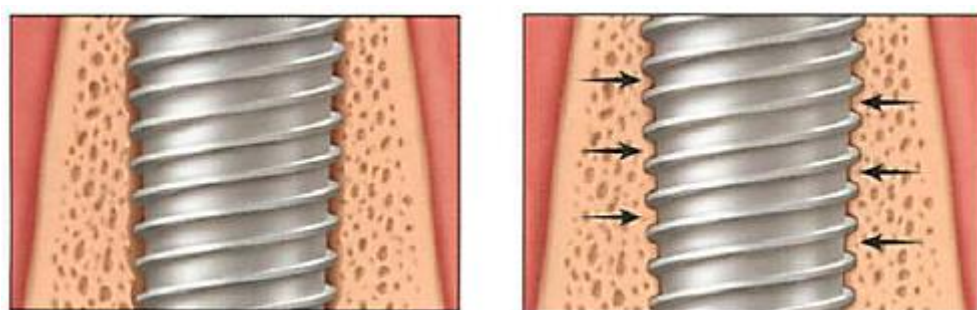


Figure 1.4: Osseointegration of the bone on the implant surface [4].

Another limitation for dental implants is their dimensions. Based on the missing tooth it replaces, the dimensions of an implant differ with length and diameter being the most critical dimensions. Length can vary from 6 mm to 16 mm while diameter must be between 3.5 mm and 6.5 mm. Since there are lots of capillary vessels and nerves around the jaw bone, the location of these living structures must also be considered [5].

In this project, the most commonly extracted tooth was selected for reasonable implant design. According to Zadik et al. [6], this is the mandibular first molar with a 45% extraction rate. Therefore, the mandibular first molar was selected as the tooth to be implanted in this project. After that, bone type must be selected. In the research of Lekholm et al. [7], type 2 bone was used for mandibulars. This classification determines the mechanical properties of the bone in FEA. Also, bone strength is crucial for analysis. Bones behave like ceramic materials and experience brittle fracture so stresses must be as low as possible. According to Harold M. Frost's work, compressive strengths of the cortical and trabecular bone are 130 MPa and 20 MPa, respectively [8].

The compression strength of the implant material is also important. In the mastication process, the force from the masseter muscle is exerted to the masticatory. During this process, compressive stresses occur around the implant. Small surface areas and high forces for exceptional loadings such as cracking nuts with teeth may lead to very high stresses on the implant and bone. Thus, such exceptional situations must be considered to avoid implant failure.

1.3 Literature Search and Parameter Settings

The so-called *in silico* approach for medical topics became popular by advanced computer technologies. Simulations and analyzes have no risk like the *in vivo* approach and they are simpler than the *in situ* approach. In dental implant research and development process, one of these approaches must be used for testing new design or material. The finite element method is applicable for dental implants tests among the *in silico* approaches. In 1990s, FEM software improved and became user friendly.

Parkhe et al. [9] worked on the thread shape of the implant to achieve better condition for cancellous and cortical bones according to stresses. They used two different models in their work. In model A, they used 30° and 60° thread angles, while in model B, they used thread

angles and thread length of 30° and 0.5 mm, 60° and 0.3 mm, 30° and 0.5 mm, 60° and 0.3 mm. After creating their 3D models, they used the ANSYS 13.0 software for FEA. They modelled only a section of the mandibular bone because a full model of the bone is costly for analysis. They modelled the cancellous bone in size of 15 mm x 20 mm x 15 mm and the cortical bone as a 2 mm thickness on the cancellous bone.

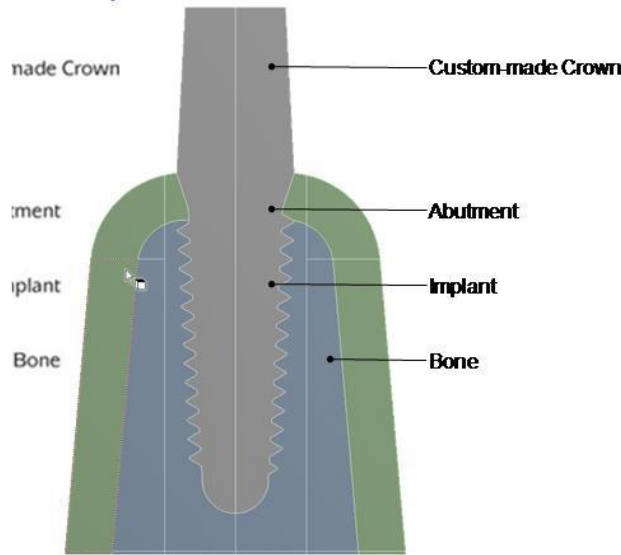


Figure 1.5: Section view of the bone geometric model [9].

They stated the supports of the model as fixed at the bottom side and frictionless at the right and left side. The cortical and cancellous bones had bonded contact. Implant and bones had frictional contact with a coefficient of 0.3. They planned four different loading conditions which were 100 N axial compression, 100 N angular (buccolingual), 50 N axial tension, and 20 N bending (buccolingual).

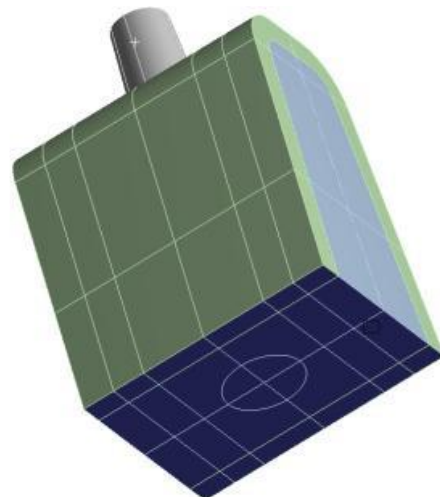
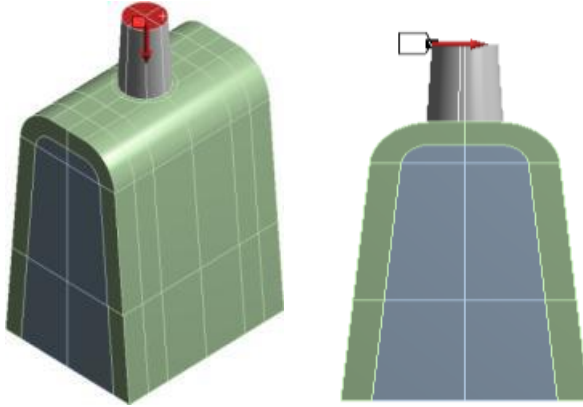


Figure 1.6: Fixed support at the bottom and frictionless supports at the right and left sides [9].



Figures 1.7 and 1.8: 100 N axial compression and 20 N bending loading (buccolingual) [9].

Implant	Compression 100N	15 Degree 100 N	Tension 50 N	Bending 20 N
Implant A	24.152	77.212	63.089	8872
Implant B	28.557	60.067	36.887	8258.4

Table: comparison of Equivalent (Von-Mises) Stress

Implant	Compression 100N	15 Degree 100 N	Tension 50 N	Bending 20 N
Implant A	0.0014	0.01035	0.0013	0.0177
Implant B	0.003	0.01476	0.0018	0.0209

Table: Comparison of Total deformation

Figure 1.9: Results table from [9].

As a conclusion, they decided a constant thread angle of 60° is the optimum choice for threads. Azari et al. [10], built a model for rapid prototyping and they tested it with FEA. They designed a new dental implant structure with just two parts which were an integrated implant and crown. Also, they used a snap-fit mechanism for implant-crown connection instead of dental cement. They modelled the bone section according to the mandibular second premolar tooth which has type-2 bone properties as stated in the classification system of Lekholm and Zarb. (Lekholm et al. [7]). The bone model had the dimensions of 24.2 mm in height and 16.3 mm in width including each 2 mm thickness of the gingiva and cortical bones on the cancellous bone. Solidworks 2005 software was used for generating 3D models.

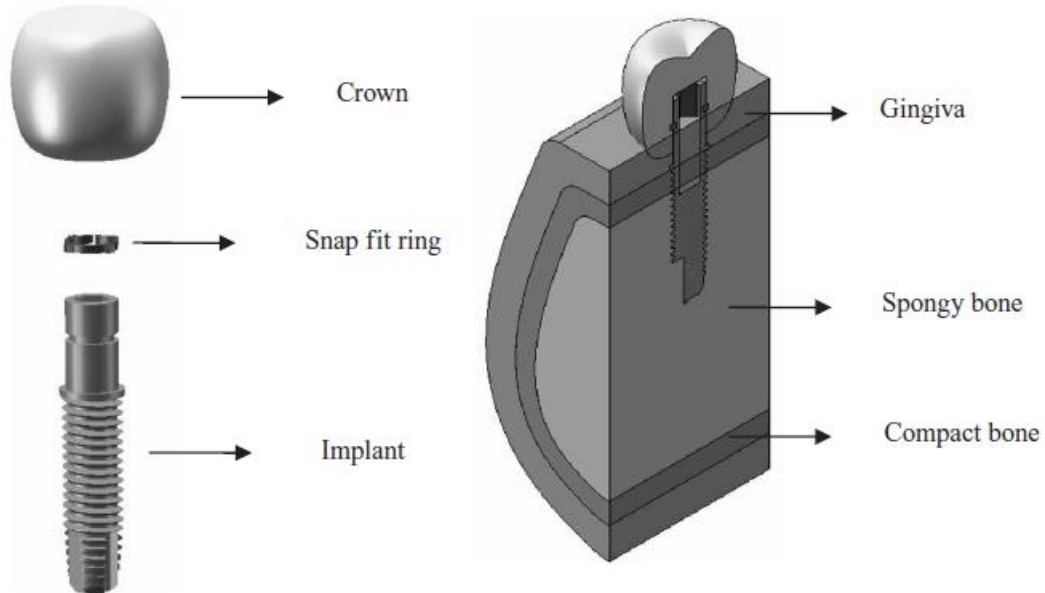


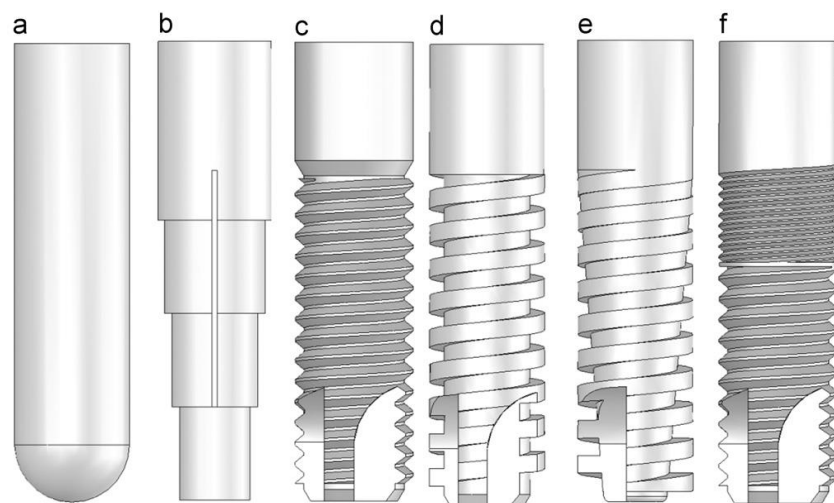
Figure 1.10: 3D models of the dental implant [10].

The FEM model described in ref. [10] had 93,099 nodes and 58,084 elements. All contact in the model were accepted as bonded contact. Cosmos Works 2005 software was used for FEA. Cobalt-Chromium for the snap-fit gauge, Ti-6Al-4V for the implant and porcelain for the crown were selected as materials. The materials were assumed to be homogenous, isotropic and linear elastic. Static and dynamic loadings were applied. Forces were 17.1 N, 114.6 N, and 23.4 N in a lingual, an axial, and a mesiodistal direction, respectively. These are the components of a 118.2 N force applied at an angle of 75° (Kayabasi, et al. [11]). Dynamic loading was described as three phases of chewing per day, 15 minutes for each phase and 60 cycles per minute. This resulted in 2,700 chewing cycles per day and nearly 10^6 cycles per year (Binon, et al. [12]). As seen in the results in Figure 1.11, they concluded that dynamic loading and fatigue conditions must be considered for dental implants.

	Equivalent (Von Misses) stress	
	Static loading (Mpa)	Dynamic loading (Mpa)
Implant	92.291	157.110
Snap fit ring	14.310	23.814
Crown	27.465	45.157
Compact bone	8.452	13.678
Spongy bone	2.912	4.875

Figure 1.11: Results table from [10].

Huang et al. [13] studied how the thread type of immediately loaded implant and surface roughness affects the stresses. They built six different implant models with three different surface roughnesses. Different surface roughnesses were imported into FEA via friction of coefficients. Friction coefficients between the bone and implant surfaces were 0.4, 0.68 and 1.0 for polished, Al₂O₃ blasted and beaded porous, respectively. They also took into account the heterogeneous structure of the bone and used anisotropic elasticity values in the FEA. Two types of loadings were applied: axial compression at the central fossa, and oblique compression with a 45° angle at the buccal cusp. They employed a real-like geometry of the bone and crown. They used fixed support at the right and left sides of the bone.



Figures 1.12 and 1.13: Models of (a) cylindrical, (b) stepped, (c) v-thread, (d) rectangular threaded, (e) tapered body of threaded implants, (f) implants with two thread sizes [13].

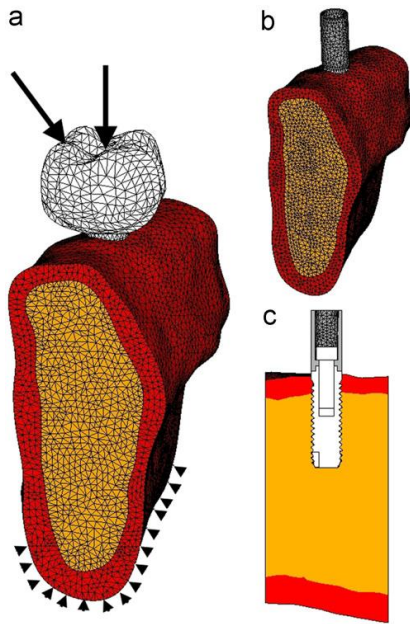


Figure 1.14: (a) Loading directions and fixed support, (b) isometric and (c) section views (from ref. [13]).

Based on Huang et al.'s [13] detailed analysis adding threads to the implant lowers the stresses on the bone significantly, rectangular threaded implants apply less stress on the trabecular bone than v-threads and surface roughness shows no clear advantage for the immediately loaded implants.

Chang et al. [14] estimated the stresses that occur in two commercial implant systems using three dimensional FEA. They made their analysis with three different variables: (i) bone level – tissue level implant, (ii) axial loading – angular loading, (iii) type 2 bone – type 4 bone. The difference between bone level and tissue level implants is the height of the implant relative to the bone surface. They used an axial 100 N compression force and a 100 N 30° oblique force. In their model, the type 2 bone had a 1.37 GPa Young's Modulus while the type 4 bone had 0.8 GPa.

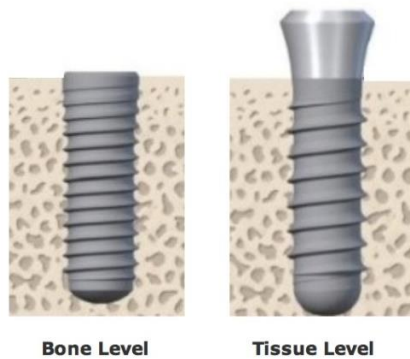


Figure 1.15: Bone level implant and tissue level implant [14].

They constructed 3D models for the maxillary second premolar tooth in the Solidworks software and performed the FEA with Abaqus 6.9. Their bone model was simple cubic with 10 mm x 10 mm x 20 mm dimensions. The thickness of the cortical bone in type 2 and type 4 bones was 2 mm and 1 mm, respectively. The cortical bone element size was 1 mm while all other parts' element size was 0.4 mm.

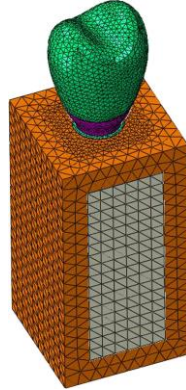


Figure 1.16: Mesh and node demonstration of the 3D model [14].

Based on Chang et al.'s [14] results, different designs of implants can be effective for different conditions. For example, the Straumann tissue level implant system yielded better results than other systems for the type 4 bone. Overall, they showed that bone level implants offered better results than tissue level implants.

Table 4 Maximum von Mises stress (MPa) in different components of NobelBiocare models in different bone qualities and different loading angles.

Products	NobelBiocare							
	Type II				Type IV			
	Active		MK III		Active		MK III	
Loading angle	0°	30°	0°	30°	0°	30°	0°	30°
Crown	7.8686	113.4610	6.8723	70.1333	7.5512	84.5432	6.9873	70.2599
Abutment	13.3162	245.4520	26.7876	662.3030	13.8777	274.2010	28.3132	583.5320
Screw	9.6096	90.1041	16.1044	200.1940	12.1696	123.0210	18.1549	253.4690
Implant	15.1580	283.7150	14.1403	312.7180	23.6874	254.6440	16.7891	463.4930
Cortex	6.0839	66.5107	7.6799	97.0723	2.3523	20.9631	3.0124	20.6457
Cancellous	1.9425	5.0874	0.9989	3.9715	2.5809	7.9157	1.8429	8.2781

Table 5 Maximum von Mises stress (MPa) in different components of Straumann models in different bone qualities and different loading angles.

Products	Straumann							
	Type II				Type IV			
	Bone level		Tissue level		Bone level		Tissue level	
Loading angle	0°	30°	0°	30°	0°	30°	0°	30°
Crown	6.4455	80.7191	16.0696	253.2560	16.1588	73.6771	22.4397	234.1630
Abutment	12.6970	247.4260	85.4391	1203.0400	16.6552	359.1300	25.8439	382.8440
Screw	10.3743	96.3107	15.9071	210.7840	10.5059	116.1950	12.1518	181.6970
Implant	11.8742	234.5430	14.4268	339.8240	33.4159	240.8820	18.1096	374.1600
Cortex	8.7094	57.5333	7.6921	94.2295	33.8099	61.1688	11.2280	104.4830
Cancellous	0.7962	3.4723	1.3093	3.7415	1.0002	4.0189	1.2033	4.9687

Figures 1.17 and 1.18: Results of NobelBiocare and Straumann [14].

Ao et al. [15] tried to optimize design of an immediately loaded implant by altering the implant thread height and width. Their thread height was between 0.2 and 0.6 mm and their thread width varied between 0.1 and 0.4 mm.

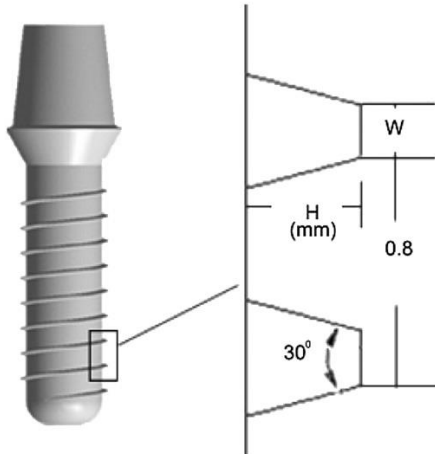


Figure 1.19: Implant thread height and width [15].

The reference model for implant optimization was the ITI brand cylindrical screwed implant and abutment 3.5 mm in height, which were merged as a united object. Mandibular first molar tooth was described for the restored crown via a structure-light scanning technique. They built their model in Pro/E software and analyzed the FEM in ANSYS Workbench 10.0. All materials were defined as isotropic, homogeneous and linear elastic. The contact between the bone and implant was frictional with a 0.3 friction coefficient. Mesh model was constructed with tetrahedron and hexahedron elements. It consisted of 220,000 elements and 310,000 nodes on average. 100 N axial compression and 30 N 45° oblique buccolingual loadings were applied separately.

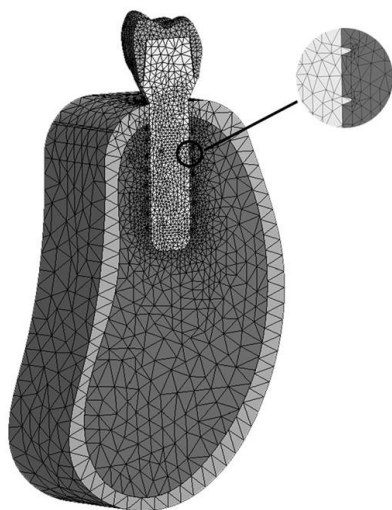


Figure 1.20: Mesh model of the implant system [15].

With different height and width values, nine models were constructed and analyzed with FEM. The results were imported to the DesignXplorer module of ANSYS Workbench. Response curves and sensitivity analysis we also done for optimal thread height and width. Sensitivity analysis shows that effectiveness of dimensions in a result; for example, a section is sensitivity analysis of maximum equivalent stress in cortical bone under axial load.

H (mm)	W (mm)	Max EQV stress in cortical bone		Max EQV stress in cancellous bone		Max displacement in implant-abutment complex	
		AX load	BL load	AX load	BL load	AX load	BL load
1	0.20	7.3225	22.652	7.8172	3.2414	0.0044796	0.0097512
2	0.20	6.5243	21.658	9.6399	3.0916	0.0044885	0.0097344
3	0.20	6.4021	21.545	7.2231	4.1950	0.0044943	0.0097108
4	0.40	6.4021	6.2955	6.5688	3.5250	0.0041196	0.0094550
5	0.40	6.6504	20.952	8.6461	4.0459	0.0041084	0.0094085
6	0.40	6.5130	20.930	8.2471	5.5875	0.0041253	0.0093637
7	0.60	6.2424	19.450	7.6951	2.3022	0.0039048	0.0092146
8	0.60	5.9432	18.941	5.3215	2.1606	0.0038815	0.0091437
9	0.60	6.0824	19.433	5.4455	3.4486	0.0038808	0.0090733

Figure 1.21: Different height and width values and their results [15].

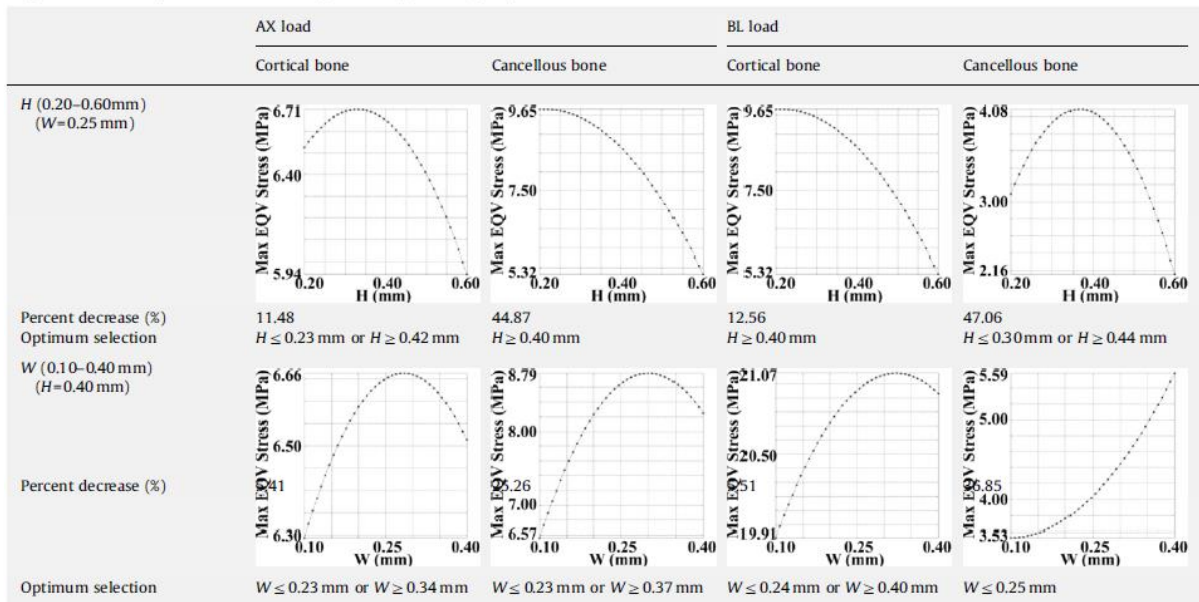


Figure 1.22: Response curve analysis for jaw bone stresses [15].

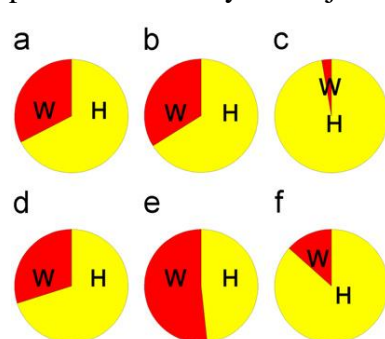


Figure 1.23: Sensitivity analysis, H=Height – W=Width [15].

In Figure 1.21, the effectiveness of parameter changes is shown. For example, height is more effective than width for cortical bone equivalent stress under axial loading in a section. As a conclusion, this study [15] shows that thread height change is more effective than thread width in terms of bone stresses and height values bigger than 0.44 mm and width values between 0.19 mm and 0.23 mm are optimal values.

Based on the information inferred from literature search, the following parameters were selected for implant design in this project:

1. Mandibular first molar tooth as the base tooth.

Zadik et al. [6] stated that molar teeth of human are exposed to very high forces during mastication and this tooth was selected because it is the most common extracted tooth [6].

2. Type 2 bone structure.

According to the work of Lekholm et al. [7], the bone type of the mandibular first molar is type 2 and it is the most powerful bone type structure.

3. Square thread.

Huang et al. [13] reported that this thread type causes lower stresses on the bone structures.

4. Tapered implant body.

Huang et al. [13] suggested this geometry to be more appropriate to the real root shape of the missing tooth.

5. 100 N axial static loading.

Parkhe et al. [9] selected this value for comparison with the literature and this load is also the average of mastication force that human jaw applies.

6. Friction coefficients: 0.3 and 0.5.

Parkhe et al. [9] employed these values for friction coefficients between the bone and implant and between metallic implant parts.

7. Bone level implant geometry.

According to the study of Chang et al. [14], bone level implants are better than tissue levels for type 2. They create lower stresses than tissue level implants.

8. 0.2 mm edge length for implant thread and 0.5 mm thread pitch.

Ao et al.'s [15] analyses suggest these values for the thread profile design.

9. Internal conical abutment design.

This geometry was selected according to the study of Saidin et al. [16]. It is not the perfect abutment type but it is the most basic one.

10. The maximum acceptable stress values, for the cortical bone: 130 MPa, for the trabecular bone: 20 MPa, and for the implant: 825 MPa.

These values were based on the studies of Frost [8] and Niinomi [17].

Most modeling work in literature employed 3D FEM, but such models are too costly in computer time. This project will show that a proper 2D FEM can yield the same results as those from a 3D FEM at a much shorter time.

1.4 Distribution of Tasks and the Gantt Chart

Two students worked in this project. Gani Melik Önder was mainly responsible for literature search and developing CAD models of the implant systems using the Siemens NX software. Veysel Mert Usta contributed to literature search but was mainly responsible for the FEA using the ANSYS Workbench software. In Figure 1.24, the Gantt chart shows the project steps and their duration time in weeks.

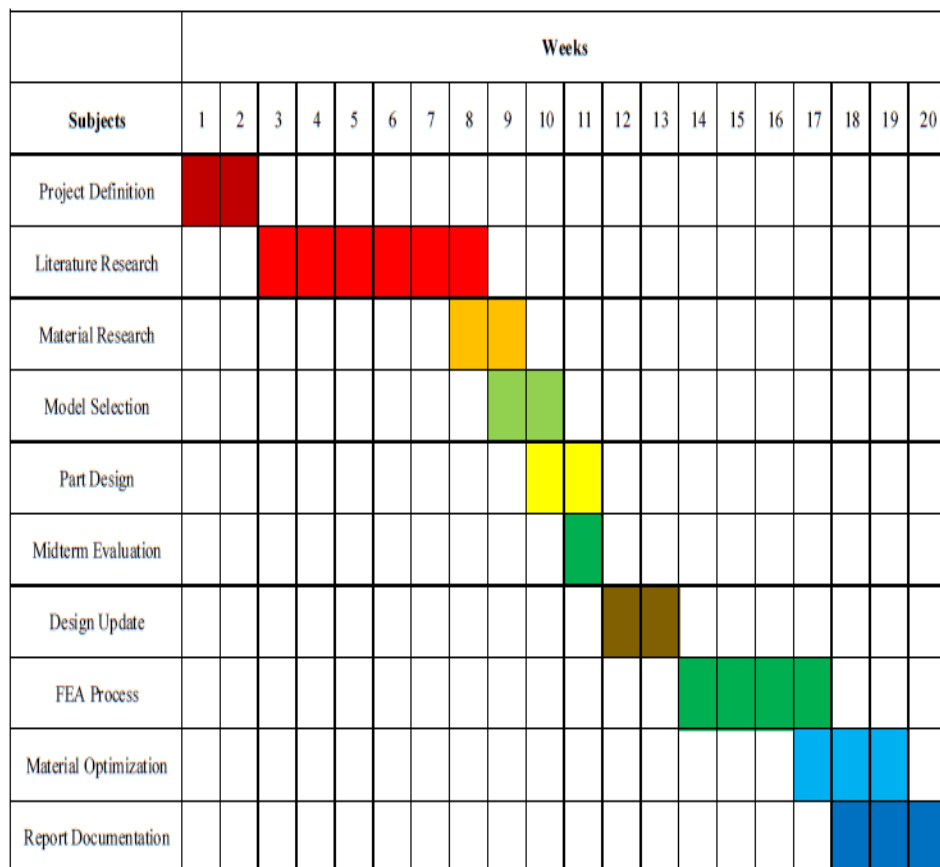


Figure 1.24: Gantt chart.

2. DESIGN OPTIONS AND SELECTION CRITERIA

In modern implant designs, companies update their implants based on feedback from patients and dentists. Failures of implant systems are the most important feedback for companies. To overcome these failures, they must be investigated using an engineering approach. This way, reasons that cause failures can be converted to more beneficial information.

One of the common failures for implants is bone resorption caused by micro cracks. Bone resorption increases with age and increasing bone stresses. One aim of this project is to reduce stresses on the jaw bone by a new design and new materials.

2.1 Design Iteration and Advantages of the New Design

Implant systems consist of mainly three parts. These are the crown, abutment and implant (Figure 2.1). Materials of all parts must be bio-compatible. Mostly, the implant and abutment are made of metal while the crown is ceramic. The implant part has the biggest contact area with the jaw bone, thus the study of the design and material of the implant is more important than the others. Design of the implant is mainly about the body and thread shape. Based on literature search, the body and thread shapes were selected as a tapered root-like body and a square thread, respectively (Figure 2.2). The general and section views of the 3D implant model employed in this project are shown in Figures 2.3 and 2.4, respectively.

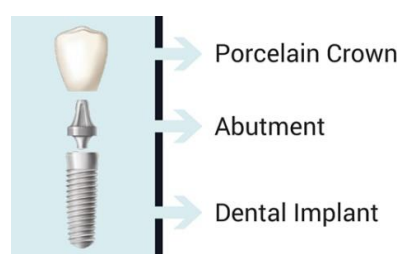


Figure 2.1: Basic implant parts.

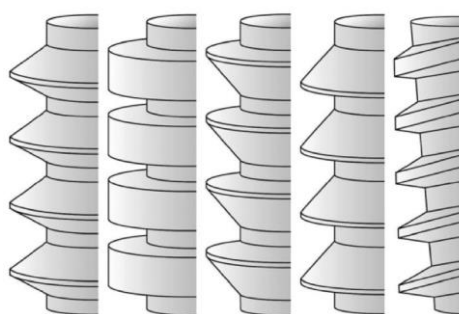


Figure 2.2: Thread types.

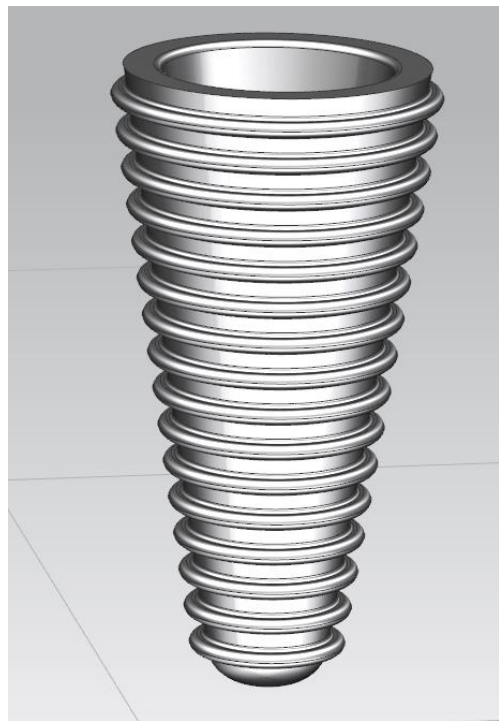


Figure 2.3: 3D model of the new implant design.

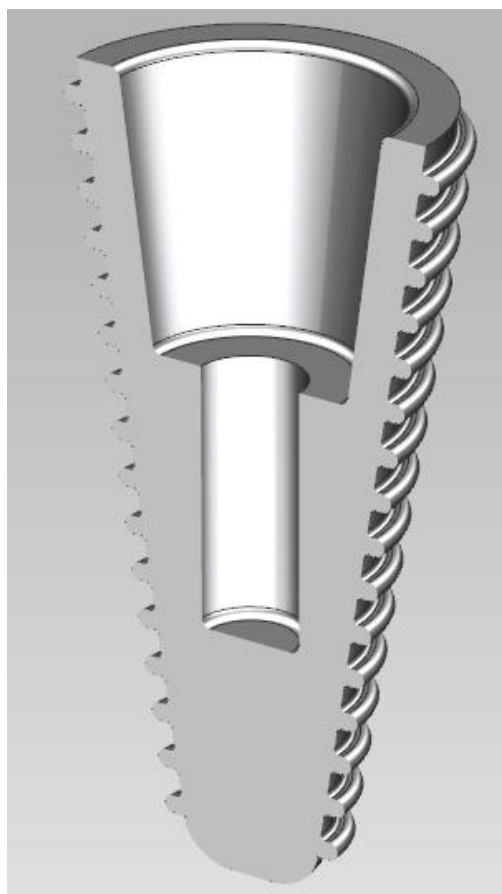


Figure 2.4: Section view of the new implant design.

Other parts of implant systems are selected as simplest form of their version. Also, retainer screw has not threads because it has no effect to the bone stresses. It will be proven by the analysis. Figures 2.5 and 2.6 are section views of bone structure and all assembled structure.

In the modern implant systems, titanium alloys are used as an implant material due to “osseointegration”. Osseointegration means reproducing of bone cells over and limitedly through the implant surfaces. Ti-6Al-4V is the common implant material but its drawback is high Young's modulus. In this project, different bio-compatible titanium alloys that have lower Young's modulus relatively Ti-6Al-4V. Reducement of bone stresses are expected when relatively low Young's modulus values. This hypothesis will be analyzed with FEA.

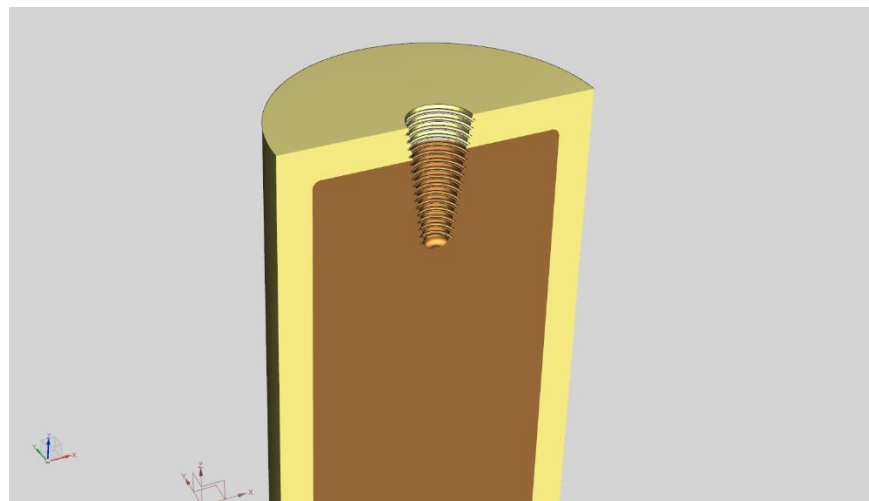


Figure 2.5: 3D model of the cortical and trabecular bone (Yellow: cortical, brown: trabecular).

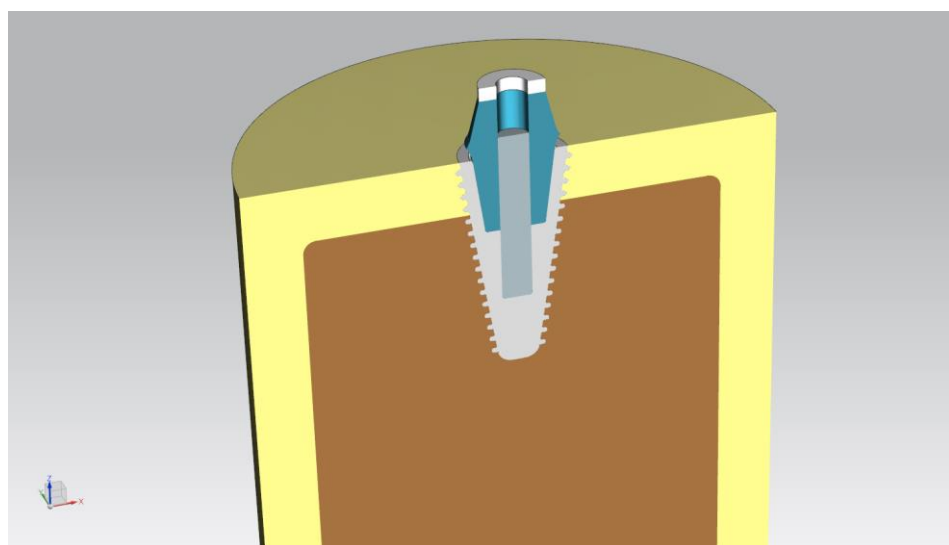


Figure 2.6: 3D model of all parts (White: crown force part, blue: abutment, gray: screw).

Bone structure is sketched with the inferred information from literature research. Its dimensions are 35 mm in height and 20 mm in diameter. Type 2 bone is accepted as a bone type so cortical thickness is 2 mm. In the Siemens NX, “Thread” tool is not specified for taper threads. To overcome this problem, section sketch of implant threads is drawn and revolved for uniting to the taper body. For tapered thread, “Variational Sweep” tool is used after “Helix”. It basically helix curve sweep of the thread section sketch. In this project, thread dimensions are selected to the literature research (Huang et al. [13]). Thread height is 0.3 mm and thread width is 0.2 mm. Pitch value of the helix that is used for “Variational Sweep” is 0.5 mm. Corner radii of the threads are 0.05 mm.

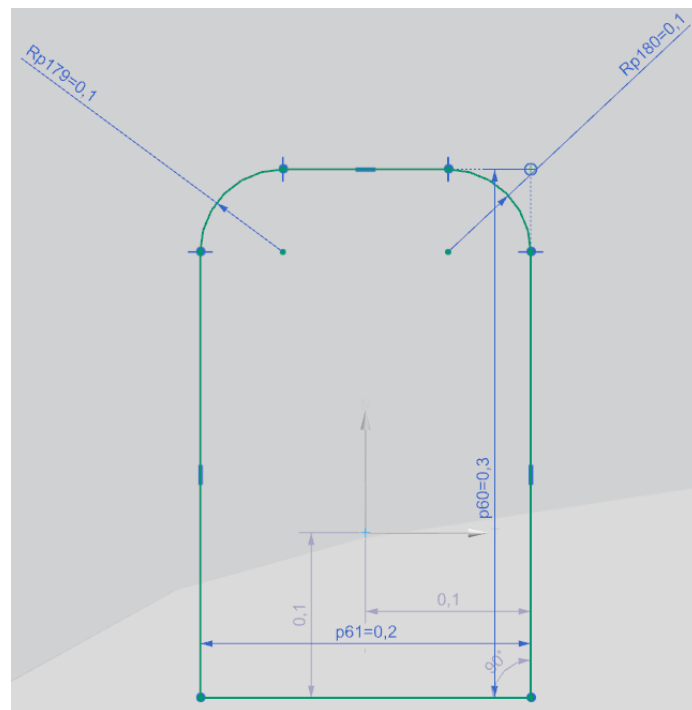
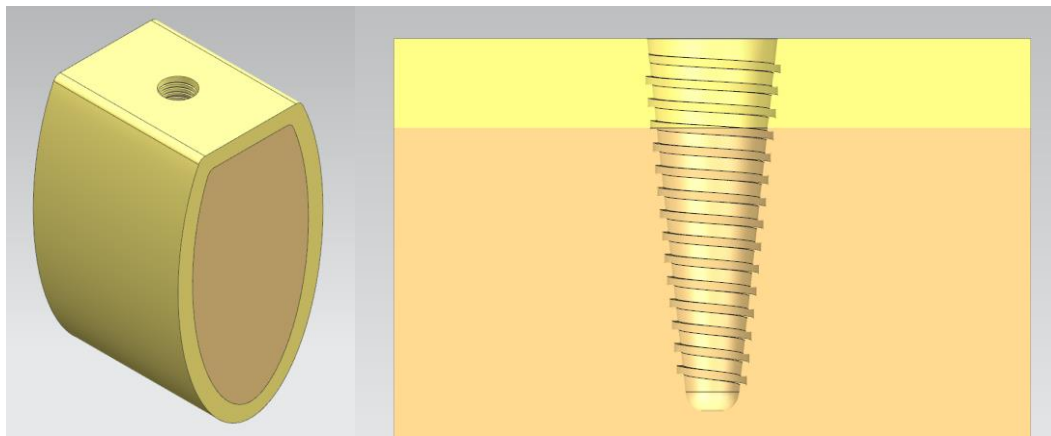


Figure 2.7: The thread profile employed in this project. Radius: 0.05mm



Figure 2.8: Tapered helix threads.

For 2D sketches, it is impossible to build a model with tapered helix thread. Therefore, only tapered thread with same thread profile is used for 2D. 3D section view is used for creating sketches of 2D via “Section Sketch” tool. For 2D analysis, bone model is analyzed for a cylinder part due to axial symmetry. Although 3D model is already created, another 3D model for cylindrical analysis is created for meaningful comparison via “Revolve” tool.



Figures 2.9 and 2.10: Real bone structure and tapered helix thread tap.

After getting the section sketches, “Bounded Plane” tool is used for creating surfaces. There is a white ceramic material for representing the crown. Force is applied to top face of ceramic. Modelling a real crown is costly in time and hardware. Our computer capacity is not enough for computing analysis with real crown so ceramic material is used for simplification.

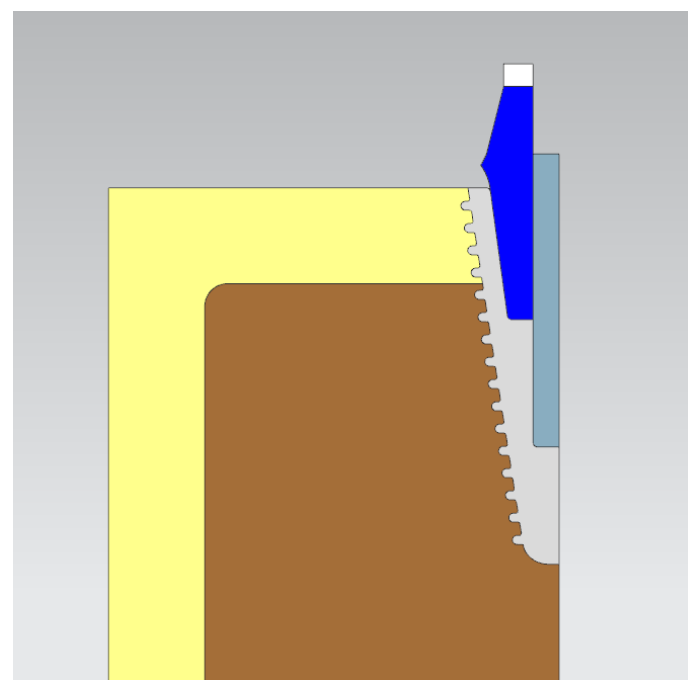


Figure 2.11: 2D model of all parts.

3. DESIGN OF AN IMPLANT SYSTEM VIA FINITE ELEMENT ANALYSIS

3.1 Introduction to ANSYS Workbench

ANSYS Workbench is a commercial simulation platform for almost all engineering projects. The interface is very user friendly. In this project, the Workbench 16.2 was used. Its toolbox consists of several analysis systems such as buckling analysis, harmonic response analysis, modal analysis, electric analysis, IC engine analysis, shape optimization, static structural analysis, thermal analysis, etc. Within the scope of this project, static structural analysis was used. In addition, there are no temperature changes, flow of a fluid, electrical or magnetic fields in the models of the project.

3.2 Project Schematic

Project schematic is kind of a white board. Different types of analysis systems can be shown as blocks by dragging them into the page from a toolbox.

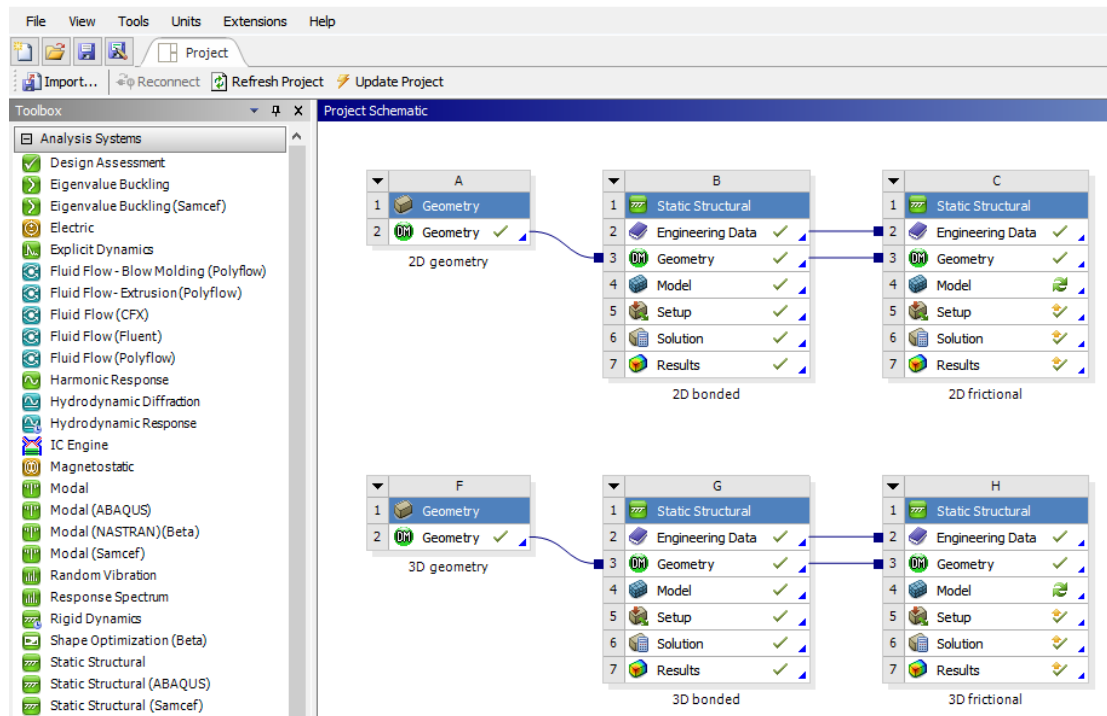


Figure 3.1: Workbench project schematic page.

Here is a presentation of this project's project schematic page in ANSYS Workbench (Figure 3.1). The blocks are linked to each other. Each link carries the information from preceding to subsequent. It provides efficiency in terms of time and accuracy, as new data input is not needed. So it is understood from the project schematic that the “2D bonded” block’s engineering data are carried to the “2D frictional” block and the “2D geometry” is same in the “2D bonded” and “2D frictional” blocks. Hence, false geometry and engineering data information are forestalled by linking the blocks.

Furthermore, in project schematic the “refresh” operation can be performed without opening the static structural. But linking the preceding geometry to the next block will cancel the current setting of the analysis and will require the user to “update” to solve it again. To overcome this problem, initially the first block analysis is solved and then duplicated. By doing so, the user prevents the very time consuming meshing operation. Duplication holds the preceding information until any change is applied to it.

When there is a geometry change, Workbench deletes the connections between parts in the geometry and the mesh because meshing is applied onto the geometry. So if there is no need to change the geometry for the next analysis, duplicating the preceding analysis will save huge time.

3.3 Geometry

The Geometry box is under the title of Component Systems in the Toolbox. Similarly, it can be dragged into the Project Schematic. By default, it captures 3D geometries but it can be adjusted to the 2D. Although Workbench has its own drawing option named Design Modeler in the Geometry box, importing external files is also possible. The main geometry files compatible with Workbench Geometry are: *.step*, *.sldprt* - Solidworks, *.x_t* - Parasolid, *.prt* - NX, *.catpart* - Catia and *.dwg* – AutoCAD. Since Design Modeler is not user friendly importing external files are so common. In this project, the Siemens NX software was used to draw the model geometry.

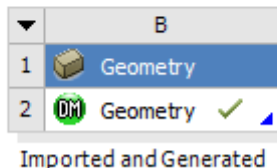
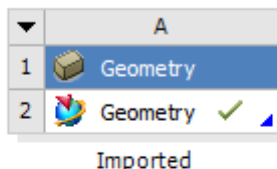


Figure 3.2: Geometry blocks on the project schematic page. Upper one is not ‘exploded’ and the latter is ‘exploded’.

The first geometry image represents the NX and the second image represents Design Modeler (Figure 3.2). After importing the NX file, it is generated in the Design Modeler and a second file is made compatible with the Workbench. The analysis can also be performed with the NX files. If it is not generated, the bodies within it are formed into one part by default. This effects the meshing. In formed geometries, a mesh element’s nodes are connected to other element’s nodes. In the static structural analysis, if there should be relative motion between parts, this may be problem. Because connected nodes inhibit the relative motion of two mesh elements. For many CFD analyses this may not be a problem as there may not be relative motion between solid parts but there may be some between solids and fluids. But in most of static structural analysis, if there is an assembly, parts move separately, and are not fixed to each other unless it is desired. To overcome this connected nodes issue, NX part must be ‘exploded’ in the Design Modeler into multiple parts as shown in the Figure 3.3.

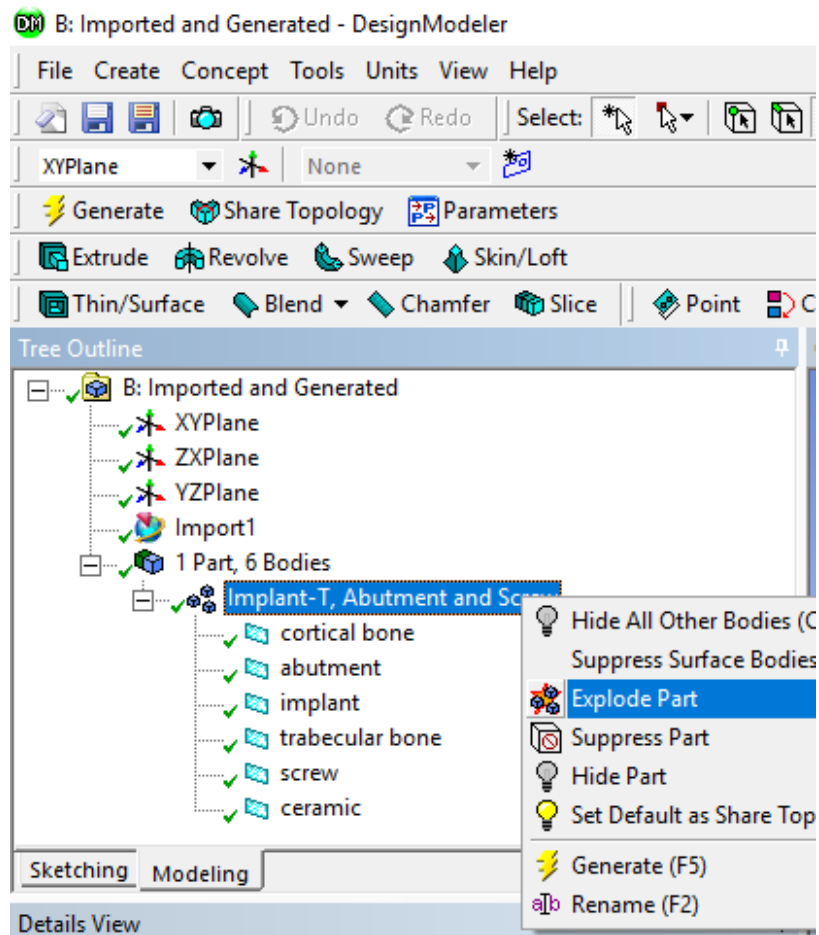


Figure 3.3: ‘Exploding’ the parts in Design Modeler.

In the ‘unexploded’ geometry meshing, it can be clearly seen that the two adjacent mesh element’s nodes are shared. When a force is applied to this part, they move together without sliding as if the two parts are bonded even if they are not. In the bonded contact case, these shared nodes do not create a problem since there is no relative motion between parts. But in the frictional contact case, the two parts must move separately because they are different materials. Their Young’s moduli are different and so is their deformation ability. In the frictional case, the fast moving element tends to deform more than the slow moving element. However, the shared nodes (Figure 3.4) do not allow the relative motion and restrict the fast ones. This effect leads to high stress concentrations in undesired locations. Also, this shared node phenomenon does not exist in nature and real life.

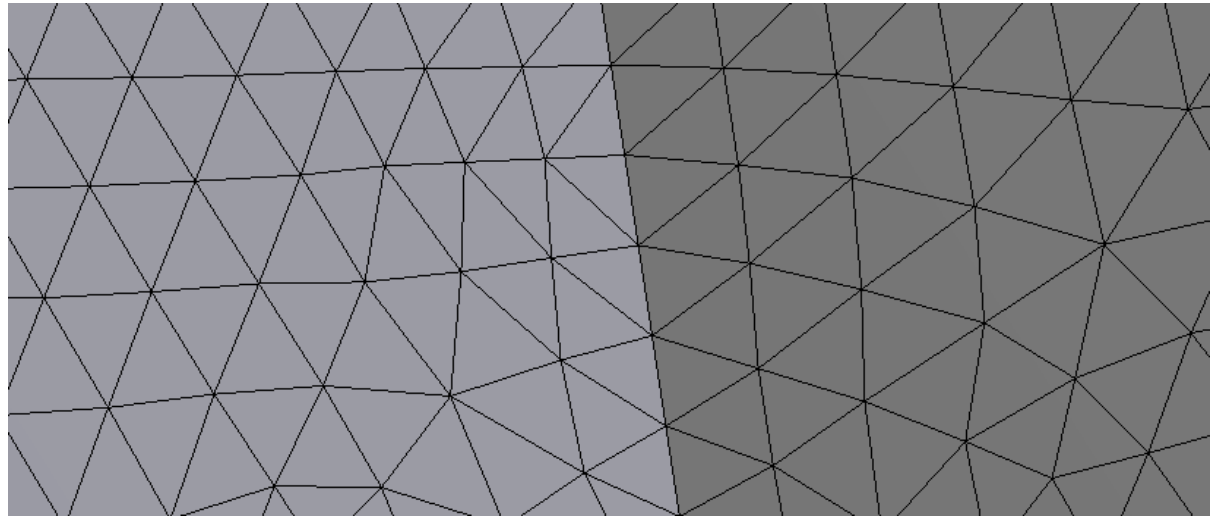


Figure 3.4: Unexploded part meshing.

In the exploded geometry meshing, the two adjacent mesh element's nodes are not shared but separated as can be seen in Figure 3.5 below. In the bonded case, the nodes are not shared but fixed. Similarly, the nodes are not shared but the elements move together. As it was stated before, independent nodes have no meaning in the bonded case. In the frictional case, because of their different deformation abilities, different parts with different materials move relative to each other and with the explosion of the parts, they can freely move. The nodes do not restrict other nodes' movement. In addition, this mimics the real life.

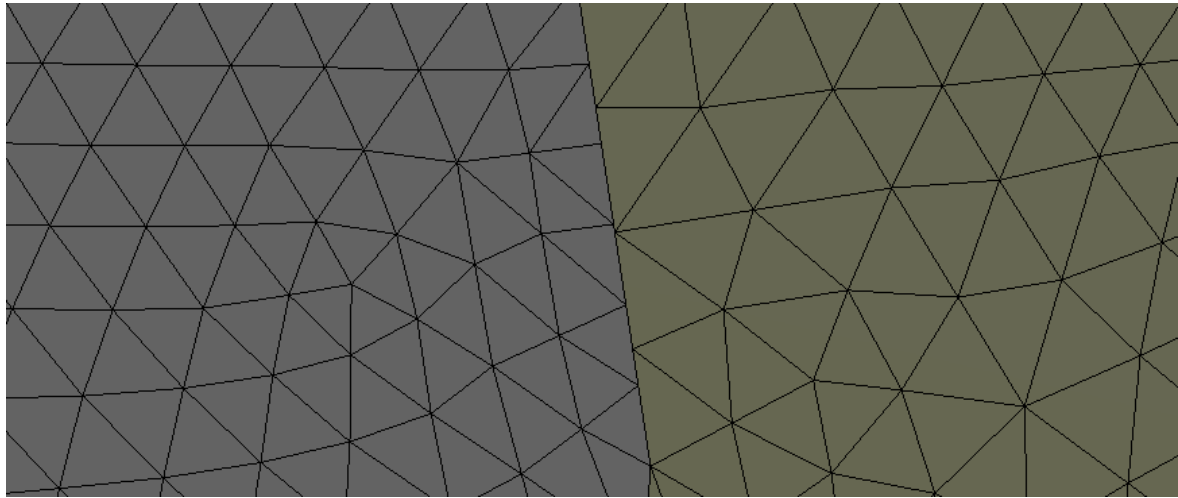
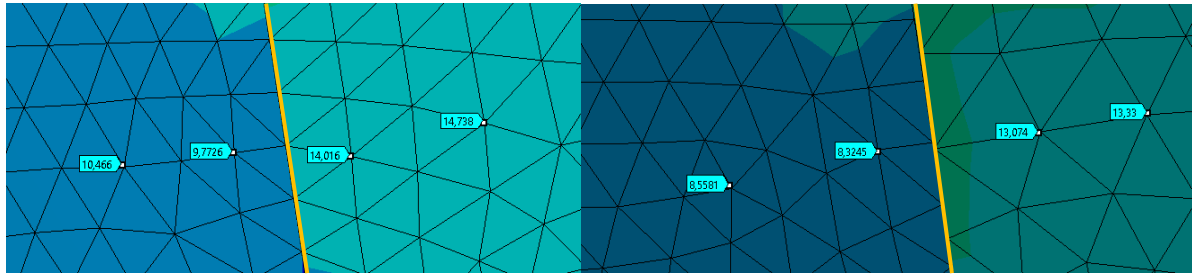


Figure 3.5: Exploded part meshing.

For just a brief comparison of the two images, it would be good to examine the results.



Figures 3.6 and 3.7: Unexploded-part stresses (left) vs. exploded-part stresses.

The left one (Figure 3.6) is not exploded, and the right one (Figure 3.7) is exploded. The von-Mises stress levels on the contact surfaces in middle (represented with yellow bars) are approximately 12.2 MPa at the left and 10.75 MPa at the right. This result shows that the poorly created models may lead to 20% more stress levels.

3.4 Static Structural

Static structural analysis is used to obtain displacements, stresses, forces and strains for the designed structures upon applied loading. The analysis can be both linear or nonlinear. In real life, most of the experiments and structures are nonlinear, only few of them can be modeled as linear. Linear analysis can be solved directly because its force-displacement curve (Figure 3.8) is well known and predictable by the ANSYS mechanical solver.

Linear static analysis operates under the equation of:

$$\mathbf{F} = \mathbf{K} \times \mathbf{x}$$

Where;

K Stiffness,

x Displacement,

F Force.

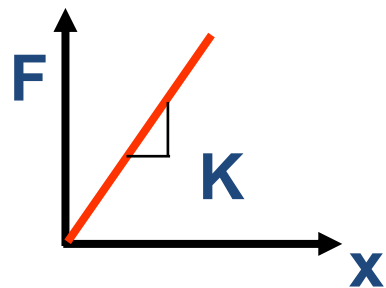


Figure 3.8: Force-displacement curve for a linear analysis.

Here, the stiffness K is assumed to be constant and the force-displacement curve is linear. But this equation is just an assumption, not the real case. However, this project is conducted under the nonlinear analysis. There are three main sources of nonlinearity: geometric, material-based and contact-based.

Geometric nonlinearities occur if there are huge deformations like in a fishing rod. In this project, there is no such big deformation. Material-based nonlinearities occur as materials experience nonlinear deformation.

Contact-based nonlinearities occur as there is no perfectly bonded interface between parts. The stiffness changes abruptly from a contacted zone to an uncontacted one. Also, the friction coefficient adds nonlinearity because a minimum relative sliding between parts may lead to change of the sign of frictional forces. Nonlinear analysis cannot be solved directly as the stiffness is dependent on displacement (Figure 3.9). The mechanical solver can only solve the model iteratively to converge the solution.

Nonlinear static analysis is based on the equation of:

$$\mathbf{F} = \mathbf{K}(x) \times \mathbf{x}$$

Where;

$\mathbf{K}(x)$ Stiffness – displacement dependent,

x Displacement,

\mathbf{F} Force.

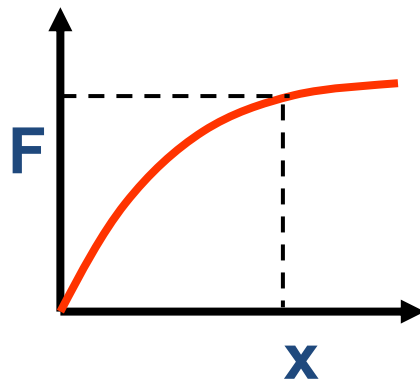


Figure 3.9: Force-displacement curve for a nonlinear analysis.

3.5 Engineering Data

Workbench requires a material property to give a stress or displacement result. The most vital part of the project is to set the proper material data in order to obtain accurate results. For example, ANSYS does not calculate the basic equation of safety factor if the user does not add the strength of material that assigned to the parts. Moreover, ANSYS does not solve the model and does not give the stress, strain or deformation results unless isotropic elasticity data is added.

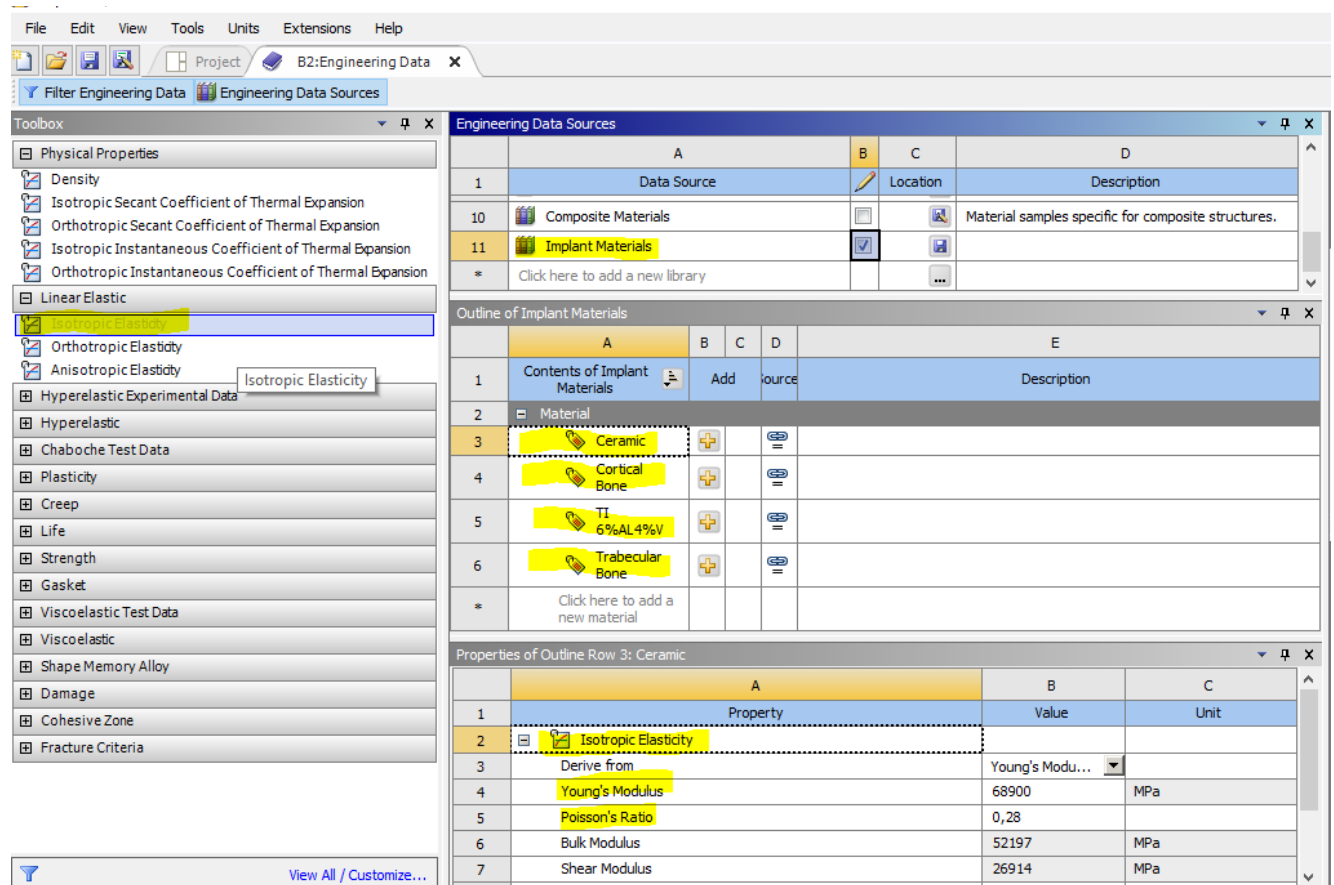


Figure 3.10: Workbench engineering data page.

Figure 3.10 shows the “Engineering Data” interface in Workbench. The toolbox on the left contains various material data. The user either can create a completely new material by selecting proper properties like strength, creep or plasticity from the toolbox or can select the predefined ones from the “Data Source”. In this project, the materials used did not exist in the “Engineering Data Source” of ANSYS. Therefore, the project materials were added as “Implant Materials” to the library. The only needed property is isotropic elasticity to solve the model and get the

results. Isotropic elasticity includes Young's modulus, Poisson's ratio, bulk modulus and shear modulus. Young's modulus and Poisson's ratio were determined from literature, while the other ones are derived and calculated by ANSYS itself.

3.6 Geometry – 2D

The 2D model consists of exploded parts which are crown, abutment, implant, screw, cortical bone and trabecular bone (Figures 3.17-3.18). The parts were imported from the NX software to the Workbench Design Modeler and then generated. After generation, parts were exploded into individual parts to separate the mesh nodes between the mesh elements of the parts.

Axisymmetric 2D behavior was selected for the geometry to represent the 360° geometry with graphical expansion with symmetry. The aim of this is to make a comparison with the real 3D model. In order to select the axisymmetric behavior, the geometry should locate on the positive (+) side of the XY plane. Axisymmetry forms around the Y axis and its normal vector is the X axis. Crown is modeled as a small rectangle for simplicity and smooth force distribution. Force was conveyed first to the abutment, as same as real life, and then next to the implant. The screw was modeled as non-threaded, again for simplicity. In real life, the screw must be threaded in order to retain the abutment and implant and tighten them into each other. In fact, a 2D analysis can solve the model with a threaded screw. But a 3D analysis cannot solve it easily because threads of the screw are very small in size and the program must use smaller mesh elements to capture this small region. Smaller mesh elements lead to high number of elements and element nodes. The smaller mesh elements and the high quantity of the element nodes affect the meshing and solution times negatively. Most importantly, the stress values on the cortical and trabecular bone, which are the scope of this project, do not change so much from a threaded screw to a non-threaded screw in 2D.

As a first experiment, the 2D screw was modeled with threads (Figure 3.12) and the second experiment was modeled with a 2D non-threaded screw (Figure 3.11). The other boundary and loading conditions were the same. The outcome shows that there is no difference between the models. The stresses on the cortical bone are 14 MPa for both two models (Figures 3.13-3.14). The stresses on the trabecular bone are 5.3 MPa in both two models (Figures 3.15-3.16) which proves that there is no need to the screw threads while modeling the experiment. Also, there is no stress distribution difference between the models.

The 2D screw thread analysis results are shown below:

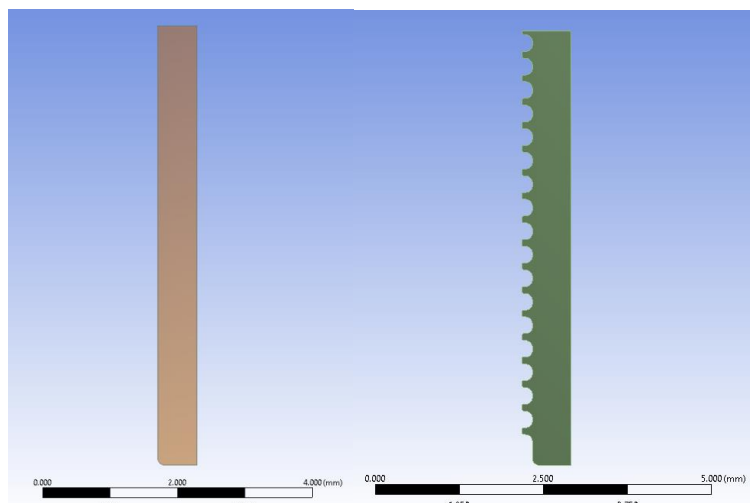


Figure 3.11 and 3.12: Non-threaded screw (left) and threaded screw.

Stress on the cortical bones:

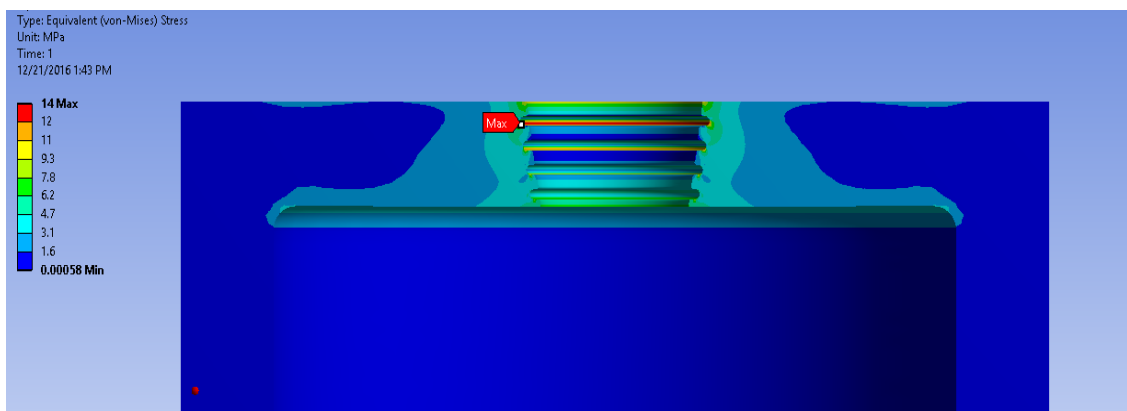


Figure 3.13: The stresses on the cortical bone with screw threads. Max. value is 14 MPa while the strength of the cortical bone is 130 MPa.

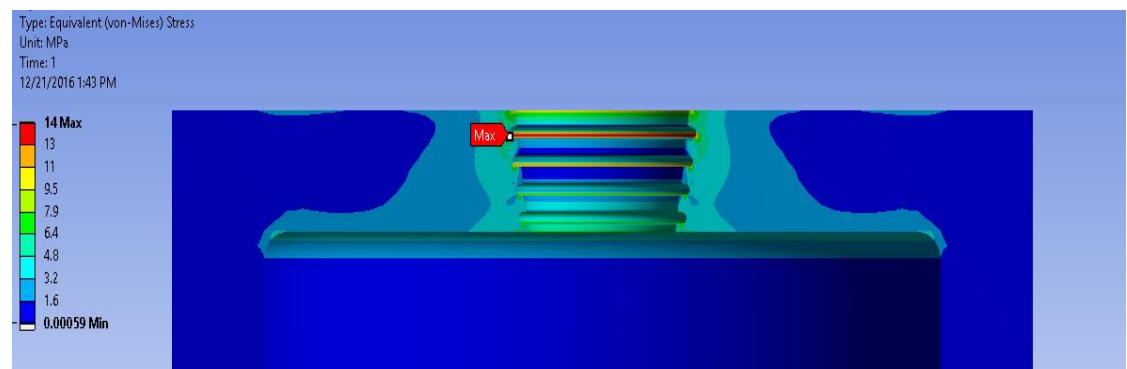


Figure 3.14: The stresses on the cortical bone without screw threads. Max. value is 14 MPa while the strength of the cortical bone is 130 MPa.

Stress on the trabecular bones:

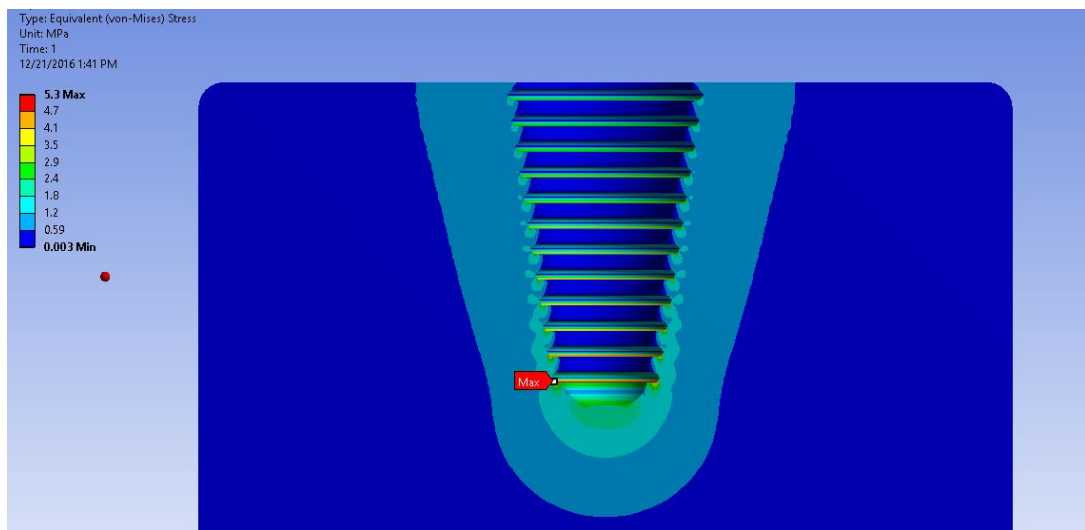


Figure 3.15: The stresses on the trabecular bone with screw threads. Max. value is 5.3 MPa while the strength of the trabecular bone is 20 MPa.

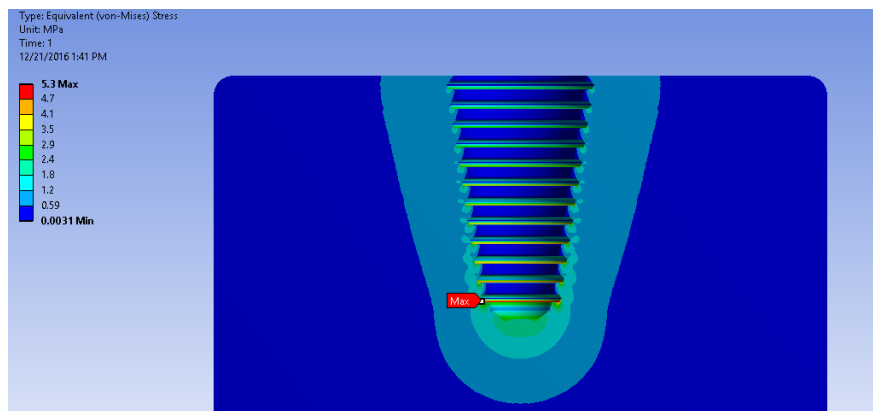


Figure 3.16: The stresses on the trabecular bone without screw threads. Max. value is 5.3 MPa while the strength of the trabecular bone is 20 MPa.

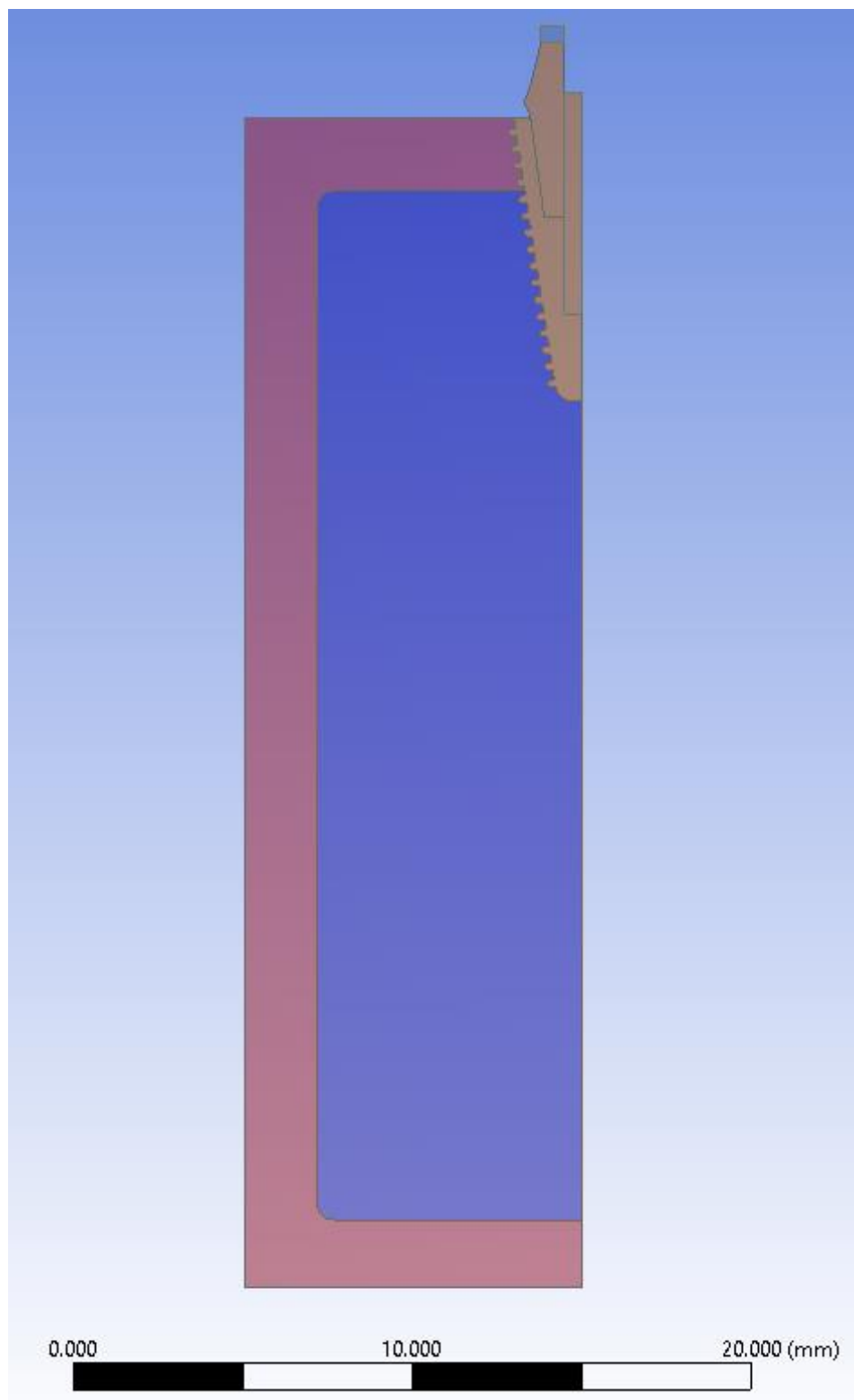


Figure 3.17: 2D surface bodies of the dental implant and bone models.

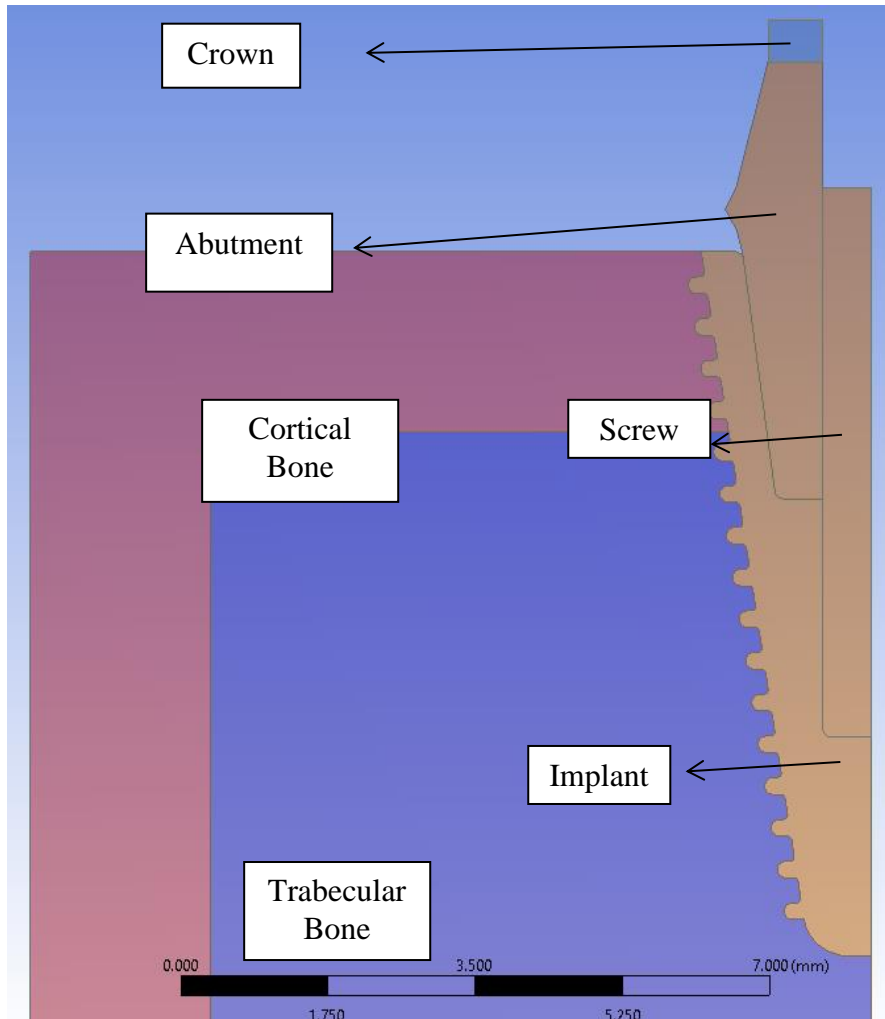


Figure 3.18: Zoomed view of the 2D surface bodies of the entire model.

3.7 Geometry – 3D

3D geometry was created with the NX software. It is nothing but the 360° rotation of the 2D sketch. After importing the NX part into the Design Modeler, it was exploded to separate the mesh nodes. It consists of 6 parts which are crown, abutment, implant, screw, cortical bone and trabecular bone (Figures 3.19 – 3.20).

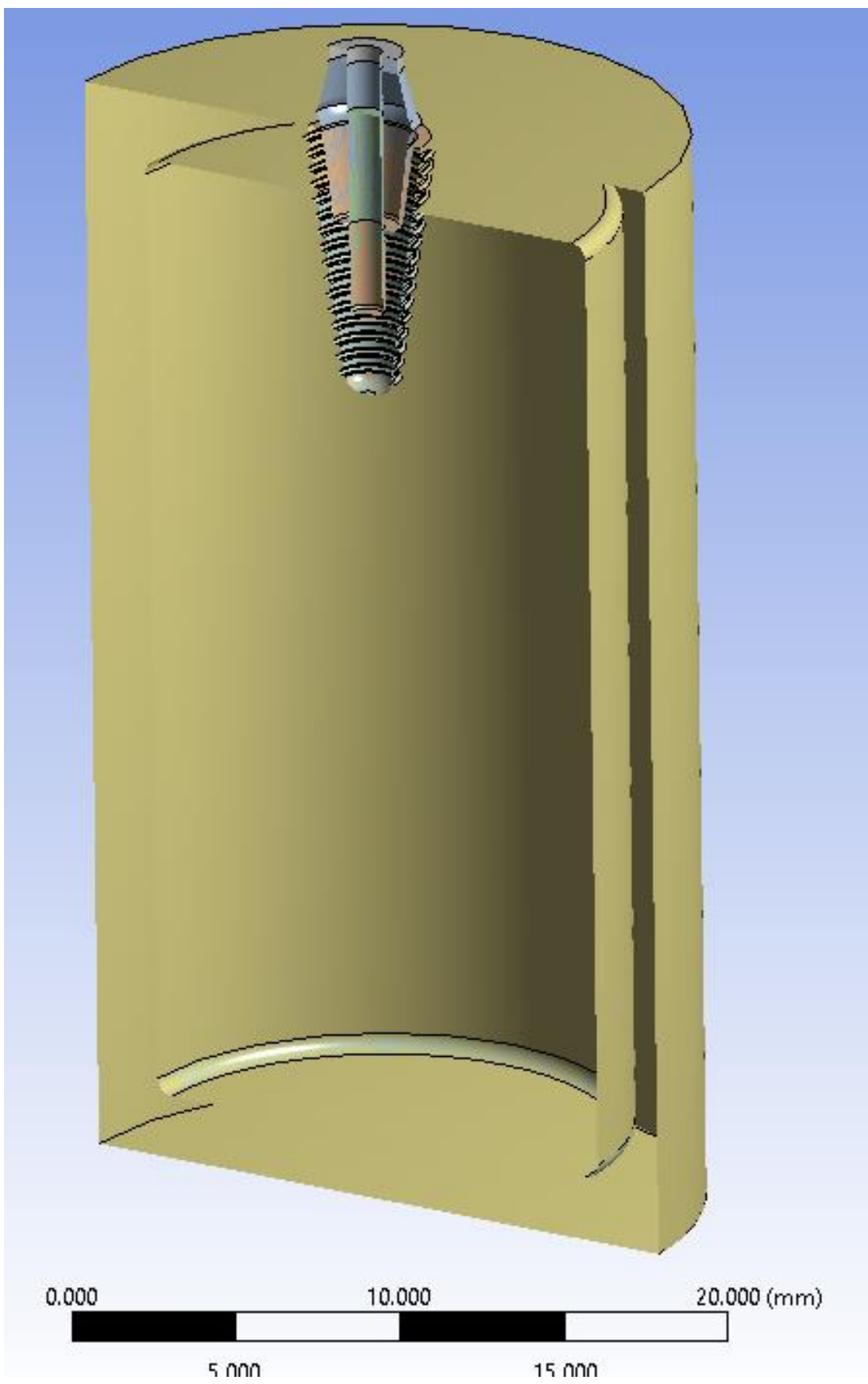


Figure 3.19: 3D section view of the model.

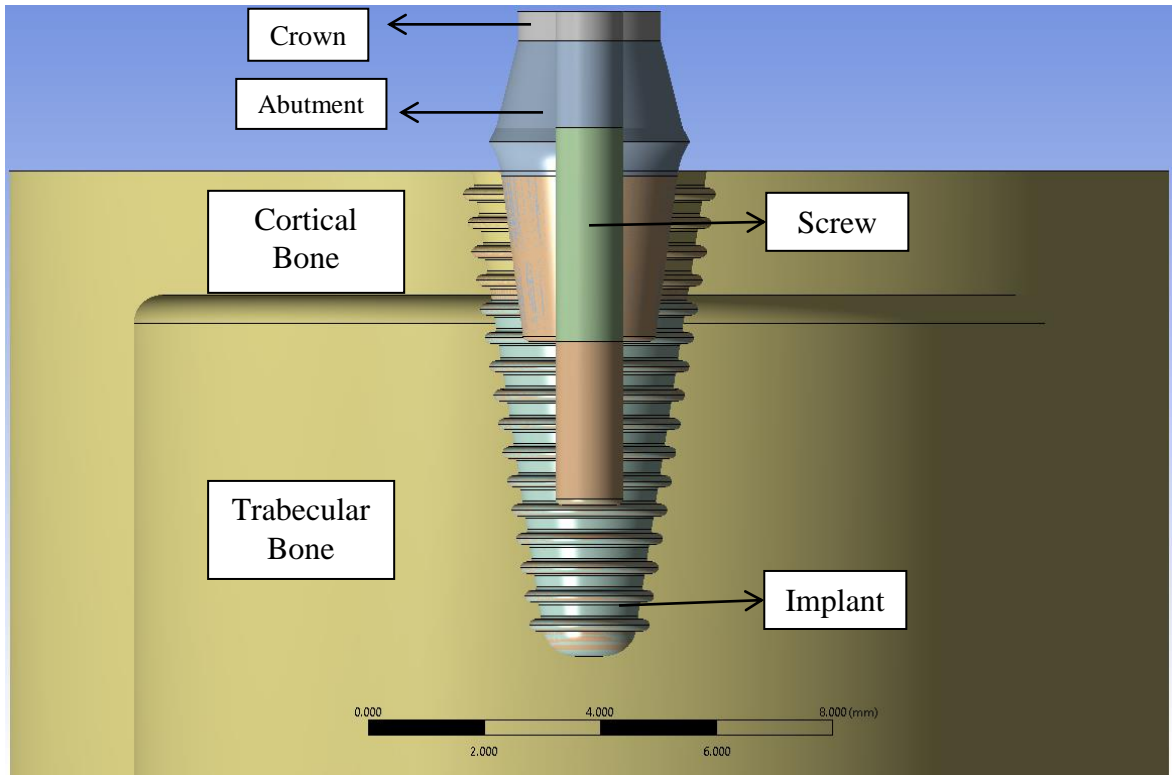


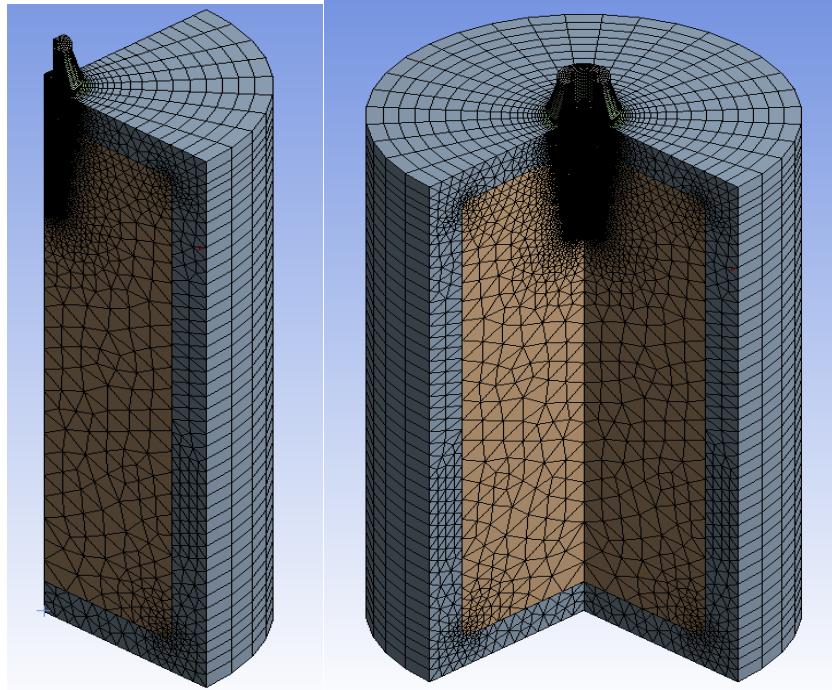
Figure 3.20: Parts of the 3D model.

3.8 Symmetry

In a 2D analysis, if the geometry is cylindrically symmetric in 3D like in shafts and hollow tubes, users can halve the real 3D model from the midsection of the geometry. So we now have a 180° model of the real model. Then halve it again from the middle of the geometry to obtain a 90° geometry. When this quarter part is looked at vertically to the surface, it represents the 2D and axisymmetric geometry sketch. If the real 3D geometry is exactly symmetric around its middle axis, the 2D sketch of its 3D 90° quarter part's normal view to the surface must be exactly the same. From this point of view, 3D analysis can be modeled in 2D to imitate the real model to reduce meshing and solving times. In this project, it was shown that the 2D and 3D analyses have nearly the same results.

Symmetry is used for graphical expansion in 2D analysis. To obtain 360° graphics of the 2D model, symmetry is preferred. It is just a turning the one 2D surface picture by 360 times around the global coordinate system. As mentioned before, the 2D geometry must be located on the positive side of the XY plane of the global coordinate system. The turning angle can be adjusted

from 1° to 360° . For example, the user can turn the 2D results by 10 times with 36° or 20 times with 18° to obtain the same graphic.



Figures 3.21 and 3.22: 90° (left) and 270° representations of the 2D surface.

Figure 3.21 was created by turning the 2D surface 9 times with 10° steps, while Figure 3.22 was created by turning it 27 times with 10° steps. They are just demonstrations or graphical expansion of the 2D sketch surface body to visualize the results more clearly.

3.9 Connections

In Static Structural there are five main types of contacts: bonded, no separation, frictionless, rough and frictional. Bonded contact does not allow separation, penetration and sliding between contact surfaces. No separation contact does not allow separation and penetration but allows frictionless sliding. Frictionless contact does not allow penetration but allows sliding and separation without resistance. Rough contact is similar to frictionless contact except sliding. This contact does not allow sliding. Frictionless contact allows sliding with resistance proportional to coefficient of friction defined by the user.

In this project, both frictional and bonded contacts were used. Bonded contacts are preferred when there is a full osseointegration because in this case the bone growth is completed over the

implant surface which has microgaps. Frictional contacts are preferred for the immediately loaded implants. In the practice, dental implants may be loaded with nearly no waiting for bone growth. In that case, due to the fact that the bone cells cannot grow into the microgaps or microcracks on the implant surface in such a small amount of time, the contact surfaces between the bone and the implant is accepted as frictional. Also the implant, abutment and screw interfaces are accepted as frictional because they are fixed with the help of the screw, and the screw cannot be fully bonded to its counterparts for disassembly. The bones are always bonded to each other anatomically. Lastly, the crown and the abutment interface is accepted as bonded because the connection is provided by gluing.

Workbench has several advanced contact formulation options which are:

1. Augmented Lagrange
2. Pure Penalty
3. MPC
4. Normal Lagrange

Normally contacts do not interpenetrate. To assure this, Workbench enforces contacts with different contact formulations. If the proper contact formulation is not used, too much interpenetration will occur and this reduces the accuracy of the solution. Augmented Lagrange and Pure Penalty are penalty-based methods. They are used for frictional contacts because they allow a little interpenetration. Because of that, in the frictional contact there is more deformation of the bodies and surfaces, some level of penetration should be allowed. Otherwise, solution convergence problems occur during the analysis.

Pure Penalty Equation:

$$F_{normal} = K_{normal} \times X_{penetration}$$

Augmented Lagrange Equation:

$$F_{normal} = K_{normal} \times X_{penetration} + \text{¥}$$

Where;

F_{normal} is contact force,

K_{normal} is contact stiffness

$X_{penetration}$ is resulting penetration.

¥ is an extra term.

This extra term ∇ leads to lower penetration without changing the contact stiffness. Since finding the real interpenetration of the dental implants and the bones is not possible, selecting the Augmented Lagrange method bypasses the changing of contact stiffness factor which is not clear. Although the high contact stiffness provides less penetration, it leads to convergence problems. For these reasons, the Augmented Lagrange method was used for frictional contacts in this project.

For a bonded case, there are two options: Normal Lagrange and MPC (multipoint constraint) (Figure 3.23). Normal Lagrange formulation adds an extra degree of freedom (contact pressure) to ensure the contact compatibility. F_{normal} is solved explicitly instead of an equation. But chattering may occur due to continuously changing contact status from open to closed as there may be very little penetration during the solution. MPC formulation uses neither compatibility equation nor extra degree of freedom but uses multipoint constraint equations to bond the nodes of the both contact and the target surfaces. This option gives precisely zero penetration for bonded conditions.

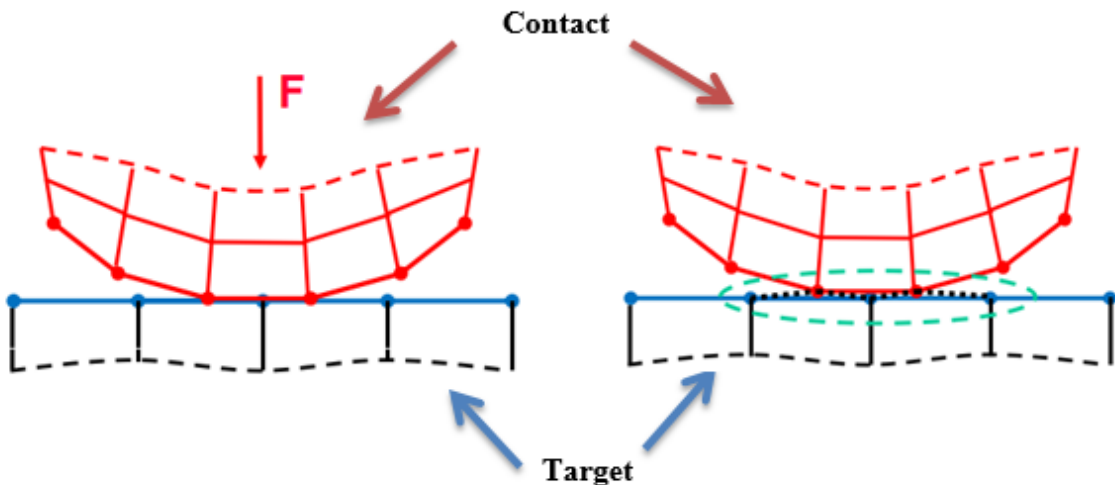


Figure 3.23: Normal Lagrange formulation on the left vs. MPC formulation on the right [46].

Normal Lagrange and MPC formulations may not capture the contact surfaces properly as they use nodal contact detection. But with a finer mesh, for instance with contact sizing meshing, nodal detection would be alleviated in a positive way over the integration point detection. To prevent chattering and convergence problems, MPC formulation was selected for the bonded contact conditions of the project.

Automatic contact stiffness update is selected as the contact surfaces are continuously changing during the analysis. Workbench updates the stiffness at every substep. This leads to long solving times but provides accuracy in terms of stresses.

To close the geometric gaps between the contact surfaces or bodies, “adjust to touch” interface treatment was used. Even if surfaces are drawn very cautiously there may still be very small geometric gaps like 7.1×10^{-17} mm which is negligible. But in order to be in the safe zone, contacts were adjusted to touch each other and the gap was accepted as 0. That means, there may still be a geometric gap but the contact adjustment makes the program understand that gaps are accepted as perfectly touched, with zero clearance. For example:

Name	Contact Side	Type	Status	Number Contacting	Penetration (mm)	Gap (mm)	Geometric Penetration (mm)	Geometric Gap (mm)	Resulting Pinball (mm)	Real Constant
Bonded - trabecular To cortical	Contact	Bonded	Closed	84.	0.	0.	3.5471e-005	3.5527e-015	9.6398e-002	7.
Bonded - trabecular To cortical	Target	Bonded	Inactive	N/A	N/A	N/A	N/A	N/A	N/A	8.
Frictional - trabecular To implant	Contact	Frictional	Closed	101.	9.3902e-015	0.	4.0205e-006	8.5183e-017	9.6398e-002	9.
Frictional - trabecular To implant	Target	Frictional	Closed	97.	7.2688e-015	0.	3.8162e-006	1.532e-017	9.6398e-002	10.
Frictional - cortical To implant	Contact	Frictional	Closed	31.	8.9229e-015	0.	3.2685e-006	7.1363e-017	9.6398e-002	11.
Frictional - cortical To implant	Target	Frictional	Closed	33.	7.7063e-015	0.	2.9266e-006	8.6381e-017	9.6398e-002	12.
Frictional - implant To abutment	Contact	Frictional	Closed	23.	3.4168e-015	0.	1.1412e-006	1.8955e-016	7.2878e-002	13.
Frictional - implant To abutment	Target	Frictional	Closed	25.	2.0139e-015	0.	1.1448e-006	2.2248e-016	7.6094e-002	14.
Frictional - implant To screw	Contact	Frictional	Closed	37.	7.322e-015	0.	2.0224e-006	4.4146e-017	9.6398e-002	15.
Frictional - implant To screw	Target	Frictional	Closed	38.	6.9323e-015	0.	2.0301e-006	1.5564e-017	9.6398e-002	16.
Frictional - abutment To screw	Contact	Frictional	Closed	41.	3.769e-017	0.	7.538e-017	7.069e-017	9.6398e-002	17.
Frictional - abutment To screw	Target	Frictional	Closed	41.	5.0912e-017	0.	1.0182e-016	3.769e-017	9.6398e-002	18.
Frictional - crown To abutment	Contact	Frictional	Closed	5.	3.2491e-015	0.	6.4982e-015	2.5374e-016	9.6398e-002	19.
Frictional - crown To abutment	Target	Frictional	Closed	4.	3.1337e-015	0.	6.2674e-015	2.0692e-016	9.6398e-002	20.

Figure 3.24: Initial contact information of the 2D frictional case.

The initial information of the contacts are shown in Figure 3.24. The highlighted row named “Frictional - cortical to implant” has an initially 8.6×10^{-17} mm geometric contact gap. But with the proper adjustments it is accepted as 0. The penetration is also an undesired subject. In real life we do not expect any penetration between the contact surfaces but the ANSYS may need it to overcome the convergence problems while solving the analysis. With the help of “adjust to touch” interface treatment, the geometric penetration 2.9×10^{-6} mm was reduced to 7.7×10^{-15} mm.

To summarize, the Augmented Lagrange formulation was used for frictional contacts. The MPC formulation was used for bonded contacts. For both cases, the “adjust to touch” interface option was employed.

3.10 Meshing

In this project, meshing was applied by selecting the element shape. Triangular elements (Figure 3.25) for 2D and tetrahedral elements (Figure 3.26) for 3D were preferred. Since relative motion between parts was desired, all parts were meshed separately. Triangular / tetrahedral elements have more capability of capturing very small curvatures than the commonly used quadrilateral / hex ones. Furthermore, the meshing must be similar in both the 2D and 3D cases for consistency.

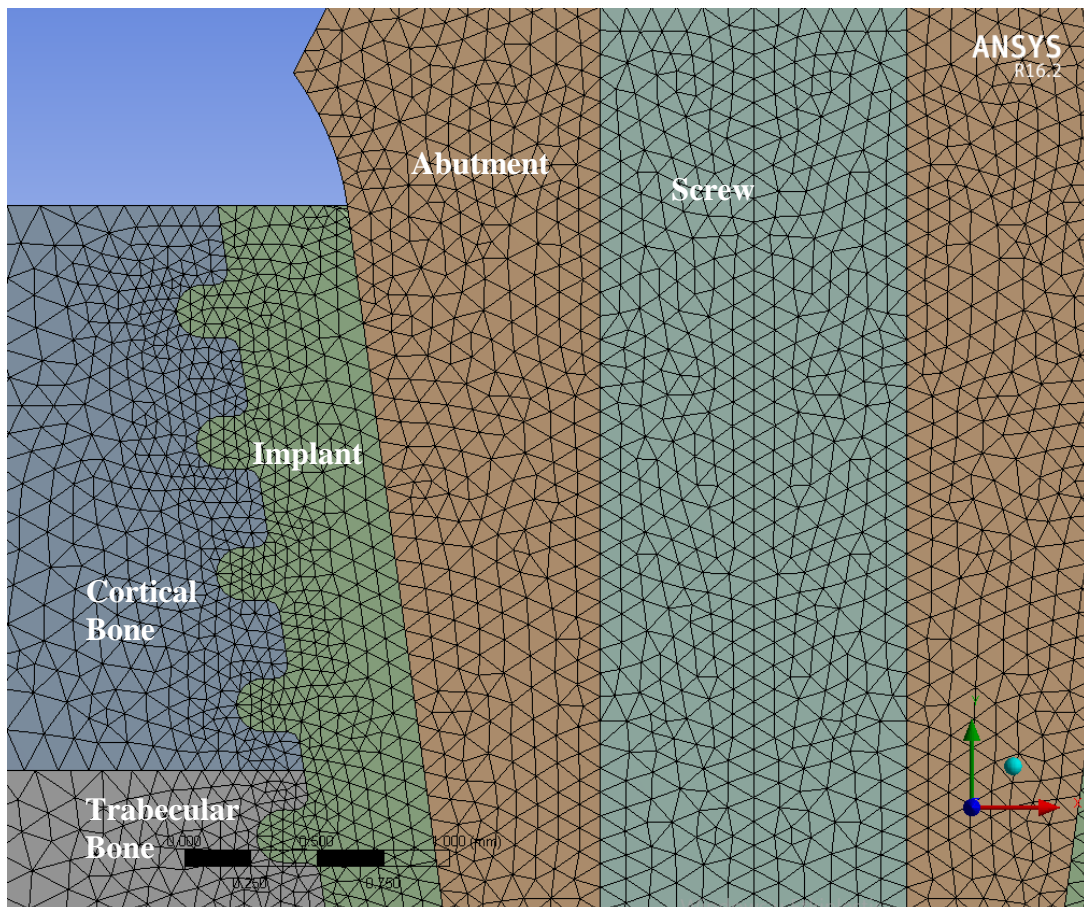


Figure 3.25: 2D meshing with triangular elements.

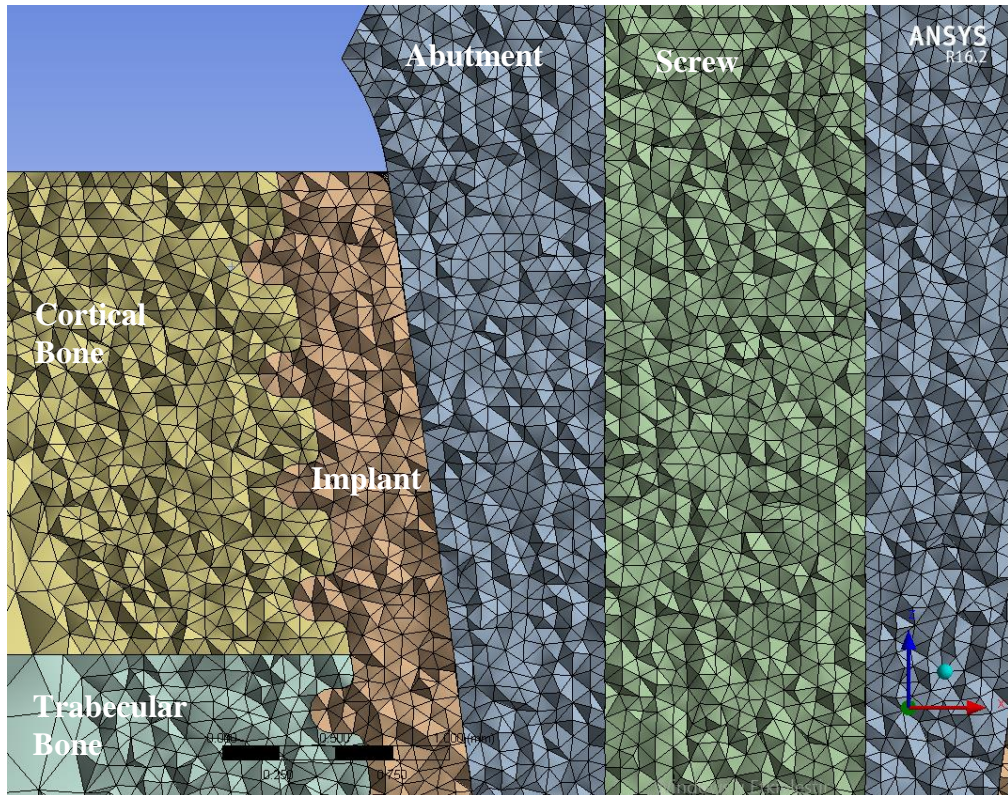


Figure 3.26: 3D meshing with tetrahedral elements.

Advanced size functions were used to avoid excessive meshing in the unimportant areas of the model. For example, the “proximity and curvature” function reduced the mesh size in curvatures like threads on the implant. The other areas like the bottom of the bone were meshed with coarse meshes. The minimum element size was determined to be 0.05 mm in both 2D and 3D models. Also the growth rate of the meshes starting from the smallest elements was fixed to 2. This means that if the smallest element size is 0.01 mm, the next adjacent element size should be 0.02 mm if the growth rate is 2.

Mesh statistics are the other important factors that must be checked. The element quality, aspect ratio and skewness values must be within acceptable limits. The element quality metric (Figures 3.27 – 3.30) scales between 0 to 1 where 1 means the best. It is computed with the equations below:

$$\text{Element Quality} = C \times \frac{\text{Area}}{\sum \text{Edge Length}^2} \quad \text{for 2D elements}$$

$$\text{Element Quality} = C \times \frac{\text{Volume}}{\sum \sqrt{(\text{Edge Length}^2)^3}} \quad \text{for 3D elements.}$$

The constant C is 6.92 for triangular elements and 124 for tetrahedral elements.

The aspect ratio metric (Figures 3.28 – 3.31) was calculated by using different algorithms in the program special for 2D and 3D mesh elements. It should be lower than 20 and the best value is 1. The skewness metric (Figures 3.29 – 3.32) measures how much the created mesh element differs from the ideal mesh element. The skewness is computed as follows:

$$Skewness = \frac{Optimal\ Cell\ Size - Cell\ Size}{Optimal\ Cell\ Size}$$

Skewness value should be lower than 0.9 in order to be in the safe zone. The 2D and 3D mesh statistics of this project are shown below.

3.10.1 2D Mesh Metrics

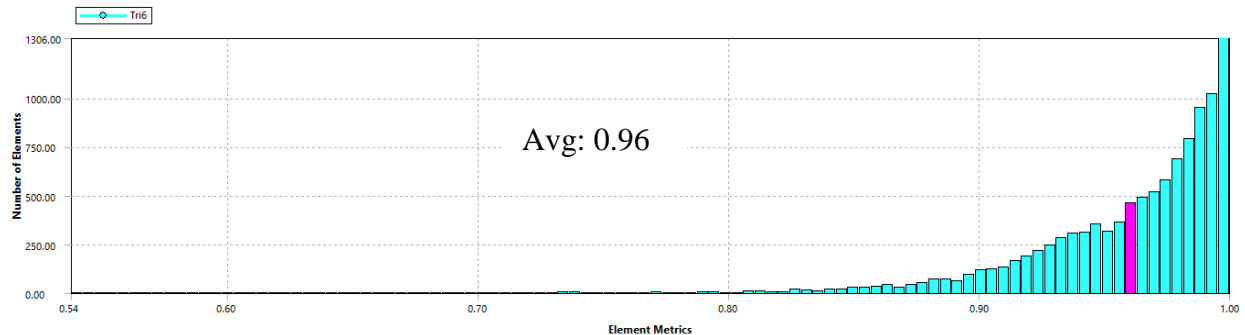


Figure 3.27: 2D element quality graph of triangular mesh. The average value is 0.96 and it should be close to the value of 1 in order to have excellent mesh quality.

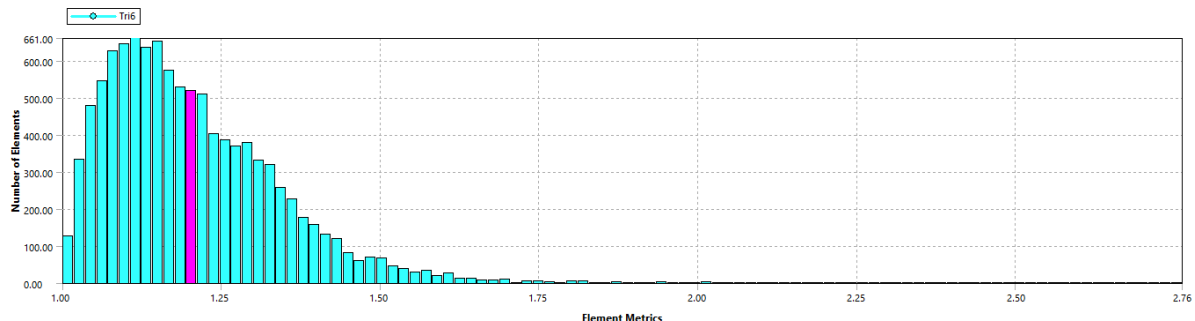


Figure 3.28: 2D aspect ratio of the triangular elements. The average value is 1.2 while the best value is 1. It should be lower than 20 in order to have fair mesh elements.

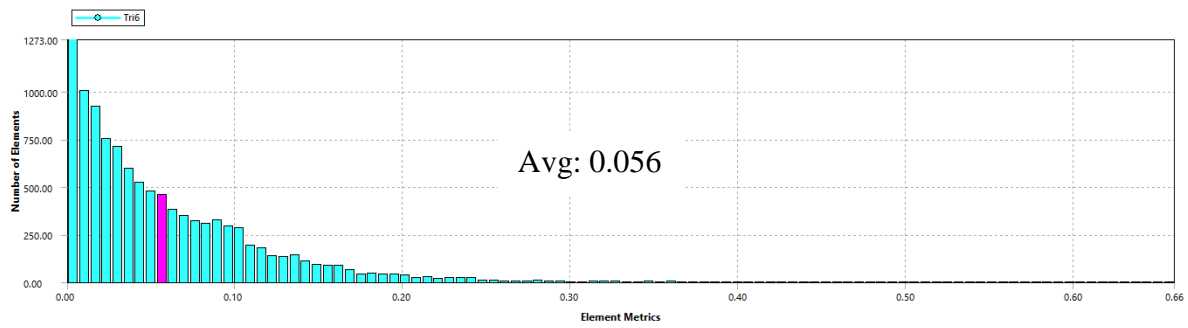


Figure 3.29: 2D skewness of the triangular elements. The average value is 0.056 and the optimum value should be 0. In order to have acceptable results, the skewness value should be lower than 0.9.

3.10.2 3D Mesh Metrics

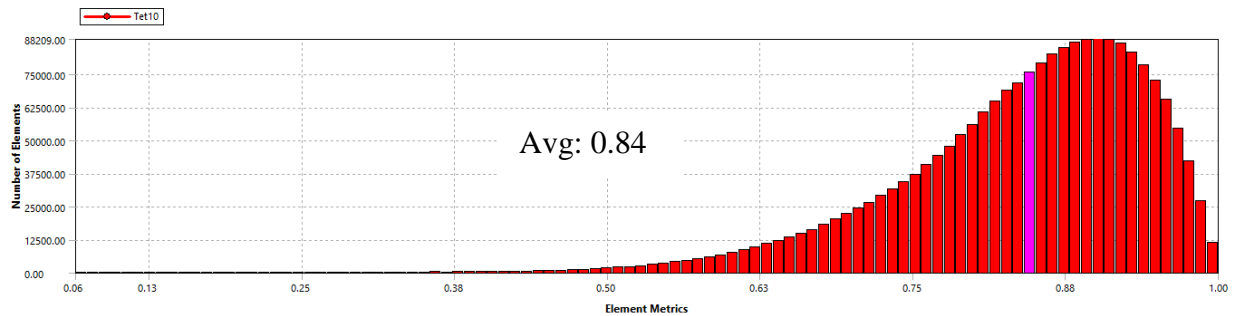


Figure 3.30: 3D element quality graph of tetrahedral mesh. The average value is 0.84 and it should be close to the value of 1 in order to have excellent mesh quality.

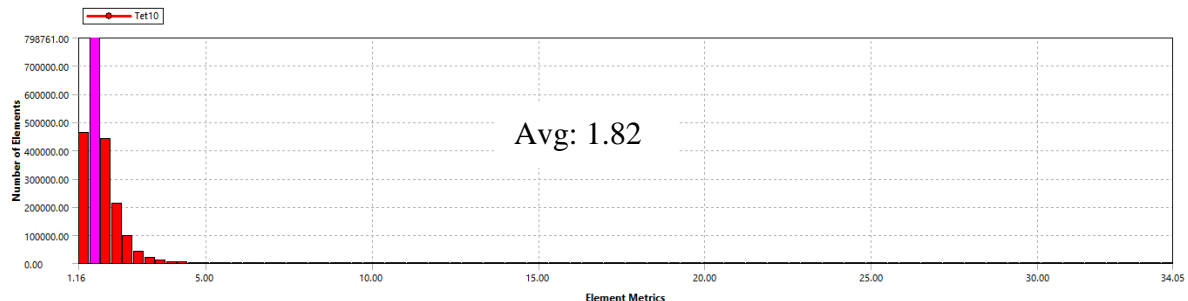


Figure 3.31: 3D aspect ratio of the tetrahedral elements. The average value is 1.82 while the best value is 1. It should be lower than 20 in order to have fair mesh elements.

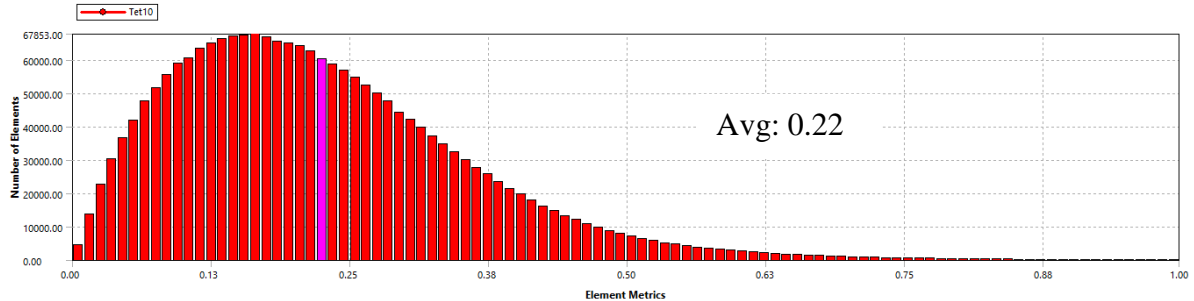


Figure 3.32: 3D skewness of the tetrahedral elements. The average value is 0.22 while the optimum value should be 0. In order to have acceptable results, the skewness value should be lower than 0.9.

The mesh metrics values are listed in Table 3.1 and they all fall within acceptable limits. The average 2D element quality is higher than the 3D case but both are near the max. value. The average 3D aspect ratio is higher than 2D and shows that the 2D elements are more properly created than the 3D elements as the min. is the best for aspect ratio. The reason of the max. value of 34 for the 3D elements may due to the lower smoothing option of the 3D meshing. But average values are lower than the acceptable 20. The average skewness of the 2D elements are lower than the 3D elements which prove that the 2D meshing is smoother and more straight than the 3D meshing. The 0.9 skewness value is acceptable for the analysis and the resulting values are lower than this value.

As it is seen in Table 3.2, the 2D meshing time is extremely shorter than that of the 3D meshing. This is because of the usage of the surface and 2D triangular elements rather than the volume and 3D tetrahedral elements. Also the mesh quantities are reduced to very low levels by 2D meshing. It brings less capacity usage of the PC while solving the analysis.

3.10.3 Tabular Data of 2D and 3D Mesh Metrics

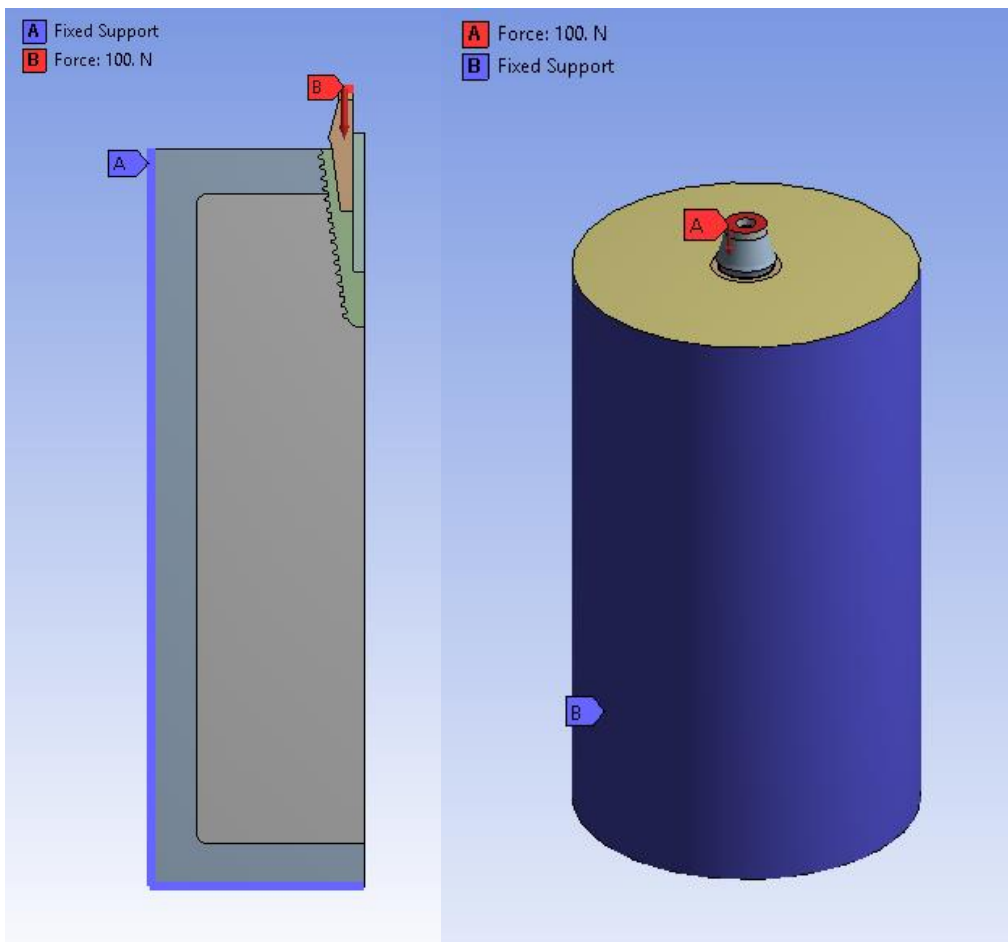
	2D	3D	2D	3D	2D	3D
	Element Quality		Aspect Ratio		Skewness	
Max.	1	1	2.76	34	0.66	0.99
Average	0.96	0.84	1.2	1.82	0.056	0.22
Min.	0.039	0.099	1	1.15	0.0000003	0.0000008

Table 3.1: Tabular data for 2D and 3D mesh metrics.

Mesh Statistics	2D	3D
Number of Mesh Elements	10,804	2,082,930
Number of Mesh Nodes	22,888	2,921,121
Meshing Time	3 s	10 h 43 min 45 s

Table 3.2: Mesh statistics for 2D and 3D meshing. It is clear that a 2D model offers huge time savings.

3.11 Loading and Boundary Conditions



Figures 3.33 and 3.34: 2D and 3D boundary conditions.

The force was applied onto the crown top surface for 3D and top edge for 2D. The load was selected as 100 N axially ($-Z$ direction). In real life, the loading magnitude may vary from 54 N to 234 N for the first mandibular premolar tooth. Under normal loading conditions, 100 N was considered a proper value.

The lateral and bottom surfaces and edges of the bone model were fixed, with zero displacement. By doing so, the displacement for the lateral and bottom bone surfaces in the 3D model, and the edges for the 2D model were restricted. In real life, the lateral surfaces of the mandibular jaw bone are free from restriction. However, this project concentrated on the modeling of an interior part of the bone. That is why the lateral surfaces were fixed. Modeling the entire jaw bone is out of the scope of the project. Nevertheless, the restriction of the bottom surface and the edges reflects real life conditions.

3.12 Material Analysis on the 2D Model

After demonstrating the similarity of results between the 2D and 3D models, the 2D model was used (due to its huge time savings) to investigate the effect of material properties on implant stresses. It is better when the mechanical properties of the bone and the implant material is similar. When the implant material is too much harder than the jaw bone, the stresses may not be conveyed properly to the bone and there may be osseointegration problems.

For this material analysis, 8 different titanium alloys were examined and studied: Ti-19Nb-14Zr, Ti-24Nb-4Zr-7.9Sn, Ti-35Nb-4Sn, Ti-25Ta-25Nb, Ti-29Nb-13Ta-4.5Zr, Ti-29Nb-13Ta-6Sn, Ti-7.5Mo-3Fe and Ti-6Al-4V (Table 3.3). (Here, the numbers in front of element names indicate wt.%) The materials were chosen from an article and they are all bio-compatible [5]. In this analysis, the only change in material properties was the Young's modulus. 14 GPa was selected as the lowest Young's modulus to make the mechanical properties closer to those of the cortical bone. Then using 10 GPa increments of the Young's modulus, its effects on the results were studied.

Alloy Designation	E (GPa)
Ti-19Nb-14Zr	14
Ti-24Nb-4Zr-7.9Sn	33
Ti-35Nb-4Sn	44
Ti-25Ta-25Nb	55
Ti-29Nb-13Ta-4.5Zr	65
Ti-29Nb-13Ta-6Sn	74
Ti-7.5Mo-3Fe	85
Ti-6Al-4V	110

Table 3.3: The Young's moduli of some titanium-based alloys [18]. The numbers in front of element names in the first column indicate wt.%.

4. RESULTS

4.1 Total Deformation

The total deformation was estimated to be 0.0037 mm in both 2D and 3D models in the bonded condition (Figures 4.1 – 4.2). It is concentrated around the crown, abutment, implant and screw as the force is applied onto the crown. Since they are all bonded to each other and their material properties are the same except the crown, the deformation value is the same for all of these parts. The deformation is spreading smoothly from the implant side to the peripheries of the model.

For the frictional case, the deformation was calculated to be 0.0044 mm in the 3D model (Figure 4.3) and 0.0042 mm in the 2D model (Figure 4.4). The distribution of the deformation from implant side to the peripheries is again smooth but its value is different if it is examined part by part. This is due to the fact that there is friction between parts and the force is absorbed while it is conveyed to the bottom sides of the model. Here logically the highest deformation value occurs on the crown as it is the first part to be in contact with the applied force. All the deformation results are consistent with the literature (see Table 5.1).

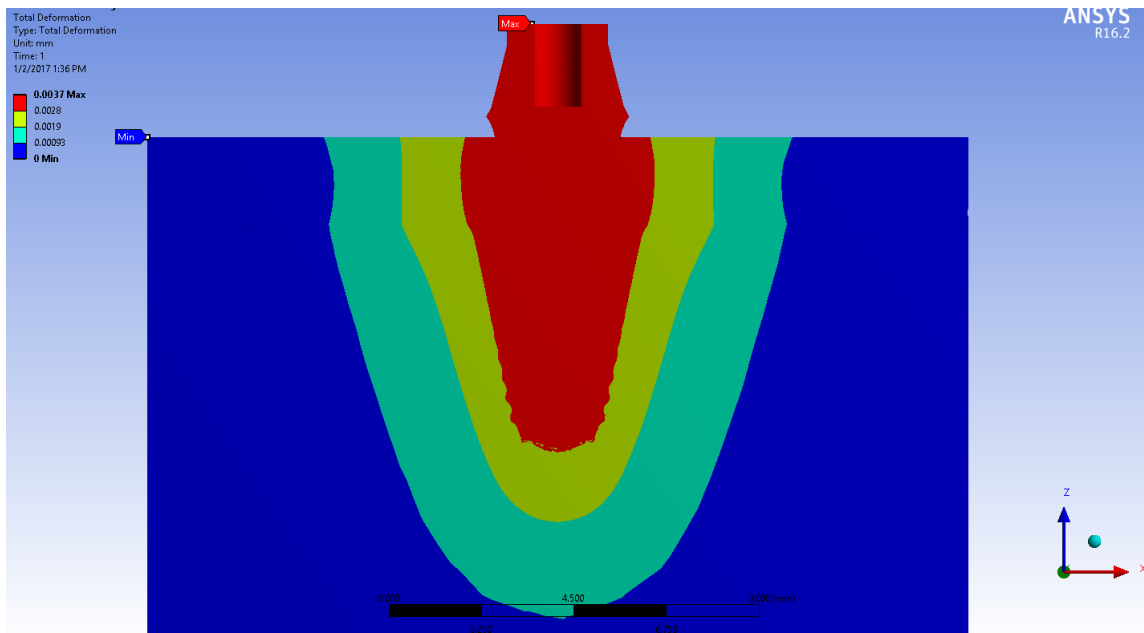


Figure 4.1: 3D bonded condition total deformation of the entire model.

Max. is 0.0037 mm.

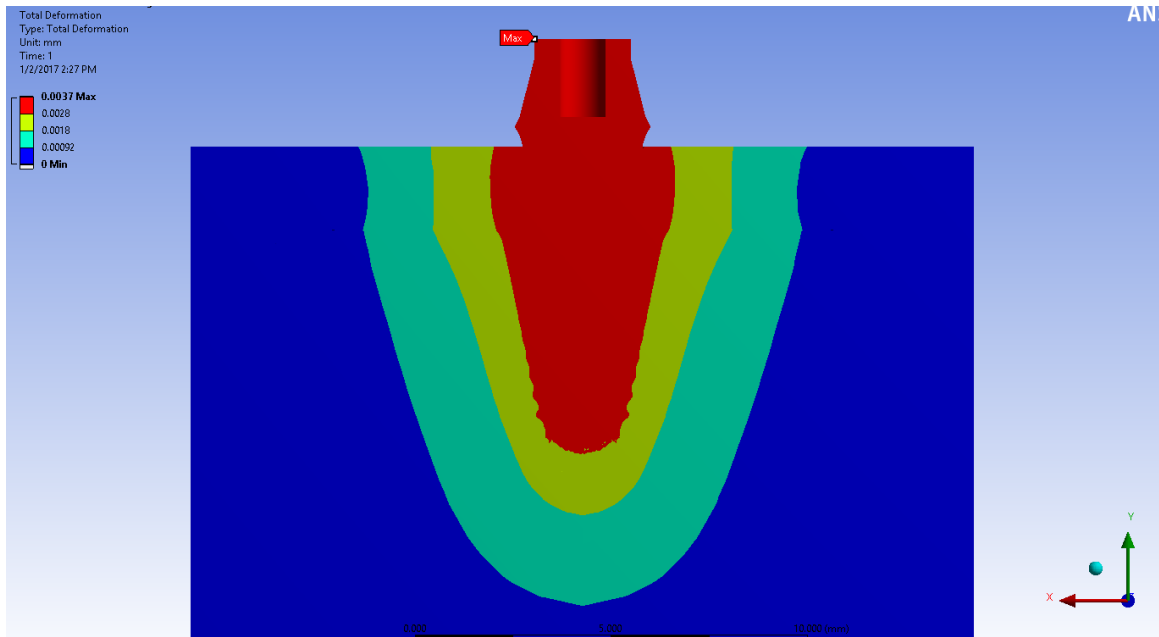


Figure 4.2: 2D bonded condition total deformation of the entire model.
Max. is 0.0037 mm.

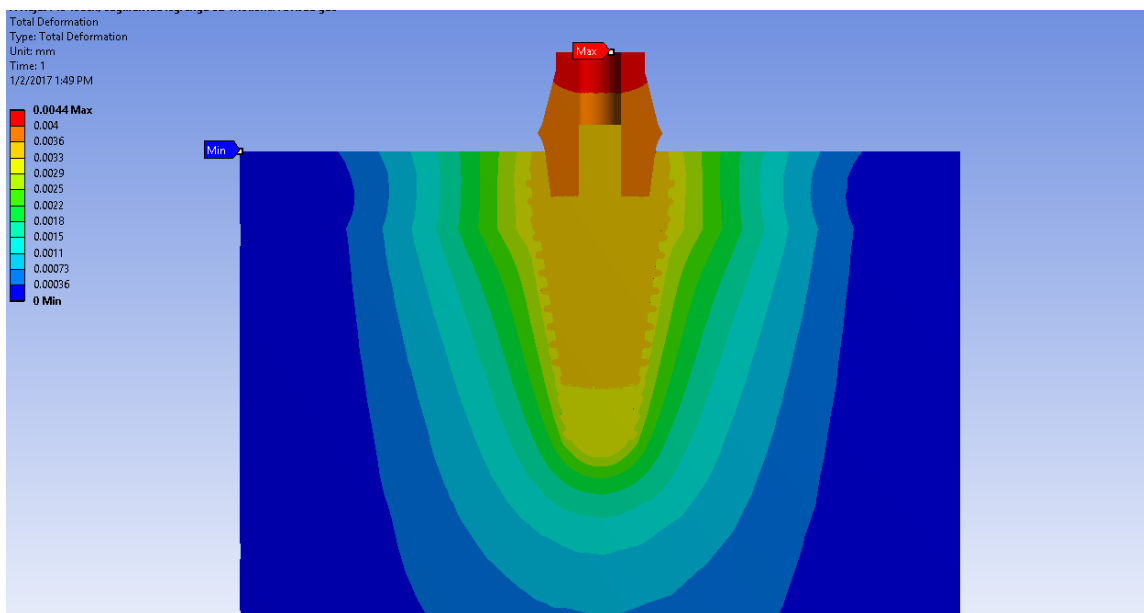


Figure 4.3: 3D frictional condition total deformation of the entire model.
Max. is 0.0044 mm.

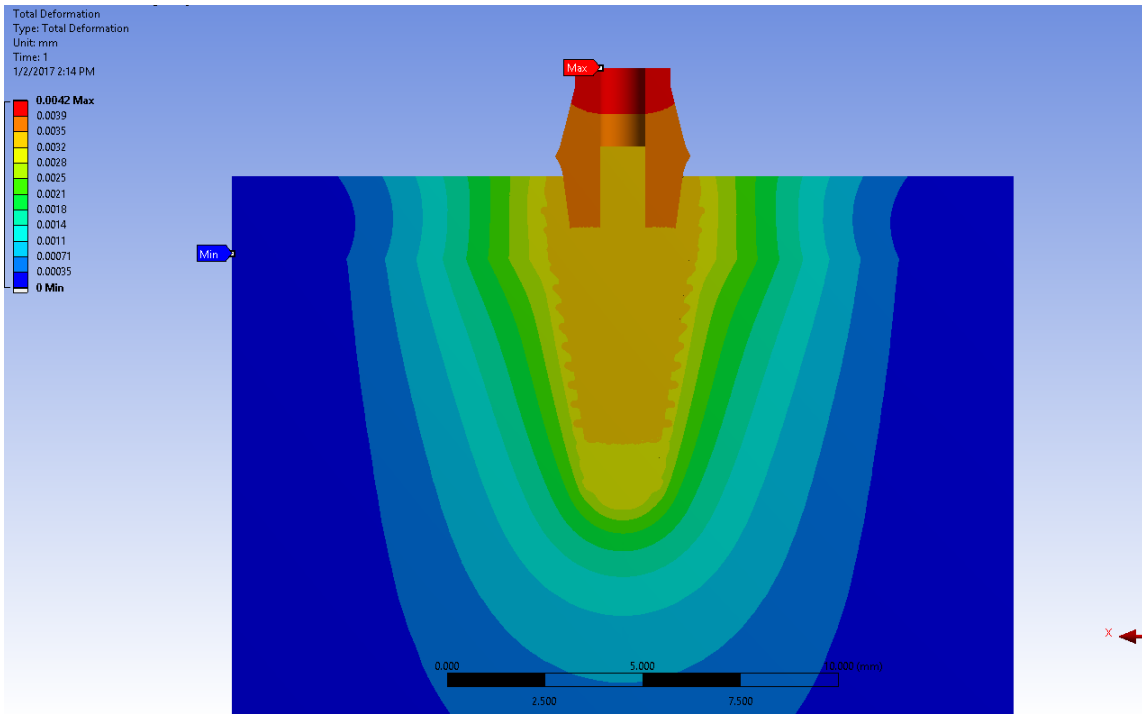


Figure 4.4: 2D frictional condition total deformation of the entire model. Max. is 0.0042 mm.

4.2 Equivalent Stresses in the Entire Model

Maximum equivalent stresses occur at the implant - abutment interface for all models but in the 3D bonded condition it occurs at the crown - abutment interface (Figure 4.5). However, its estimated values are similar in both cases: 41 MPa vs. 35 MPa. In the case of the bonded condition, which is fully osseointegrated, the max. equivalent stresses are 41 MPa for both 2D (Figure 4.6) and 3D models. The general stress distribution is very similar in all models. For the frictional case, which is an immediately loaded condition, the stresses are 35 MPa in the 3D (Figure 4.7) and 40 MPa in the 2D (Figure 4.8) models. The max. stresses occur along the implant - abutment interface and on the abutment part. Since there is relative motion in the frictional case, the stress distribution is less smooth than the bonded condition. The harder cortical bone absorbs most of the loading as it is seen in the figures below. As a result of this, stresses are distributed to the cortical bone peripheries in bonded cases (Figures 4.5–4.6). But in the frictional case, the stresses may have a chance to affect also the trabecular bone because the friction coefficient can inhibit just some amount of relative motion between parts, not all. Thus rather than clinging to the cortical bone, the implant will go down to the trabecular bone. It is understood from Figures 4.7–4.8 that the stresses are expanded to the trabecular bone

peripherals. That is why the stress distribution in the cortical bone decreases and that in the trabecular bone increases.

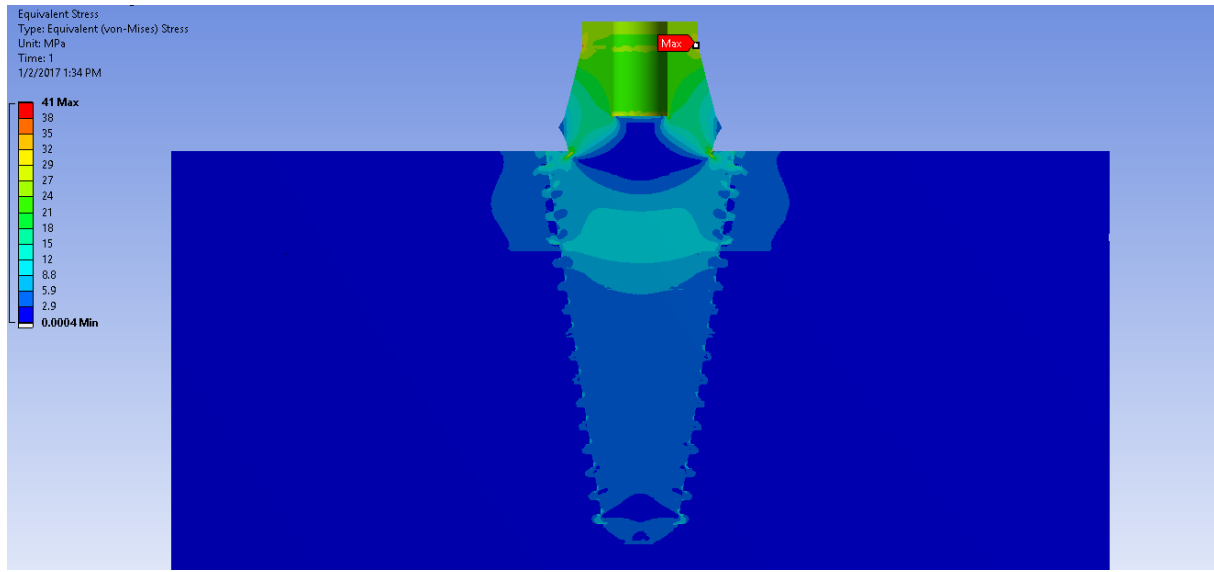


Figure 4.5: 3D bonded condition equivalent stresses in the whole model. Max. occurs on the top of the abutment which is 41 MPa while the strength of the abutment is 830 MPa.

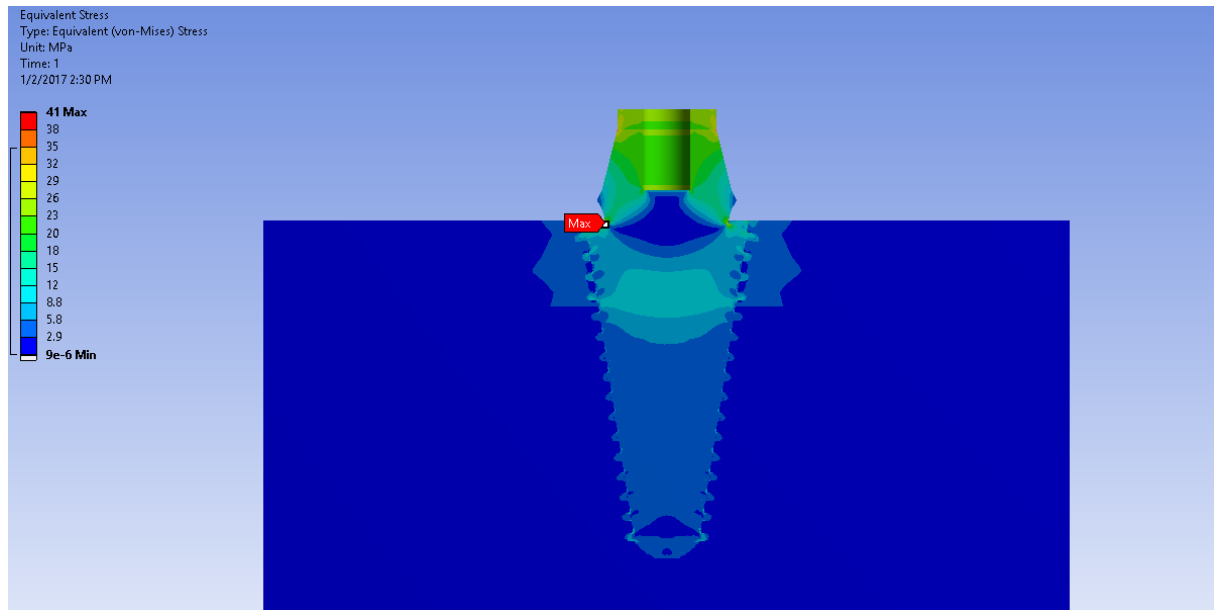


Figure 4.6: 2D bonded condition equivalent stresses in the whole model. Max. occurs on the implant which is 41 MPa while the strength of the implant is 830 MPa.

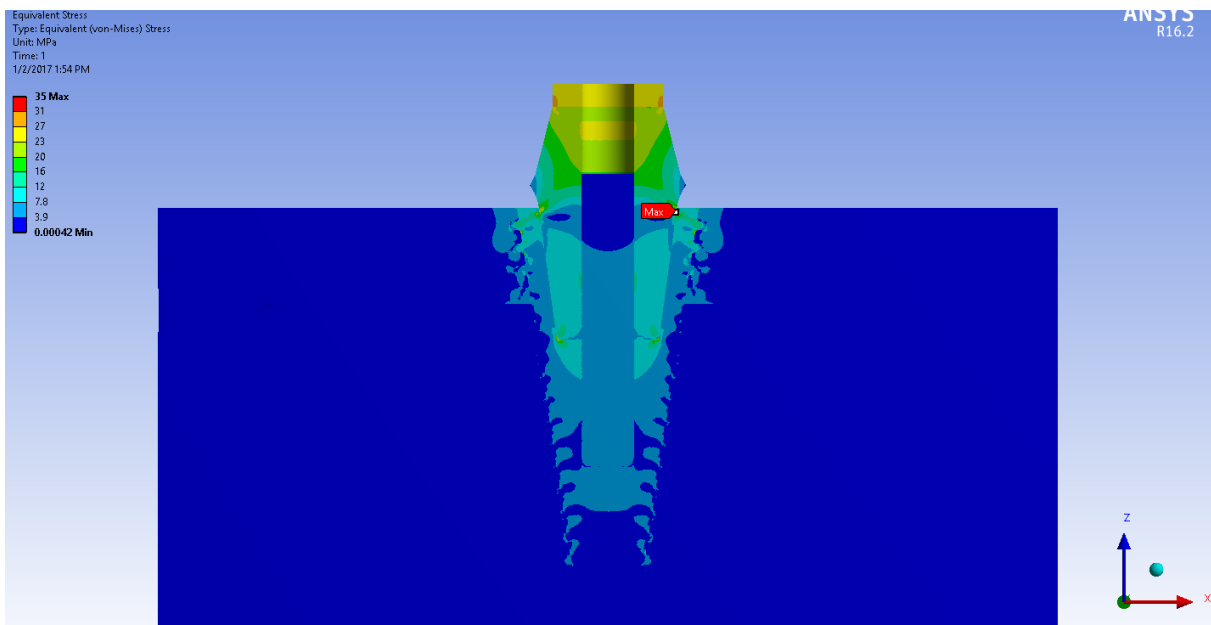


Figure 4.7: 3D frictional condition equivalent stresses on the whole model. Max. occurs on the abutment which is 35 MPa while the strength of the abutment is 830 MPa.

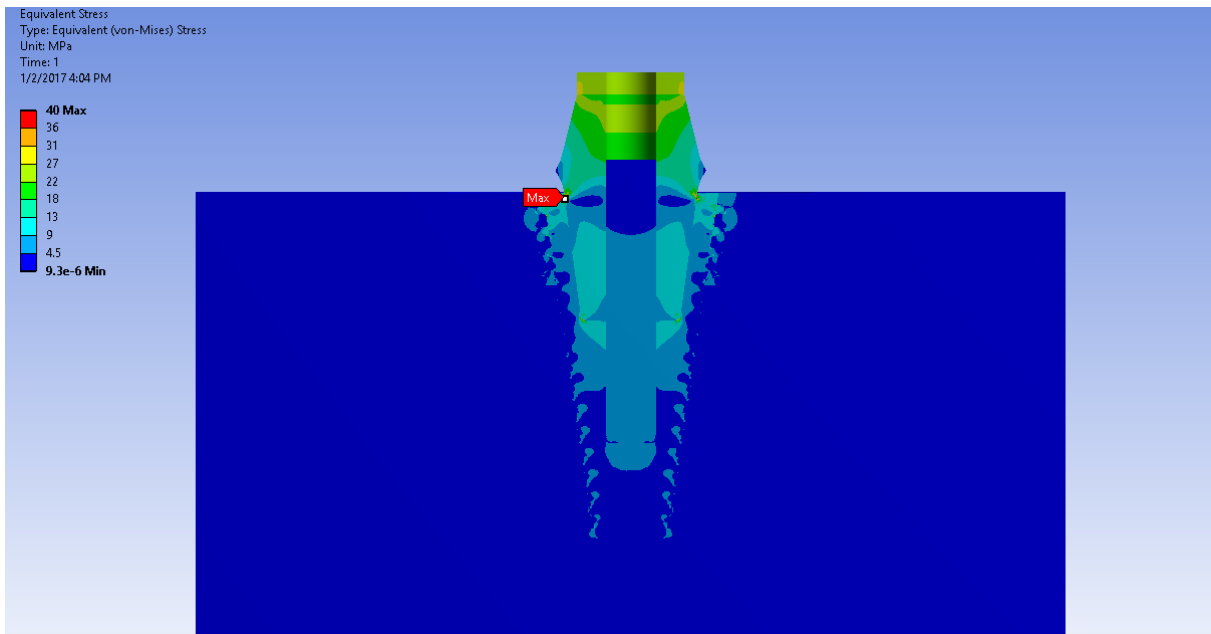


Figure 4.8: 2D frictional condition equivalent stresses on the whole model. Max. occurs on the implant which is 40 MPa while the strength of the implant is 830 MPa.

4.3 Equivalent Stresses in the Cortical Bone

Maximum equivalent stresses on the cortical bone in the bonded condition were calculated to be 9.8 MPa in the 3D (Figure 4.9) and 8.4 MPa in the 2D (Figure 4.10) models. The location of the max. stresses are on the top the first thread profile and it is same for each model. Also the stress distribution is the same. The reason for the max. stress location is that it is the initial contact interface of the stable bone structure and the force-driven implant structure. The implant forces the first layer of the cortical bone and since the cortical bone resists, high stresses occur. In the frictional case, the max. stresses were found to be 14 MPa for both the 2D (Figure 4.12) and the 3D (Figure 4.11) models. This time, the max. stress location is the second thread profile of the cortical bone as there is no restriction of movement. The implant can engage with the cortical bone rather than sticking to it at the first contact point as was the case in the bonded condition. This engagement results in higher stress values but a lower stress distribution toward the peripheries of the cortical bone.

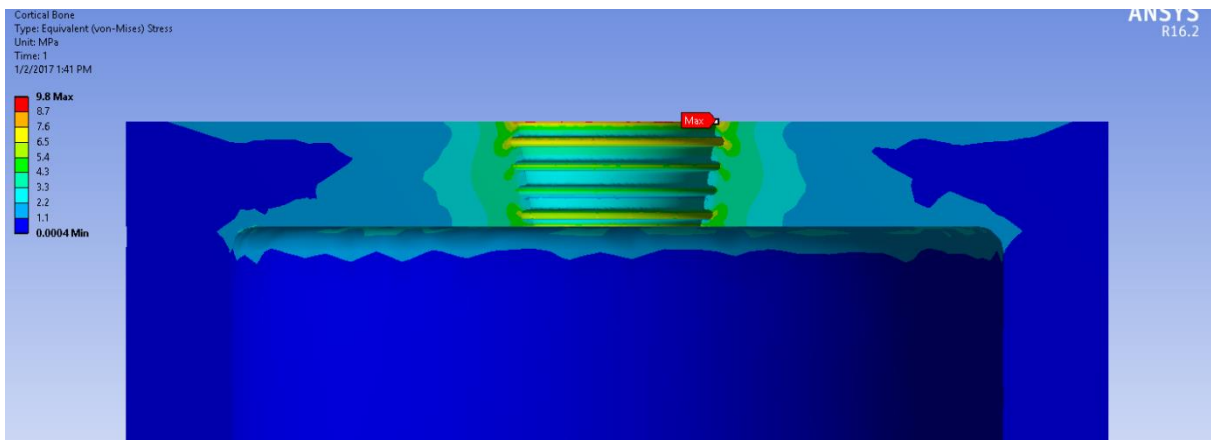


Figure 4.9: 3D bonded condition equivalent stress on the cortical bone. Max. value is 9.8 while the strength of the cortical bone is 130 MPa.

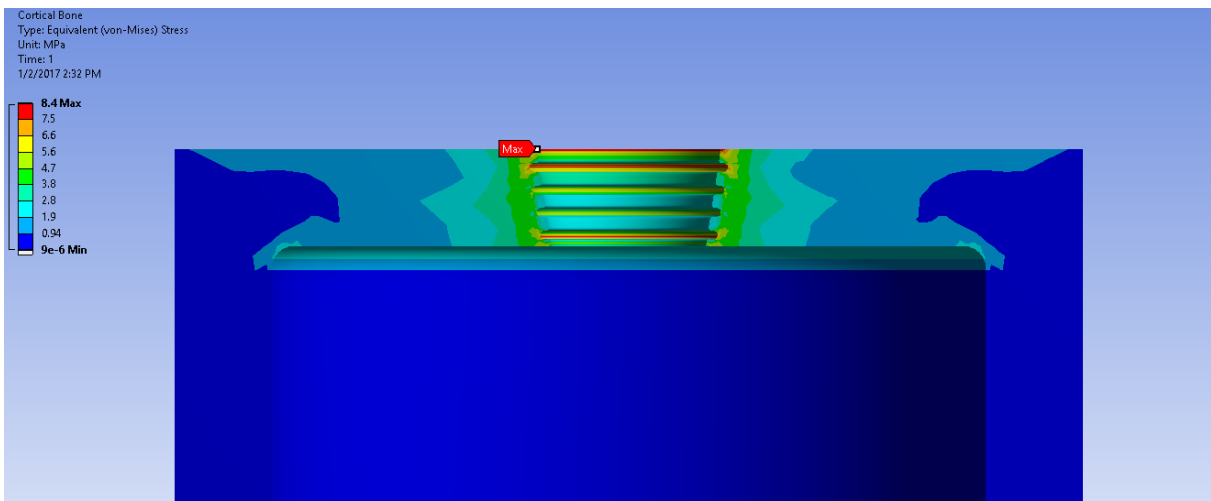


Figure 4.10: 2D bonded condition equivalent stress on the cortical bone. Max. value is 8.4 MPa while the strength of the cortical bone is 130 MPa.

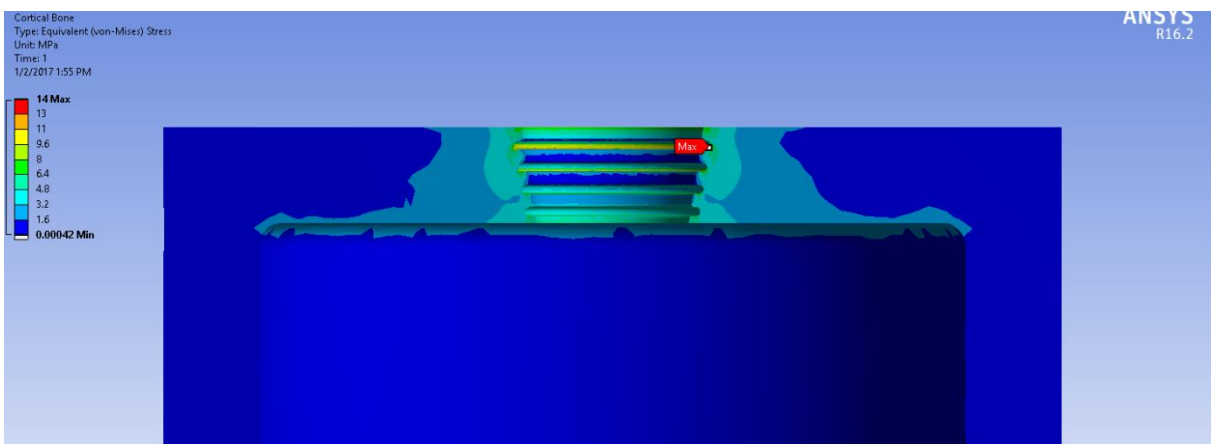


Figure 4.11: 3D frictional condition equivalent stress on the cortical bone. Max. value is 14 MPa while the strength of the cortical bone is 130 MPa.

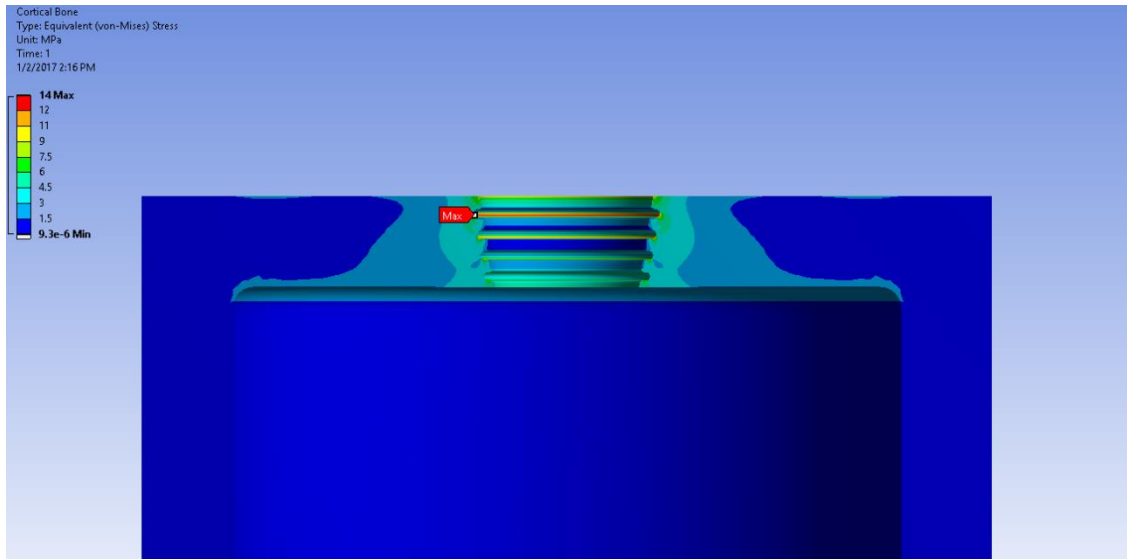


Figure 4.12: 2D frictional condition equivalent stress on the cortical bone. Max. value is 14 MPa while the strength of the cortical bone is 130 MPa.

4.4 Equivalent Stresses in the Trabecular Bone

The max. equivalent stress values on the trabecular bone in the bonded case were found to be 3.3 MPa for the 3D and 3.5 MPa for the 2D models. In the 3D model (Figure 4.13), the highest stress occurs on the bottom thread profile as same as the 2D model (Figure 4.14). Since the implant cannot move toward the trabecular bone, high stresses occur at the last thread profile and the bottom surface of the bone. The difference in the stress distribution can be seen between the frictional and bonded cases. In the frictional case, the distribution decreases toward the peripheries as it allows more penetration to the bone.

In the frictional case, the max. equivalent stresses were 4 MPa in the 3D (Figure 4.15) and 4.7 MPa in the 2D model (Figure 4.16). The reason for the lower stresses found in the bonded condition than the frictional condition is that the bonded contacts do not allow relative motion between parts and the implant cannot go down to the trabecular bone.

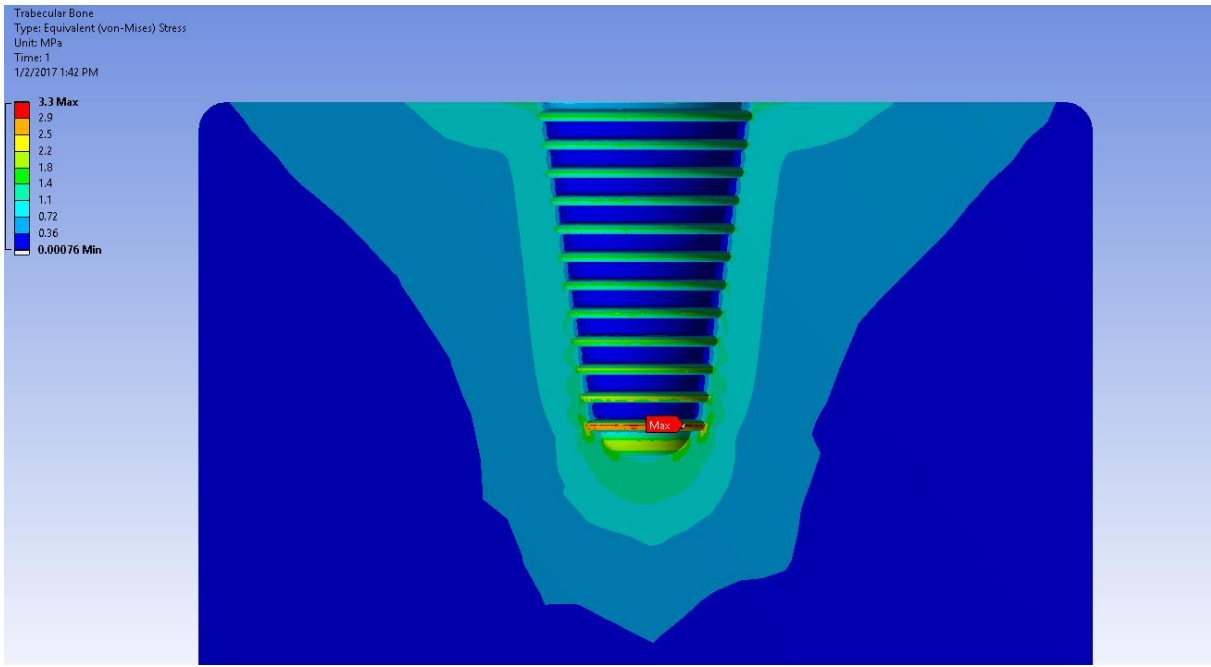


Figure 4.13: 3D bonded condition equivalent stress on the trabecular bone. Max. value is 3.3 MPa while the strength of the trabecular bone is 20 MPa.

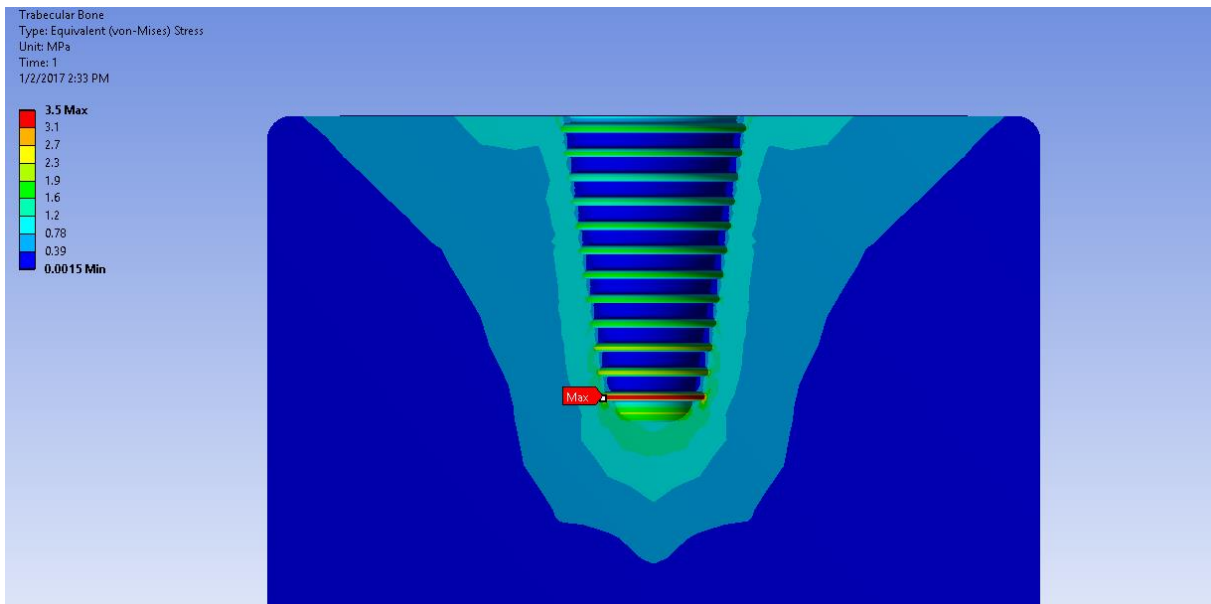


Figure 4.14: 2D bonded condition equivalent stress on the trabecular bone. Max. value is 3.5 MPa while the strength of the trabecular bone is 20 MPa.

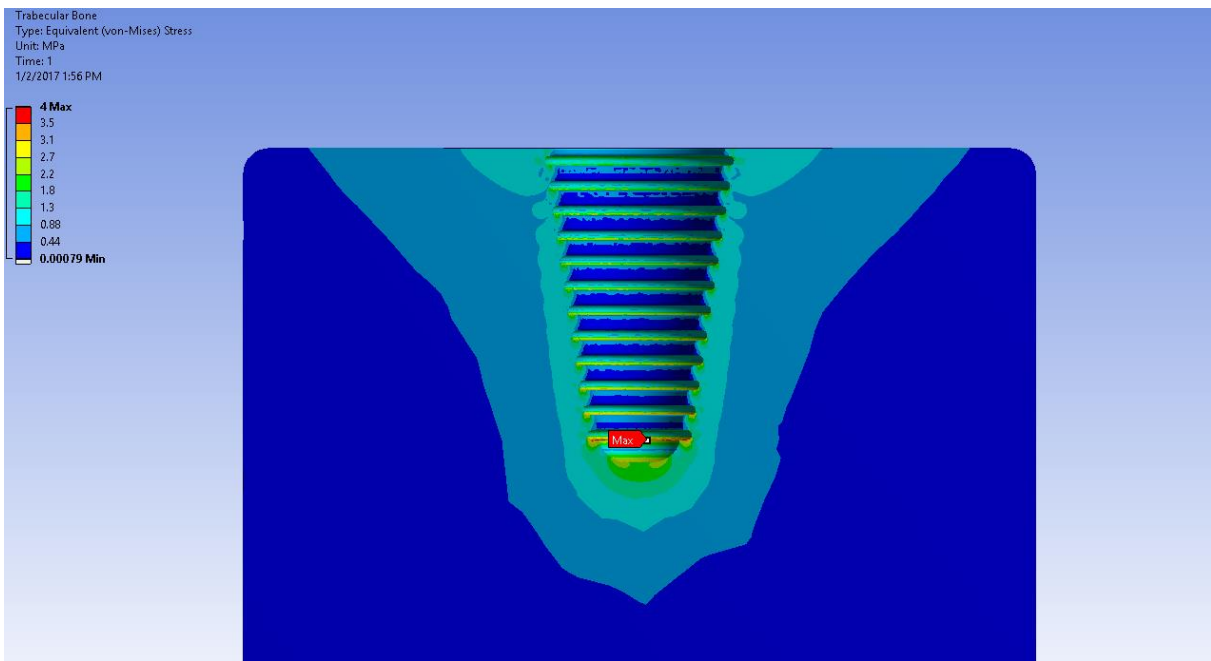


Figure 4.15: 3D frictional condition equivalent stress on the trabecular bone. Max. value is 4 MPa while the strength of the trabecular bone is 20 MPa.

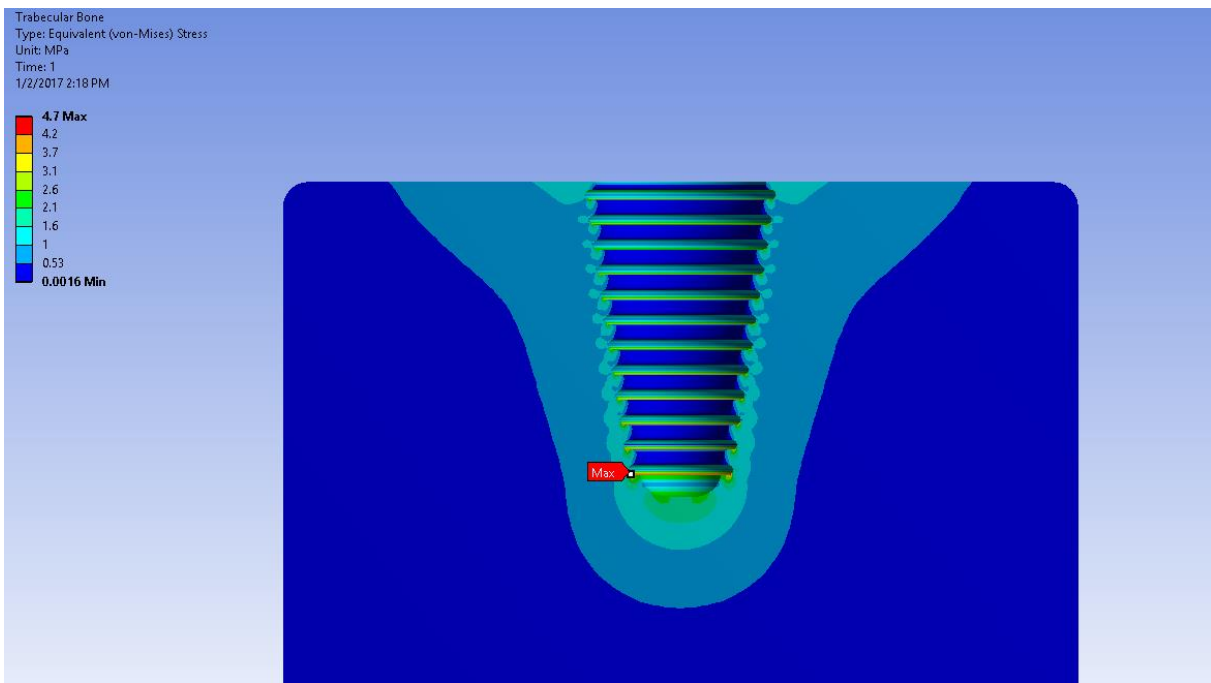


Figure 4.16: 2D frictional condition equivalent stress on the trabecular bone. Max. value is 4.7 MPa while the strength of the trabecular bone is 20 MPa.

4.5 Tabular Data of the Stress and Deformation Results

To interpret the results accurately, Table 4.1 was created. Since the scope of this project was analyzing the stress values on the bones, the cortical and the trabecular bone stress values are more remarkable. For the cortical bone, in the 2D bonded case 8.4 MPa was obtained while in 3D bonded case it was 9.8 MPa. The difference is 14.3% which still can be acceptable as they are much lower than the limit value of 130 MPa. In the 2D frictional case it was 14 MPa as same as in the 3D frictional case. For the trabecular bone, in the 2D bonded case, 3.5 MPa was obtained while in the 3D bonded case it was 3.3 MPa. The difference is 5%. In the 2D frictional case it was 4.7 MPa while in the 3D frictional case it was 4 MPa. The difference is 14.9%. Also the other stress values on the remaining parts are similar to each other.

	2D Bonded	2D Frictional	3D Bonded	3D Frictional
Deformation (mm)	0.0037	0.0042	0.0037	0.0044
Max. Stress in Implant (MPa)	41	40	41	35
Max. Stress in Cortical Bone (MPa)	8.4	14	9.8	14
Max. Stress in Trabecular Bone (MPa)	3.5	4.7	3.3	4
Max. Stress in Crown (MPa)	33	32	39	32
Max. Stress in Abutment (MPa)	36	37	41	35
Max. Stress in Screw (MPa)	20	7	25	7.6
Max Stress in Implant (MPa)	41	40	35	33

Table 4.1: Deformation and stress results from the 2D and 3D models.

4.6 FEM Solution Times

The solution times are shown in Table 4.2. This project proves that axisymmetric designs can be modeled and solved in 2D to avoid time consuming analysis and excessive usage of PC resources. As there is no penetration in the bonded cases, they are faster than the frictional cases in terms of solution times. The 2D bonded case takes 5 seconds while the 2D frictional case lasts 15 seconds. On the other hand, the 3D bonded takes 44.7 minutes to solve while the 3D frictional case takes 2 hours 57 minutes and 5 seconds. This project therefore shows that the solution times can be reduced 99.8% for the bonded case and 99.85% for the frictional case while there are no significant changes in the results.

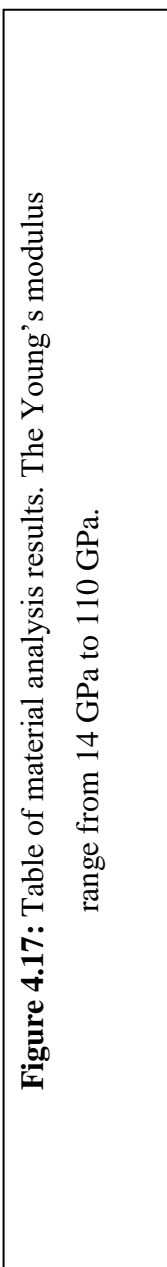
	2D Bonded	2D Frictional	3D Bonded	3D Frictional
Solution Time	5 sec.	15 sec.	44.7 min.	2 h. 57 min. 5 sec.

Table 4.2: FEM solution times for the tested models.

4.7 Material Analysis Results

The material analysis results are shown in Figure 4.17. To get low deformation (Figure 4.18), the materials with high Young's modulus like Ti-6Al-4V or Ti-7.5Mo-3Fe should be chosen. To lower the max. equivalent stress on the whole model (Figure 4.19), a material with a modulus of 50 GPa should be chosen. But separately a modulus of 75 GPa is recommended for the frictional case and 35 GPa for the bonded case. To lower the stress values on the cortical bone (Figure 4.20), moduli within the range 14 GPa – 20 GPa can be selected. Separately, the alloy Ti-29Nb-13Ta-4.5Zr with a 33 GPa modulus for the bonded case, and the alloy Ti-24Nb-4Zr-7.9Sn with a 65 GPa modulus for the frictional case is recommended. To lower the trabecular bone stress values (Figure 4.21) 30 GPa is ideal. On the other hand, the alloy Ti-19Nb-14Zr ($E = 14$ GPa) is recommended for the bonded case and the alloy Ti-24Nb-4Zr-7.9Sn ($E = 33$ GPa) seems appropriate for the frictional case.

	A	B	C	D	E	F	G	H	I	J	K
1	Name ►	P1 - Frictional Case Young's Modulus	P6 - Bonded Case Young's Modulus	P2 - Total Deformation Maximum	P3 - Equivalent Stress Maximum	P4 - Cortical Maximum	P5 - Trabecular Maximum	P7 - Total Deformation Maximum	P8 - Equivalent Stress Maximum	P9 - Cortical Maximum	P10 - Trabecular Maximum
2	Units	MPa	► MPa	mm	► mm	MPa	► MPa	mm	► MPa	MPa	► MPa
3	DP 0 (Current)	1.4E+04	1.4E+04	0.00953	40.5	11	4.05	0.0079	51	7.51	3.59
4	DP 1	3.3E+04	3.3E+04	0.00612	35.9	10.5	4.12	0.00521	39.9	7.95	2.68
5	DP 2	4.4E+04	4.4E+04	0.00546	35.9	11.3	4.33	0.00468	37.3	7.76	2.77
6	DP 3	5.5E+04	5.5E+04	0.00505	37	11.8	4.47	0.00436	35.7	7.52	2.98
7	DP 4	6.5E+04	6.5E+04	0.0048	37.8	12.3	4.55	0.00416	34.7	7.44	3.12
8	DP 5	7.4E+04	7.4E+04	0.00463	38.5	12.6	4.6	0.00403	34.1	7.72	3.22
9	DP 6	8.5E+04	8.5E+04	0.00447	39.2	12.9	4.65	0.0039	34.7	8.03	3.33
10	DP 7	1.1E+05	1.1E+05	0.00422	40.3	13.5	4.73	0.0037	36.3	8.69	3.5



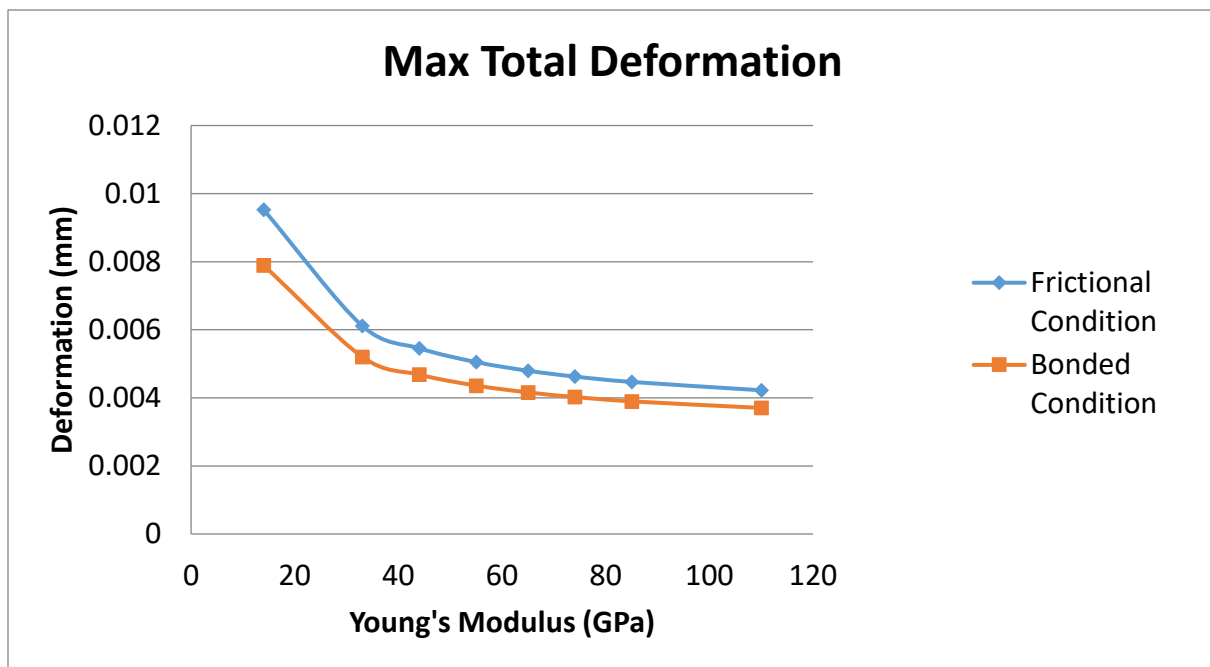


Figure 4.18: Deformation graph for both bonded and frictional cases.

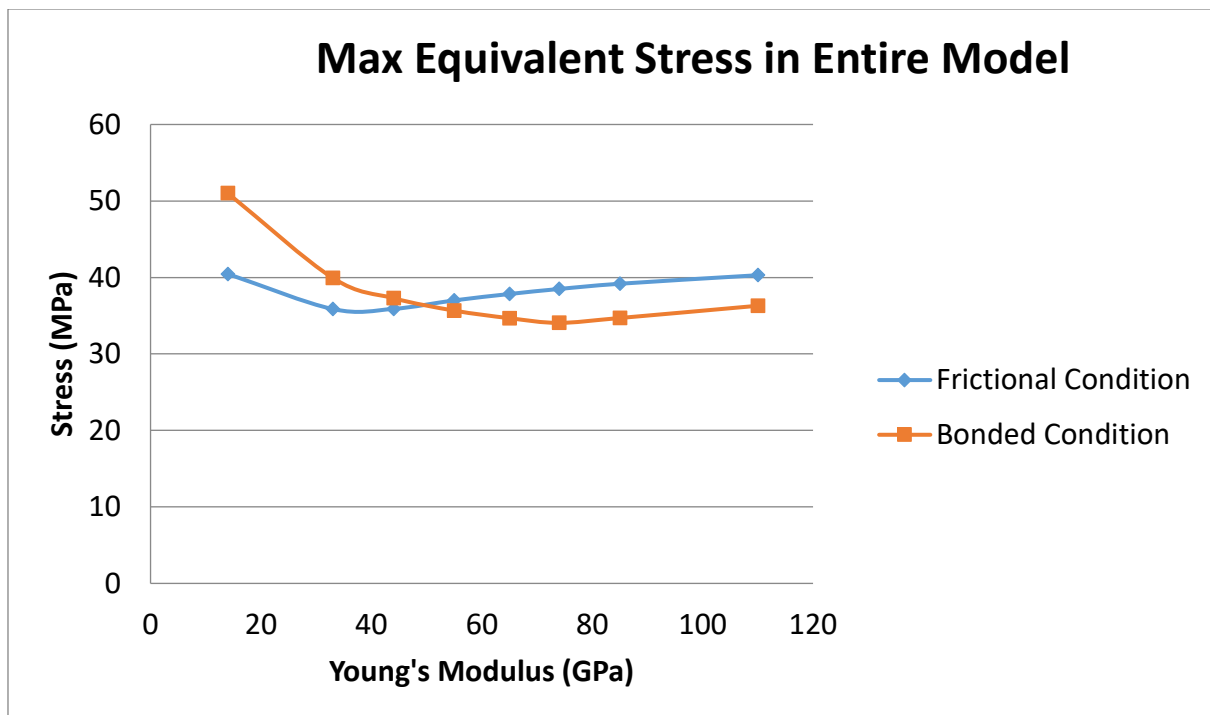


Figure 4.19: General max. equivalent stress graph for both bonded and frictional cases.

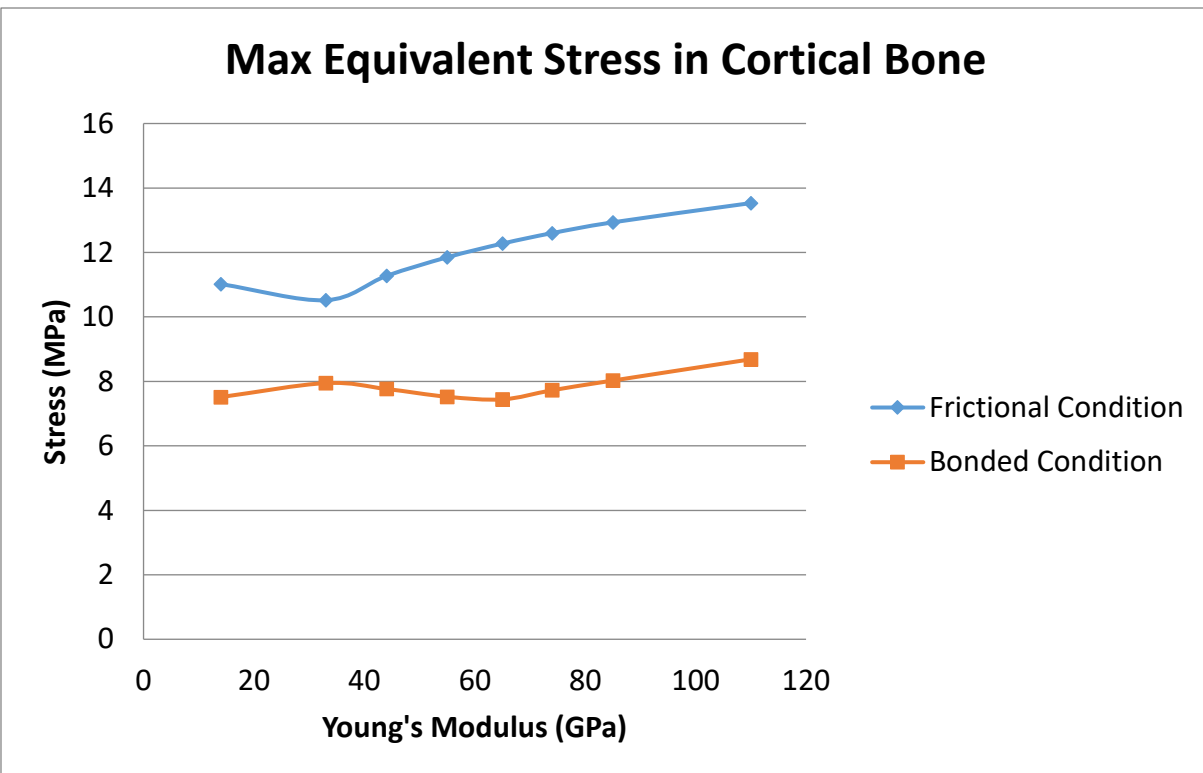


Figure 4.20: Cortical bone max. equivalent stress graph for both bonded and frictional cases.

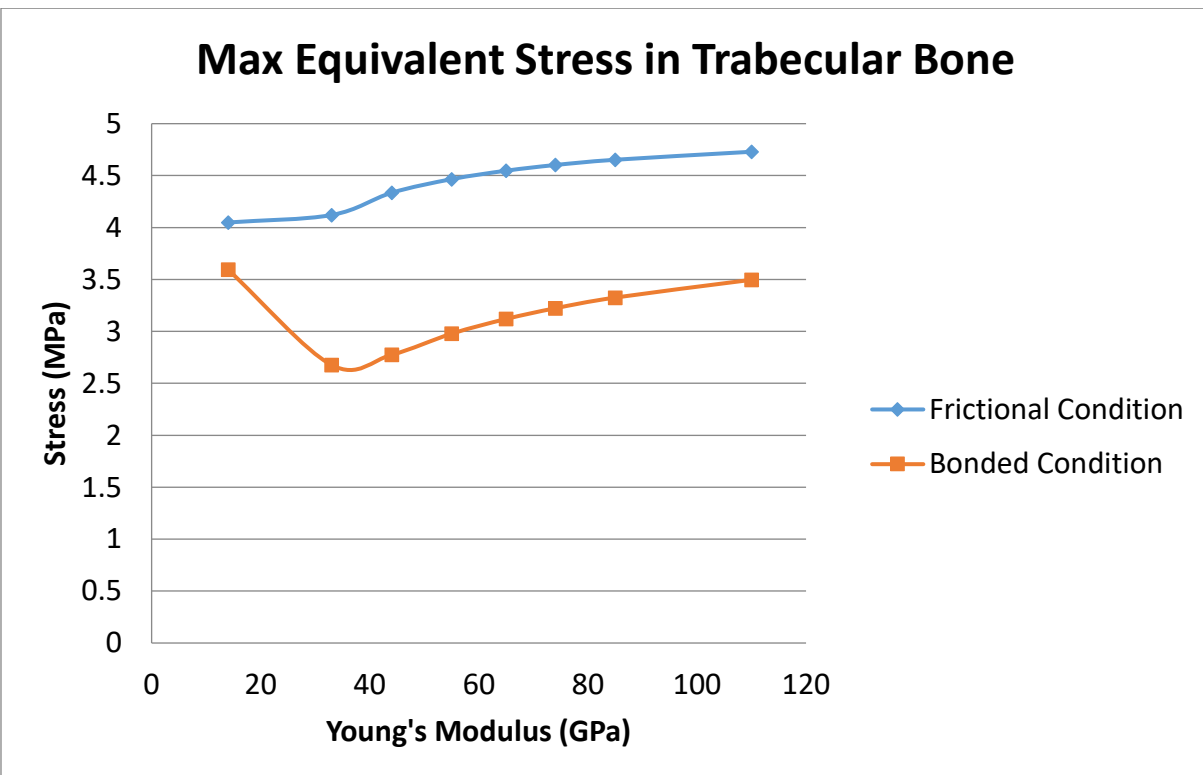


Figure 4.21: Trabecular bone max. equivalent stress graph for both bonded and frictional cases.

5. EVALUATION, DISCUSSION AND SUGGESTIONS

At the beginning of this project, the literature was broadly reviewed with regards to implant modeling. As a result of that review, bone level and tapered implants were chosen. Actually the square thread was also suggested to reduce the stress levels on the bones but it is left as a future work. Throughout the literature search lots of implant models were encountered. Some of them had just a single implant embedded into the bone and some of them had an implant with different parts similar to the geometry of this project. Most of the implant models with multibody parts did not have screw threads while some of them even had no screw. For exactness and the accurate representation of the real bone-implant structure, the screw was used in this project. Based on the screw thread analysis, it was found that screw threads do not affect the stress values on the cortical and trabecular bone. Also, the very small thread curvatures like 0.05 mm cannot be captured easily while meshing, especially with 3D mesh elements. With those facts in mind, the screw threads were eliminated in both the 2D and 3D models.

Contacts between different parts were studied for bonded and frictional cases. In real life, there is almost zero or very low interpenetration of the contact surfaces. But in a digital environment, there are always errors. Specifically for this project, there were geometric gaps like $1.6 \times 10^{-17}\text{ mm}$ and some level of initial geometric penetration like $2.0 \times 10^{-6}\text{ mm}$. With proper contact formulations, the geometric gap was reduced to 0 and the penetration was reduced to $6.9 \times 10^{-15}\text{ mm}$ which can be accepted as negligible.

For the bonded case, the MPC (multipoint constraint) formulation was chosen to zero the initial penetration and the initial gap. For the frictional case, the Augmented Lagrange formulation was preferred to reduce the penetration by adding an extra safety constant to the contact force equation rather than changing the contact stiffness which is a bit uncertain.

Meshing was adjusted to make the 2D and 3D meshes similar. As was shown in the meshing section, the 2D and 3D mesh elements are very close each other in terms of size and shape. Also, since the stress and deformation results were found to be very close to each other in both 2D and 3D models, the costly 3D model can safely be replaced with a 2D surface model. By doing so, not only the meshing time but also the solving time can be significantly reduced. For example, it takes 10 h 43 min 45 s to mesh a 3D model with 2,082,930 mesh elements and 2,921,121 mesh nodes. But for the 2D model, it takes only 3 s to mesh 10,804 elements and

22,888 nodes. This corresponds to a 99% mesh time reduction which is very remarkable. Although there was a huge difference in the mesh statistics, the results were same. Loading may vary to 54 N to 234 N for the mandibular first premolar tooth. But it can also accelerate to the 900 N in the extreme cases. The literature mostly preferred 100 N axial load to simulate the mastication. To get better comparison results, an axial 100 N was chosen as loading condition. The lateral and bottom surfaces or edges were fixedly supported.

The analysis using the alloy Ti-6Al-4V yielded very enlightening results. It proved that there is no distinct difference between 2D and 3D results. To avoid the very time consuming 3D analysis, 2D analysis can be preferred. The 2D and 3D results are consistent with themselves and with the literature (Table 5.1).

100 N Axial Loading	Cortical Bone (MPa)	Trabecular Bone (MPa)	Total Deformation (µm)
Zhang et al.	19.6 - 20.2	1.8 - 5.7	6.39 – 11.49
Huang et al.	5.9 - 16.9	3.0 - 20.8	1.6 – 1.9
Ao et al.	5.9 - 7.3	5.3 - 9.6	4 – 5
Chang et al.	2.3 - 33.8	0.7 - 2.5	N/A
Rahmati et al.	8.4 - 13.6	2.9 - 4.8	N/A
Our Model with Ti-6Al-4V	8.4 - 14	3.5 – 4.7	3.7 – 4.4
Our Model with Ti–24Nb–4Zr–7.9Sn (Proposed)	7.9 – 10.5	2.7 – 4.1	5.2 – 6.1

Table 5.1: Tabular data of literature stress and deformation results on the bones compared to our results.

To examine the Young's modulus effect, material analysis was conducted. Roughly it showed that the lower the Young's modulus, the lower the stress values on the cortical and trabecular bones but the higher the deformation values.

6. FINANCIAL COST ANALYSIS

In a new research and development project, cost is as essential as requirements. For this project, costs can be classified into four groups, which are license fees for journals used in literature search, computer hardware costs, design and analysis software license fees and labor costs.

License fees for journals was supported by Istanbul Technical University Library Department. If this project were a commercial research and development project, the cost of the literature license would be \$3,000 for each journal associated with dentistry in 2016. In our literature review, five important dentistry journals were mostly used, so it would cost around \$15,000 in journal license fees [19].

The computer hardware used in this project was supported by the Smart CAD Laboratory of ITU Mechanical Engineering Department. It has an Intel i7 6700 processor, an EVGA GTX970 graphic card, a 16 GB RAM and an MSI MS-7978 motherboard. Such hardware costs around \$2,000 in the open market in 2016.

Software licenses were supported by ITU Computer Center. For this project, the Siemens NX 10.0 in design and the ANSYS Workbench 16.2 in FEM analysis were used. If this project were a commercial project, the cost of the NX and Workbench would be around \$20,000 each annualy in 2016.

Labor costs involve funds paid to researchers for commercial projects. The two members of this project worked 2.5 days per week for 5 months. If \$500 per month is assumed given to a full time researcher, \$2,500 would be the total labor cost of this project.

In summary, \$59,500 would be spent for this project if it were a commercial project.

7. FUTURE WORK

In this project, the basic implant problem was stated and new solutions were recommended. A new implant model was developed and analyzed. The improvements can be grouped into two topics, which are material and design.

In this project, there were two important issues for material selection. One of them was strength and the other one was bio-compatibility. Strength is a crucial material selection criteria because forces applied by the human jaw can go up to 900 N. This may seem as a small value but these implants are very small objects and stress concentration must be under control. In addition, bio-compatibility must be considered in selecting implant materials. It must not cause any complication with the living tissues. Also, implants must allow bone regeneration and osseointegration over the implant surfaces. As a future work, material systems such as a gradient inner structure, a porous structure, outer nanoparticles and bone-like materials (hydroxyapatite) can be studied. These materials may increase strength, bio-compatibility or both.

Design is another significant part of projects. Model or analysis design can dictate the project needs. Moreover, detailed designs can reveal the real situation clearly and help the problems easily. In this project, the implant system was designed very basically. It focused on just the implant. In the future, real square spiral threads can be studied using the FEM models developed in this project. In future projects, other parts with different designs and their effects should be examined for a better implant system. Furthermore, design analysis of the implant may expand. For example, real data from CT scan images may be used. Such images can offer implant systems specific for each patient. Another future study may involve real crown geometries. Additionally, adjacent teeth or the whole set of teeth may be attached to the design for a more realistic analysis. Finally in FEA, topology optimization can be applied to the implant. This will optimize the design of the implant and reduce the manufacturing costs.

REFERENCES

- [1] **Indian dental academy Follow** (2014). History and development of Dental implants / dental courses. Retrieved January 02, 2017, from <http://www.slideshare.net/indiandentalacademy/anurag-dani-history-and-devpt-of-implants>
- [2] **Moraschini, V., Poubel, L. D., Ferreira, V., & Barboza, E. D.** (2015). Evaluation of survival and success rates of dental implants reported in longitudinal studies with a follow-up period of at least 10 years: a systematic review. International Journal of Oral and Maxillofacial Surgery, 44(3), 377-388.
- [3] **Branemark, P.** (1983). Osseointegration and its experimental background. The Journal of Prosthetic Dentistry, 50(3), 399-410.
- [4] **Introduction to Dental Implants.** (n.d.). Retrieved January 03, 2017, from <http://www.robertsimondds.com/introduction-to-dental-implants>
- [5] **Straumann USA.** (n.d.). Retrieved December 30, 2016, from http://www.straumann.us/content/dam/internet/straumann_us/resources/brochurecatalogue/product-catalogs/en/USLIT.007.2016.US.Product.Catalog.pdf
- [6] **Zadik, Y., Sandler, V., Bechor, R., & Salehrabi, R.** (2008). Analysis of factors related to extraction of endodontically treated teeth. Oral Surgery, Oral Medicine, Oral Pathology, Oral Radiology, and Endodontology, 106(5).
- [7] **Lekholm U, Zarb GA, Albrektsson T.** (1985). Patient selecting and preparation. Tissue integrated prostheses. Chicago: Quintessence Publishing Co. Inc.
- [8] **Frost, H. M.** (2003), Bone's mechanostat: A 2003 update. Anat. Rec., 275A: 1081–1101.
- [9] **Parkhe, N., Hambire, U., Hambire, C., Gosavi, S.**, (December 2015). Enhancing dental implant model by evaluation of three dimensional finite element analysis, International Journal of Engineering Science Invention, 4(12), 26-33.
- [10] **Azari, A., Kheirollahi, H., & Rahmati, S.** (2009). Analysis and fabrication of new designed dental implant using rapid prototyping technology. Innovative Developments in Design and Manufacturing.
- [11] **Kayabaşı, O., Yüzbasioğlu, E., & Erzincanlı, F.** (2006). Static, dynamic and fatigue behaviors of dental implant using finite element method. Advances in Engineering Software, 37(10), 649-658.
- [12] **Binon, P.P. & McHugh, M.J.** (1996). The effect of eliminating implant/abutment rotational misfit on screw joint stability. Int J Prosthodont; 9:511–9.
- [13] **Huang, H., Hsu, J., Fuh, L., Lin, D., & Chen, M. Y.** (2010). Biomechanical simulation of various surface roughnesses and geometric designs on an immediately loaded dental implant. Computers in Biology and Medicine, 40(5), 525-532.

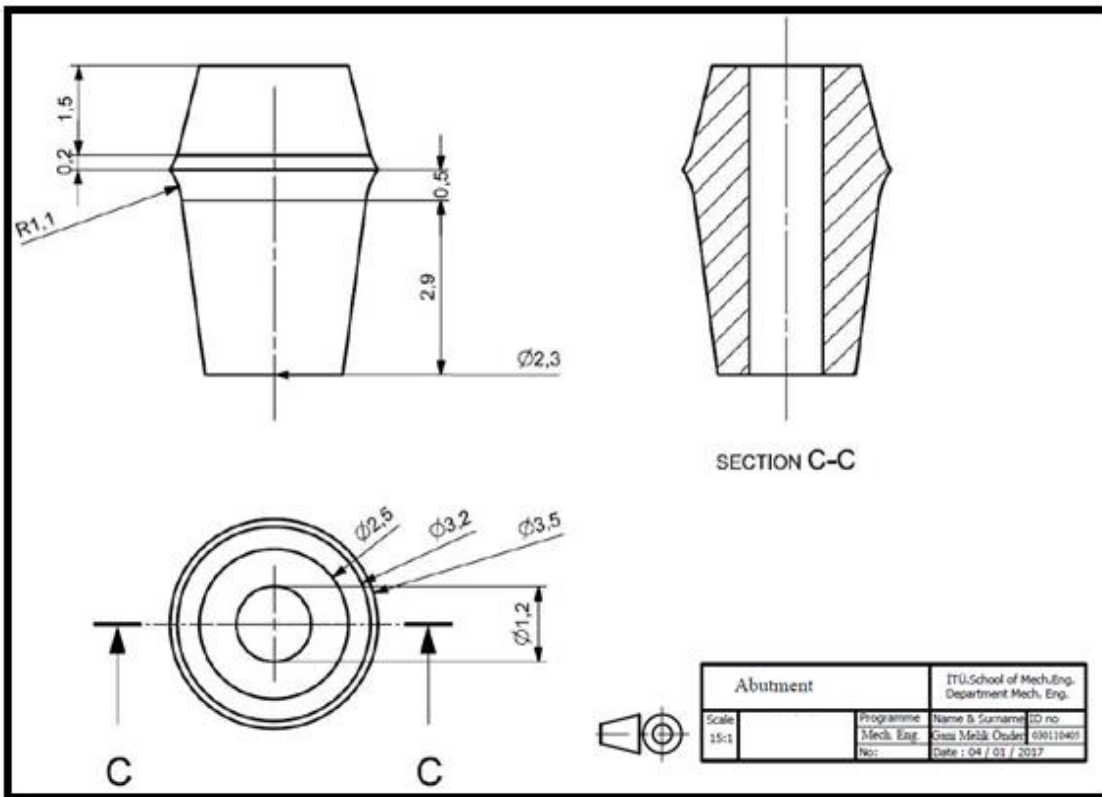
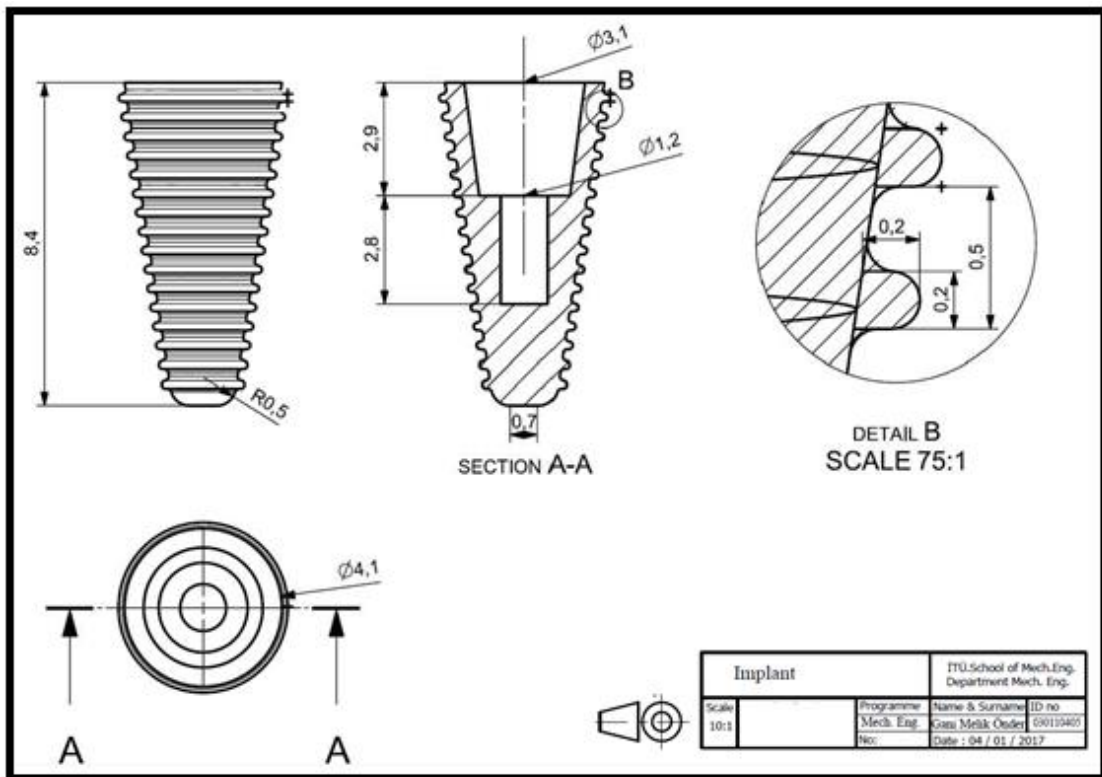
- [14] **Chang, H., Chen, Y., Hsieh, Y., & Hsu, M.** (2013). Stress distribution of two commercial dental implant systems: A three-dimensional finite element analysis. *Journal of Dental Sciences*, 8(3), 261-271.
- [15] **Ao, J., Li, T., Liu, Y., Ding, Y., Wu, G., Hu, K., & Kong, L.** (2010). Optimal design of thread height and width on an immediately loaded cylinder implant: A finite element analysis. *Computers in Biology and Medicine*, 40(8), 681-686.
- [16] **Saidin, S., Kadir, M. R., Sulaiman, E., & Kasim, N. H.** (2012). Effects of different implant abutment connections on micromotion and stress distribution: Prediction of microgap formation. *Journal of Dentistry*, 40(6), 467-474.
- [17] **Niinomi, M.** (1998). Mechanical properties of biomedical titanium alloys. *Materials Science and Engineering: A*, 243(1-2), 231-236.
- [18] **Mohammed, M., Khan, Z., Siddiquee, A.** (2014). 'Beta Titanium Alloys: The Lowest Elastic Modulus for Biomedical Applications: A Review'. *World Academy of Science, Engineering and Technology, International Science Index 92, International Journal of Chemical, Molecular, Nuclear, Materials and Metallurgical Engineering*, 8(8), 822 - 827.
- [19] **Elsevier** (n.d.). Pricing. Retrieved December 30, 2016, from <https://www.elsevier.com/about/company-information/policies/pricing>
- [20] **Achour, T., Merdji, A., Bouiadjra, B. B., Serier, B., & Djebbar, N.** (2011). Stress distribution in dental implant with elastomeric stress barrier. *Materials & Design*, 32(1), 282-290.
- [21] **Albogha, M. H., & Takahashi, I.** (2015). Generic finite element models of orthodontic mini-implants: Are they reliable? *Journal of Biomechanics*, 48(14), 3751-3756.
- [22] **Alkan, I., Sertgöz, A., & Ekici, B.** (2004). Influence of occlusal forces on stress distribution in preloaded dental implant screws. *The Journal of Prosthetic Dentistry*, 91(4), 319-325.
- [23] **Brunski, J. B.** (1992). Biomechanical factors affecting the bone-dental implant interface. *Clinical Materials*, 10(3), 153-201.
- [24] **Chang, C., Chen, C., Huang, C., & Hsu, M.** (2012). Finite element analysis of the dental implant using a topology optimization method. *Medical Engineering & Physics*, 34(7), 999-1008.
- [25] **Chen, J., Chen, X., Zhang, X., Eichstädt, O., Du, R., Deng, F., & Zhang, Z.** (2014). Computer-aided design and manufacturing of dental implants with irregular geometries. *Biodental Engineering III*, 51-56.
- [26] **Chen, Y., Chen, W., Chang, H., Huang, S., & Lin, C.** (2014). A novel dental implant abutment with micro-motion capability—Development and biomechanical evaluations. *Dental Materials*, 30(2), 131-137.

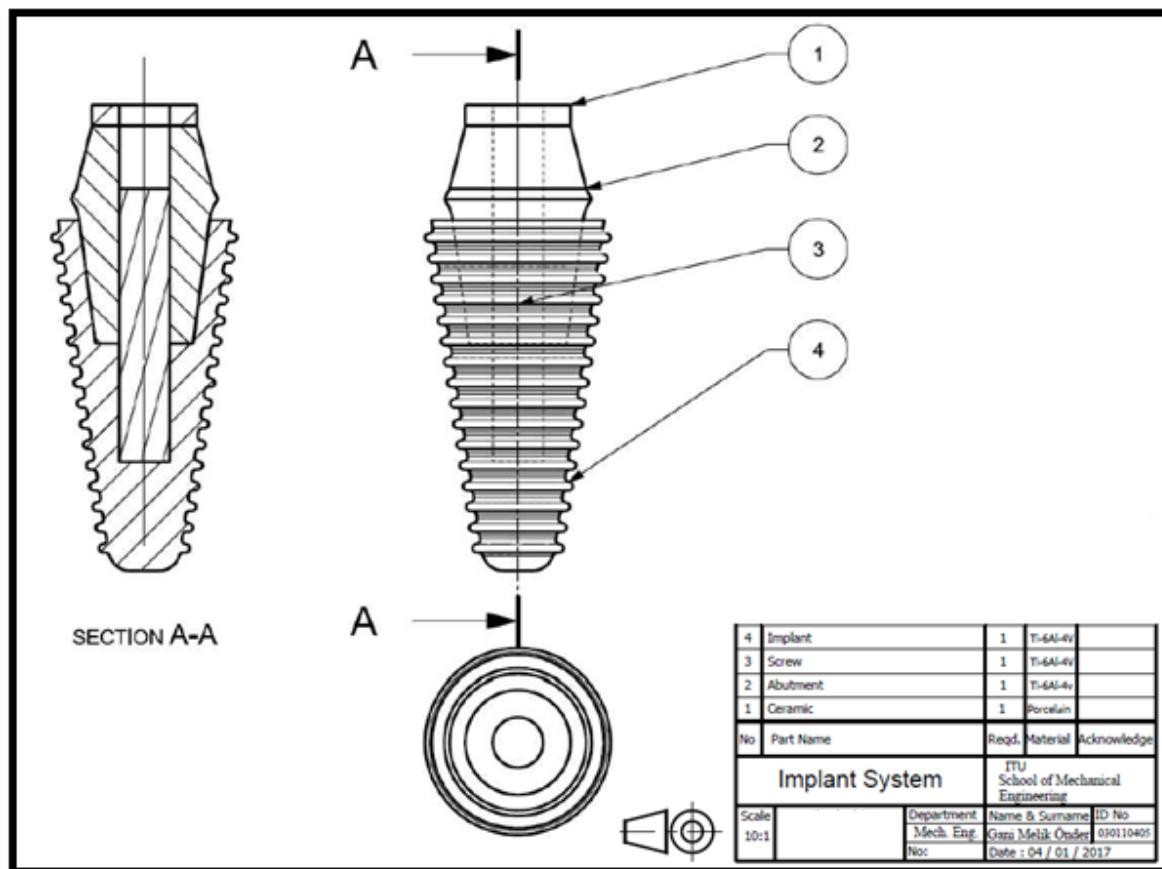
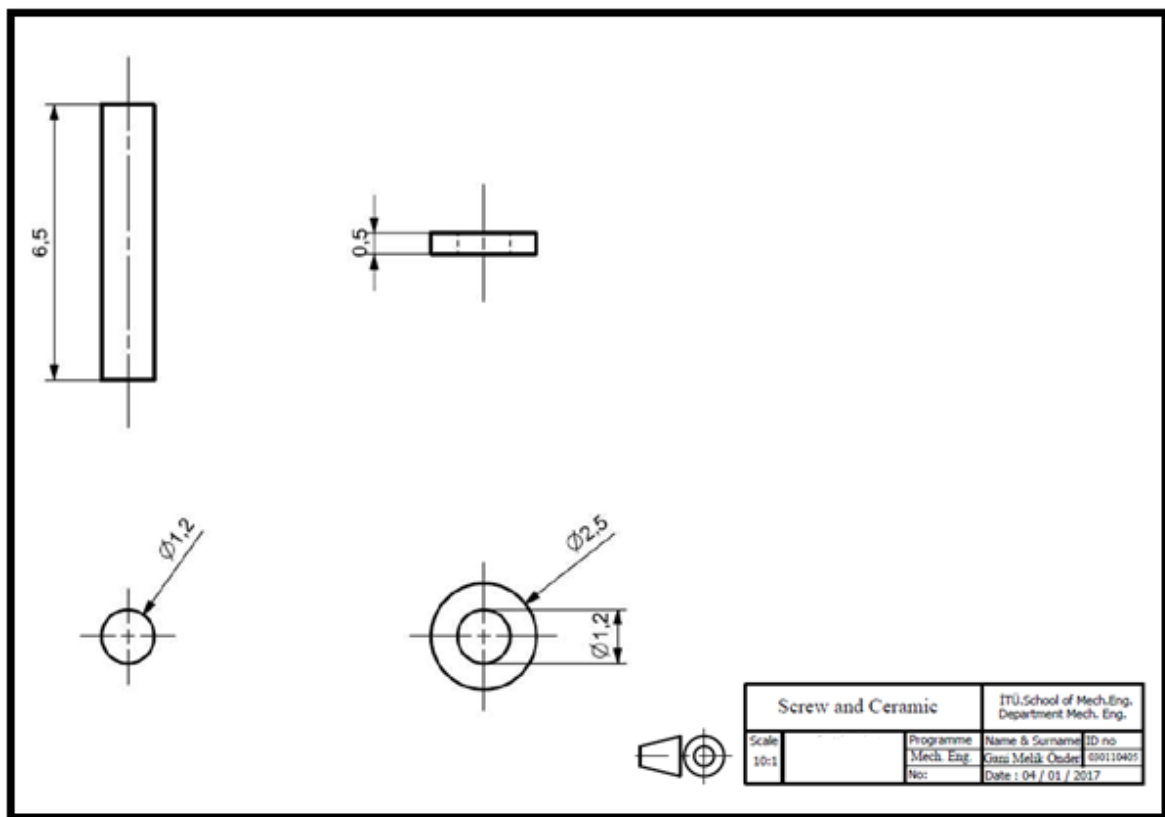
- [27] **Desai, S. R., Karthikeyan, I., & Singh, R.** (2012). Evaluation of Micromovements and Stresses around Single Wide-Diameter and Double Implants for Replacing Mandibular Molar: A Three-Dimensional FEA. *ISRN Dentistry*, 2012, 1-10.
- [28] **Eliaz, N.** (2012). Degradation of implant materials. New York: Springer.
- [29] **Ellingsen, J. E., & Lyngstadaas, S. P.** (2003). Bio-implant interface: improving biomaterials and tissue reactions. Boca Raton, FL: CRC Press.
- [30] **Geng, J., Yan, W., & Xu, W.** (2008). Application of the finite element method in implant dentistry. Hangzhou: Zhejiang University Press.
- [31] **He, Y., Hasan, I., Keilig, L., Chen, J., Pan, Q., Huang, Y., & Bouraue, C.** (2016). Combined implant-residual tooth supported prosthesis after tooth hemisection: A finite element analysis. *Annals of Anatomy - Anatomischer Anzeiger*, 206, 96-103.
- [32] **He, Y., Hasan, I., Chen, J., Keilig, L., & Bouraue, C.** (2016). The influence of residual root number and bone density on combined implant-residual tooth supported prosthesis after tooth hemisection: A finite element study. *Annals of Anatomy - Anatomischer Anzeiger*, 208, 103-108.
- [33] **Hisam, M., Lim, J., Kurniawan, D., & Nor, F.** (2015). Stress Distribution Due to Loading on Premolar Teeth Implant: A Three Dimensional Finite Element Analysis. *Procedia Manufacturing*, 2, 218-223.
- [34] **Indian dental academy Follow** (2014). History and evolution of dental implants / academy of fixed orthodontics. Retrieved January 02, 2017, from <http://www.slideshare.net/indiandentalacademy/2-newhistory-and-evolution-of-implants1>
- [35] **Kumar, G., Kovoor, L., & Oommen, V.** (2011). Three-dimensional finite element analysis of the stress distribution around the implant and tooth in tooth implant-supported fixed prosthesis designs. *Journal of Dental Implants*, 1(2), 75.
- [36] **Lu, S., Li, T., Zhang, Y., Lu, C., Sun, Y., Zhang, J., & Xu, D.** (2013). Biomechanical optimization of the diameter of distraction screw in distraction implant by three-dimensional finite element analysis. *Computers in Biology and Medicine*, 43(11), 1949-1954.
- [37] **Mehdi, G., Belarbi, A., Mansouri, B., & Azari, Z.** (2015). Numerical study of effect of elastomeric stress absorbers on stress reduction in bone-dental implant interface. *Journal of Applied Oral Science*, 23(1), 87-93.
- [38] **Mellal, A., Wiskott, H. W., Botsis, J., Scherrer, S. S., & Belser, U. C.** (2004). Stimulating effect of implant loading on surrounding bone. *Clinical Oral Implants Research*, 15(2), 239-248.

- [39] **Noorthoek, D.R.**, (2013), Macroscopic and Microscopic Dental Implant Design: A Review of the Literature (Master's Thesis), Retrieved from http://ufdcimages.uflib.ufl.edu/UF/E0/04/58/59/00001/NOORTHOEK_D.pdf
- [40] **The History of Dental Implants** (n.d.). Retrieved January 02, 2017, from <http://www.thedentalgeek.com/2015/03/the-history-of-dental-implants/>
- [41] **Toniollo, M. B., Macedo, A. P., Rodrigues, R. C., Ribeiro, R. F., & Maria Da Glória Chiarello De Mattos.** (2013). A three-dimensional finite element analysis of the stress distribution on morse taper implants surface. *Journal of Prosthodontic Research*, 57(3), 206-212.
- [42] **Verri, F. R., Batista, V. E., Santiago, J. F., Almeida, D. A., & Pellizzer, E. P.** (2014). Effect of crown-to-implant ratio on peri-implant stress: A finite element analysis. *Materials Science and Engineering: C*, 45, 234-240.
- [43] **Wu, A. Y., Hsu, J., Chee, W., Lin, Y., Fuh, L., & Huang, H.** (2016). Biomechanical evaluation of one-piece and two-piece small-diameter dental implants: In-vitro experimental and three-dimensional finite element analyses. *Journal of the Formosan Medical Association*, 115(9), 794-800.
- [44] **Yokoyama, S., Wakabayashi, N., Shiota, M., & Ohyama, T.** (2004). The influence of implant location and length on stress distribution for three-unit implant-supported posterior cantilever fixed partial dentures. *The Journal of Prosthetic Dentistry*, 91(3), 234-240.
- [45] **Zhang, X., Chen, X., Zhang, G., & Chen, J.** (2014). Biomechanical analysis of typical structured dental implants and surrounding bone tissues. *Biodental Engineering III*, 235-239.
- [46] **ANSYS Mechanical Structural Nonlinearities.** (n.d.). Retrieved from http://inside.mines.edu/~apetrell/ENME442/Labs/1301_ENME442_lab6_lecture.pdf

APPENDIX – 1 TECHNICAL DRAWINGS

All units are in mm.





APPENDIX – 2

STUDENT RESUMES

RESUME - 1



Name Surname: Veysel Mert Usta

Birth Place and Date: Zonguldak / 30.11.1993

Contact: mertusta@gmail.com

RESUME - 2



Name Surname: Gani Melik Önder

Birth Place and Date: Kayseri / 09.10.1993

Contact: ganimelikonder@gmail.com